Synthetic Aperture Radar Application for Agricultural Land Use Classification in Java Island, Indonesia

(インドネシア、ジャワ島における農業的土地利用分類のための
の合成開口レーダ画像の応用)

Prima Rizky Mirelva

2019

Synthetic Aperture Radar Application for Agricultural Land Use Classification in Java Island, Indonesia

A dissertation presented to

The United Graduate School of Agriculture Sciences, Tottori University

in partial fulfillment of the requirements for a degree of Doctor of Philosophy

by

Prima Rizky Mirelva

Approved by

Professor Ryota NAGASAWA

Faculty of Agriculture, Tottori University

The United Graduate School of Agricultural Sciences

Tottori University, Japan

August, 2019

Prima Rizky MIRELVA (2019)
Synthetic Aperture Radar Application for Agricultural Monitoring in Indonesia
The United Graduate School of Agricultural Sciences, Tottori University, Japan
August 2019
Ph.D Thesis

Declaration

This thesis is submitted for the degree of Doctor of Philosophy at the United Graduate School of Agricultural Sciences, Tottori University. This dissertation is the result of my own work and has not been and is not being, in part or wholly, submitted for another degree, diploma, or similar qualification.

Prima Rizky Mirelva

Acknowledgements

All praises and gratitude belong to Allah for everything that has been given to me, especially health and ability to finish my study in Japan.

I would like to express my gratitude to my academic supervisor, Professor Ryota Nagasawa, for his endless support, advice, and motivation during my study in this university. His deep knowledge in agriculture and remote sensing helped me in conducting this research. I wish to pass my gratitude to my teacher, Professor Ketut Wikantika, for his guidance and encouragement in my study. I am also grateful for Professor Yoshiyuki Hioki and Professor Hirokazu Haga for their beneficial suggestions in my study.

Many thanks and appreciation goes to my beloved parents, Maimirza and Maria Elva, sister, Karina, brother, Abyan, and especially my husband, Prayudha. Without them, this journey would be difficult to handle. Their unconditional love, trust, and understanding, inspired me to finish my study.

Special appreciation is to my colleagues in Landscape Ecology and GIS Laboratory, especially Lissa Fajri, and Dandy Aditya, for their recommendation in my study. I would also like to thank my kind hearted friends: Sukontip Vianmana, Kansuma Burapapol, Koera Takuya, and Kono Tatsuya that made living in Tottori cheerful and unforgettable. Last but not least, I would like to extend my gratitude to my warm hearted Indonesian friends and Tottori muslim community.

Finally, I want to acknowledge the financial support of Ministry of Education, Culture, Sports, Science, and Technology Japan. I am thankful for the opportunity to be able to study and gain knowledge in Tottori University as well as to experience rich Japanese culture.

Table of Contents

List of Figures

List of Tables

List of Abbreviations

ASEAN **:** Association of Southeast Asian Nations
ALOS : Advanced Land Observing Satellite
dB : decibel unit
DEM : Digital Elevation Model
ESA : European Space Agency
FAO : Food and Agriculture Organization
FBD : Fine Beam Dual polarization
FBS : Fine Beam Single polarization
FD : Freeman and Durden Polarimetric Decomposition
GEE : Google Earth Engine
GIS : Geographic Information System
HH : Horizontal transmit - Horizontal receive polarization
HV : Horizontal transmit - Vertical receive polarization
ISODATA : Iterative Self-Organizing Data Analysis Technique
JAXA : Japan Aerospace Exploration Agency
KC : Kappa coefficient
MLC : Maximum Likelihood Classification
NDPI : Normalized Difference Polarization Index
NEST : Next ESA SAR toolbox
OA : Overall Accuracy
OLI : Operational Land Imager
PALSAR : Phased Array type L-band Synthetic Aperture Radar
PolSARpro : Polarimetric SAR Data Processing and Educational Tool
Quad-pol : quad polarizations
radar : radio detection in ranging
RAR : Real Aperture Radar
RGB : composition of red, green, and blue band
SAR : Synthetic Aperture Radar
SI : Separability Index
SLAR : Side Looking Aperture Radar
SNAP : Sentinels Application Platform
UTM : Universal Transverse Mercator
VH : Vertical transmit - Horizontal receive polarization
VV : Vertical transmit - Vertical receive polarization
Y4 : Yamaguchi 4 components polarimetric decomposition

Chapter 1
Introduction

1.1 Research Background

Agricultural activities are beneficial and important sector for almost every country. The countries in the tropical region are most benefited the climate condition to do agricultural activities in all year round. The majority of ASEAN (Association of Southeast Asian Nations) countries depend to the agriculture sector for national income, national food consumption, and it provides high quantity of job for the countries' rural citizen. According to Food and Agriculture Organization (FAO) data of 2010 the rice or paddy is the main commodity for mostly ASEAN countries. Maize and cassava are also well known commodity in ASEAN countries. It is followed by other economically valuable commodity such as oil palm, sugarcane, or vegetables and tropical fruits, such as mango, coconut, pineapple and banana.

Based on the Statistic of Indonesia for 2010-2014 (Badan Pusat Statistik, 2015), the agriculture, forestry and fishing sectors give valuable contribution to the national Gross Domestic Product with 13.38 percent contribution. It is below the manufacturing sector and above the mining and quarrying sector. The agriculture sector consists of food crops, horticultural crops, and plantation crops, livestock, and agriculture services, gives 75 percentage distributions amongst agriculture, forestry, and fishing sectors.

The topographic with many active volcanoes provides fertile soil that is suitable for cultivating agriculture crops (Wahyunto et al. 2012). One of central agricultural activities areas in Indonesia is located in Java Island. The population density in Java is high with around more than 800 people per kilometer square (Verburg et al. 1999). There are five provinces in Java including the capital of Indonesia, DKI Jakarta. The population distributes in the supported cities (suburban) around DKI Jakarta, such as Tangerang (Banten Province), Bekasi, Depok, and Bogor (West Java province). According to commuter statistic from the Statistical Indonesia agency, more than 2 million people commute within, into or out the capital city for various activities purpose (Badan Pusat Statistik, 2014).

The urbanization is high in other cities in Java such as Bandung (West Java Province), Semarang (Central Java Province), Surabaya, and Yogyakarta (Special Region of Yogyakarta Province) as the central provincial government as well as center for trade and manufacturing (Firman 2016). As these cities growth and focus on the industry, the smaller cities became the support system to provide commodity, including agriculture product, for distributed and traded in the big city. It is common to have the farmers in the smaller city deal directly to suppliers from big city (Van der Wouden 1997 in Firman 2016). Although all provinces have their own agricultural areas, more intensive agricultural fields are concentrated in rural area of Central Java and East Java

provinces. The frequent eruptions of Merapi Volcano has been influenced the soil condition near the slope of Merapi Volcano in Central Java. There were four volcano eruptions within two decades. The frequent eruptions increased the amount of soil nutrition which is beneficial for agricultural activities (Wahyunto et al. 2012). Majority of people living near the slope of Merapi Volcano are working as smallholder farmer. They afford and manage agriculture in the small fields. Generally, the agricultural fields in Central Java are small in scale with size around 0.3 Ha per household (Agis and Manikmas 2003). In addition, the agricultural fields are often located near slope of Merapi Volcano and often in irregular shape to fit the hilly topography.

Besides the irregular shape of agricultural fields, the intercropping systems which follow the seasonal pattern are also widely adapted by the Javanese farmers. This practice is beneficial to increase yield and to obstruct the pest invasion. The common practice of intercropping system are rice planting which cultivated with other subsidiary crops such as maize in dry season or intercropping between maize and other horticultural crop types.

Due to the unsystematic and complex agriculture areas in Java, it is challenging to do detail mapping in the agricultural area. According to Geospatial Information Agency of Indonesia, the national standard for topographic mapping with scale 1:10000 differentiate the agricultural area into three general categories, irrigation paddy field, rain-fed paddy and crop field (Badan Standardisasi Nasional 1999). Nowadays, the specific land use and land cover mapping of agriculture become important as basis of decision maker to support the sustainability of agriculture. As the most populated island, population in Java is continuing to grow. The increase population gives pressure to the agricultural land due to the need for infrastructure (Widiatmaka et al. 2016). The statistic of agriculture commodity is heavily obtained by direct survey to the field which is time consuming. In brief, mapping agriculture area in Indonesia face several challenges such as the complexity of the agricultural fields, the unsystematic planting system, extensive labor needs for survey, and the land cover and land use change. The additional monitoring, such as using geo-spatial technology whether GIS or remote sensing, is essential to enhance the information about agricultural croplands in shorter time process. In addition, the remote sensing technology with good temporal data acquisition will be significant for updating the agriculture map.

There are two kinds of remote sensing to monitor the agriculture area the optical and microwave (radar) remote sensing. However, the cloud that often covers tropical area becomes one of limitation for optical remote sensing system (Inoue et al. 2002). The microwave remote sensing such as Synthetic Aperture Radar (SAR) is good option to overcome limitation of optical remote sensing for discriminating the agriculture area in tropical country. There are a lot of satellites which mounted with different wavelength band SAR system sort from the shorter to longest wavelength such as X-band (2.5-4 cm), C-band (3.75-7.5 cm), and L-band (23-30 cm).The X-band carried by the satellite TerraSAR-X or Radarsat-2. The Sentinel-1 satellite mounted with C-band SAR. Meanwhile the L-band wavelength is carried by the ALOS/PALSAR and ALOS2/PALSAR2.

Previous studies performed agriculture or land cover analysis by using SAR data. For example, the dual polarization of ALOS PALSAR data was used for paddy field identification in China (Zhang et al. 2011). The paddy field identification by using the ALOS PALSAR data in the tropical area such as Indonesia has also been conducted (Shofiyati, et al. 2011). Another study used multi-temporal of ALOS PALSAR data for determining area that potential for crop extension (Milisavljevic et al. 2012). The (McNairn et al. 2009) presented that full polarization data of ALOS PALSAR gave promising result for crop classification. The polarimetric data of ALOS PALSAR was used to differentiate hay pasture, soybean, corn and cereal. The sensor combination between ALOS PALSAR, TerraSAR-X, and ENVISAT is also used for monitoring sugarcane crops (Baghdadi et al. 2008).

The previous studies presented that the importance and the ability of SAR data in agricultural monitoring and identification. However, the studies about classifying the complex agricultural in tropical area are still limited. In addition, the land covers and land use mapping in agricultural area especially in Indonesia, is time –consuming. The SAR data, further, could be integrated with the cloud based systems such as Google Earth Engine (GEE) to maximize the efficiency and reduce the time for mapping process. Therefore, in this study, three types of SAR satellites, namely ALOS/PALSAR, ALOS2/PALSAR2, and Sentinel-1, were utilized for discriminating the agriculture croplands area in tropical area. The ALOS/PALSAR and ALOS2/PALSAR2 were Japanese radar system with L-band SAR satellite. ALOS-2/PALSAR-2 has revisit time around 14 days. It is higher than previous ALOS/PALSAR with 46 days of revisit time. In order to get detail capability knowledge about the ALOS/PALSAR and ALOS2/PALSAR2, two different study sites and two types of dataset were prepared. Besides the L-band wavelength SAR satellites, the Sentinel-1 with C-band wavelength with 12 days revisit time was also utilized and will especially be integrated with the cloud based system. These SAR data will be further used to analyze the effectiveness of SAR data in classifying the complex agricultural croplands as well as for updating the land use and land cover mapping process by implementing the cloud based system, such as GEE.

1.2 Research Objectives

The primary objective of this research is to understand the ability of remote sensing in classifying the complex agricultural croplands, especially the active remote sensing. The active remote sensing depends on the wavelength used by the synthetic aperture radar satellites, such as L-band or C-band. The agricultural croplands properties such as structure and condition influence the backscatter value of the synthetic aperture radar. Furthermore, the backscatter value can be modified by using polarimetric decomposition or performed arithmetic conditions to obtain the best backscatter value for identifying and classifying the complex agricultural croplands area. Therefore, the objectives of the research were formulated as follows:

(1) to examine the characteristic of complex agriculture cropland that can be identified by using active

remote sensing data,

(2) to explore the ability of ALOS/PALSAR full polarization mode and the most effective of backscatter value parameter for identifying complex agricultural croplands,

(3) to perform classifying and mapping of Sentinel-1 by using the cloud based system of GEE

(4) to investigate the multi-temporal of ALOS-2/PALSAR-2 for identifying and classifying the agricultural croplands,

(5) to analyze the influence of sample points selection based on the backscatter value characteristic for classification process

1.3 Outline of Dissertation

This dissertation composed in six chapters. The first chapter is dedicated to describe the introduction of this study which separated into three sections, namely the background, the objectives of this study and the last is the outline of dissertation.

The second chapter mainly explains about the characteristic of agricultural system in Indonesia as well as the basic theory of remote sensing focus in the Synthetic Aperture Radar.

The third chapter discussed about the ALOS/PALSAR data implementation in classifying agricultural croplands in study area in Central Java. This chapter emphasized the possible methods to achieve good classification result of full polarimetric for classifying agricultural croplands.

The fourth chapter, the multi-temporal of C-band SAR satellite named Sentinel-1 was performed in the GEE to develop methodology for faster identifying and classifying in agricultural croplands.

In the fifth chapter, the second generation of ALOS/PALSAR name ALOS2/PALSAR2 was obtained for classifying more complex agricultural cropland than study area in the third chapter. There are four satellite imageries used such as three dual-polarization satellite image and one full polarization of ALOS2/PALSAR2. This chapter use different method for collecting sample points in order to achieve the third objective of this study.

The last chapter is general discussion and recommendation all of the third to the fifth chapters.

Chapter 2
Theoretical Framework

2.1 Agricultural system in Indonesia

According to the Center for Agricultural Data and Information system of Indonesia in 2014, the agriculture area in Indonesia can be divided into six types based on the agricultural type and the cultivation process. The six types of agriculture area in Indonesia are paddy field, irrigated paddy field, non-irrigated paddy field, dry field, shifting cultivation land and also temporarily unused land. From the statistical survey obtained by the Statistics Indonesia between 2014 until 2016 and the preliminary value for 2017, the agricultural area utilization in Indonesia can be seen in Table 2-1.

Table 2-1 Agricultural area in Indonesia in 2014-2017

In Hectare value

No.	Land type	Year			
		2014	2015	2016	2017*
1	Paddy field:	8,111,593	8,092,907	8,187,734	8,162,608
	Irrigated paddy field	4,763,341	4,755,054	4,782,642	4,745,027
	Non-irrigated paddy field	3,348,252	3,337,853	3,405,092	3,417,581
2	Dry field	12,033,776	11,861,676	11,539,826	11,730,930
3	Shifting cultivation	5,036,409	5,190,378	5,074,223	5,222,066
4	Temporarily unused land	11,713,317	12,340,270	11,941,741	12,016,778
	Total	36,895,095	37,485,231	36,473,524	37,132,382

Agriculture in Indonesia is mainly located in Java Island. The large agricultural area distribution in Java is influenced by several factors such as climate condition and soil type. The different climate condition and soil type also led to the cropping system to maximize the agricultural production. The combination of climate, soil type, and also topographic condition increased the agriculture monitoring difficulties due to the random pattern of cropping system.

2.1.1 Climate condition

Climate in Indonesia is mostly classified as Af climate based on Köppen-Geiger classification or tropical rainforest climate that identified with average temperatures above 18^{o}C and average rainfall more than 60 mm. The monsoon climate, classified as Am based on Köppen-Geiger classification, can also be found in the central and eastern part of Java island, and small area in Sulawesi Island. This type of climate is identified to have less

pronounced dry seasons and extraordinary rainfall to complement the dry season. The southern part of Indonesia such as West Nusa Tenggara and East Nusa Tenggara have tropical savanna climate (Aw) based on Köppen-Geiger classification which have long dry season. Due to the climate condition, most of the agriculture in Indonesia is largely located in Java Island.

The agricultural is highly related to the rainy or wet season for determining the suitable planting season. The rainfall in Indonesia is influenced by the austral-Asian monsoon (Naylor et al. 2002) and El Nino-Southern Oscillation (Hamada et al. 2002). The dry season in Java starts between April to September and the rainy season starts in October to March. However, the western and central and eastern part of java has different climate system. The central and eastern part of Java is drier than the western part of Java since it has the monsoon climate. Due to the different climate condition, the agricultural activities were varies follow the climate condition

2.1.2 Soil type

Java Island has various mountainous topographic conditions with many active volcanoes that provide levels of elevation and fertile soil which are suitable for cultivating various crops. Based on the soil exploratory map from Ministry of Agriculture Government of Indonesia, the soil types in Java consist of inceptisols, ultisols, andisols, mollisols, and vertisols (Sarwani et al. 2015). In Central Java, the soil types consist of vertisols, andisols, and inceptisols. The agriculture in Central Java is affected by the existence of Merapi volcano. The Merapi volcano is one of the most active volcanoes in Indonesia which has erupted many times (1872, 1883, 1906, 1930, 1954, 1957, 1992, and 1998), and the last eruption occurred on 10 November 2010. The soil around Merapi volcano is dominated by andisols and alfisols which are formed from volcanic material and rich in organic material (Wahyunto et al. 2012). Thus the agricultural fields in Java are widely distributed near the mountainous area due to its high amount of fertile soil (Lavigne et al. 2008).

2.1.3 Cropping system

Agricultural fields in Java are generally small in scale and irregular shape to fit the hilly topography. The cropping system in Central Java is also depended on the weather and climate condition that affected the water supply. Therefore, the cultivation is rotated. In addition, the intercropping systems that follow seasonal patterns are also widely implemented by Javanese farmers to increase yield and obstruct pest invasions.

Farmers in Central Java have their own traditional calendar for calculating the season and forecasting time to start cultivating their crops called as Pranatamangsa which means the arrangement of seasons (Daldjoeni, 1984). The calendar has the same length with the Gregorian calendar and is calculated based on the cosmology, animal behavior and the phenology of plant. Thus each month can be different in length. The pranatamangsa divides year into four seasons, mangsa rendheng (wet season), mangsa labuh (beginning of rainy season), mangsa

mareng (ending of rainy season), and mangsa katiga (dry season). Nowadays, the pranatamangsa is not suitable for predicting the cultivation time due to the unpredictable seasonal change. Thus based on those pranatamangsa, the new cropping system was developed. In Central Java, there are three cropping times, called as cropping time I (MT-I) in rainy season between November to February for paddy cultivation, cropping time II (MT-II) in dry season between March to June, and the last is cropping time III (MT-III) in the second dry season for vegetables and horticultures.

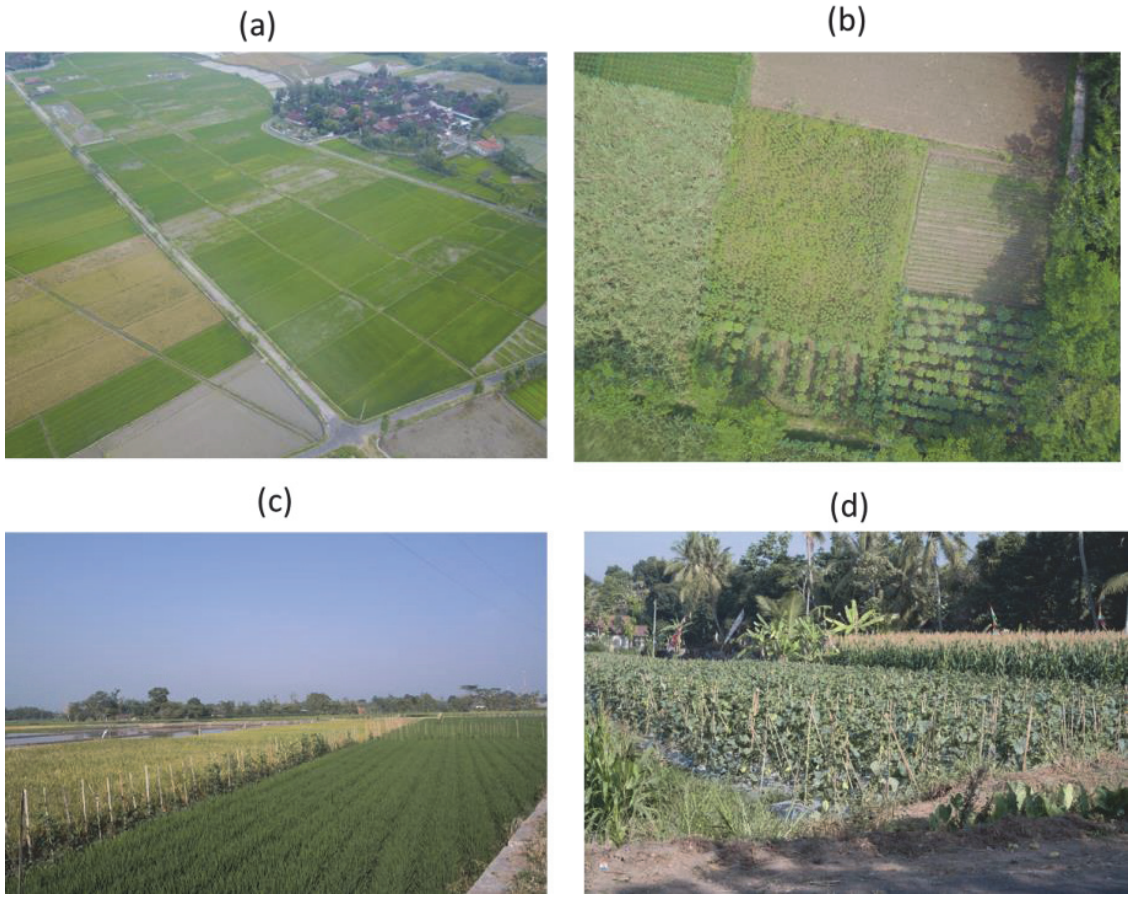

Fig. 2-1 The different cultivation stage of (a) paddy fields image taken from drone, (b) the various horticultural crops image taken from drone, (c) different stage of paddy fields, (d) the maize and chayote are planted side by side

In order to understand the cropping system in recent years, the field survey was done in the 2017 in Central Java. The paddy fields planted in different stage which indicated the different planting time of paddy fields. One of the examples of different cultivation stage of paddy fields which can be easily identified shows in Fig. 2-1. This picture was taken by drone in March 2017 on Central Java agricultural area. The large and complex agricultural fields in Java were also influenced by the uneven condition of the irrigation system.

Besides paddy fields, there are other plant varieties that often found in Central Java area such as maize, soy bean, peanuts, cassava, and sweet potato. The horticulture types are also widely planted in this area, some of

which are: shallots, potato, and chili. The intercropping systems can be found in the upland fields where rice is cultivated along with other subsidiary crops such as maize. In Fig. 2-1shows the different cultivation stage of paddy fields as well as typical various horticultural crops in Central Java.

2.1.4 Mapping agricultural in Indonesia

Indonesia is known as archipelago country with thousands of islands. The large area of Indonesia was separated by the sea. This condition leads to the difficulty of detail mapping process. The land use and land cover mapping with high precision is important to gain knowledge about valuable socio-economic sectors. It is beneficial for the government and stockholders to implement right policy for increasing the economic in one area. The topography map is also known as RBI (Rupa Bumi Indonesia) map.

Table 2-2 The availability of topography map in Indonesia until 2017

No.	Topography scale map	National coverage (MSN*)	Map availability in MSN			Not yet available	Availability up to 2017 in percentage
			Up to 2015	Up to 2016	Up to 2017		
1	1 :1,000	-					
2	1 : 5,000	377824	590	3922	3922	373902	1.04
3	1 : 10,000	91547	1074	1074	1074	90473	1.17
4	1 : 25,000	13020	3894	4781	4781	8239	36.72
5	1 : 50,000	3899	3201	3506	3506	393	89.92
6	1 : 100,000	1259	26	26	26	1233	2.07
7	1 : 250,000	309	309	309	309	0	100.00
8	1 : 500,000	103	103	103	103	0	100.00
9	1 : 1,000,000	37	37	37	37	0	100.00

MSN*: map sheet number, source: (Abidin & BIG Staff, 2018)

Based on the presentation of (Abidin and BIG Staff, 2018), the demand of map with higher precision and detail is increasing. However the availability of map especially large scale is still low. The Table 2-2 shows the availability of topography map as well as the number of map needed up until 2017. The large scale map with scale such as below 1:25,000 is lack of updating even though it is important for the land use and land cover planning. The remote sensing and other technology such as drone were also utilized for updating the topographic map as well as to enhance the spatial information as well as for mapping. The mapping of agricultural croplands area has unique difficulties. The cropping pattern was dynamic. Therefore, the high precision mapping for agricultural cropland is hard to achieve. However, the temporal monitoring can be fulfilled by the remote sensing which later can be used as based for further mapping and field survey.

2.2 Basic theory of Synthetic Aperture Radar

The remote sensing system offers promising technology to provide wide range of imageries dataset for agricultural monitoring. Remote sensing is defined as the science and art of obtaining information about an object, area, or phenomenon through the analysis of data acquired by a device that is not in contact with the object, area, or phenomenon under investigation (Lillesand et al. 2008). Therefore, the remote sensing technology is often used to gather and to obtain information from limited access to the area or in particular range of time. The type of data or information from the remote sensing technology is highly correlated with the sensor and the electromagnetic wavelength that mounted to the satellite. According to the sensor, remote sensing technology can be divided into two, passive remote sensing and the active remote sensing. The sensor of passive remote sensing works as our eyes see object, the sunlight contains electromagnetic waves which received and absorbed by the object in the earth, and the residual of electromagnetic waves reflected back and captured by the sensor. Therefore, the objects will give different spectral characteristic which is beneficial for monitoring purposes. The passive remote sensing is often limited by the atmospheric condition such as clouds which cover the monitoring area.

The active remote sensing system acquired data by transmitting the electromagnetic energy to the earth surface. It receives the scatter from the objects which often called as backscatter. The active remote sensing used the radar (radio detection in ranging). Radar wavelength is called as the microwave bands and in range between around 1 mm to 1 m. Based on the Fig. 2-2 (Berens, 2006), the microwave bands are almost 100% can penetrate the atmospheric condition. Therefore, these wavelengths are used for radar imaging. The term on radar imaging refers to the image acquisition by using radar that mounted to the aircraft or spacecraft.

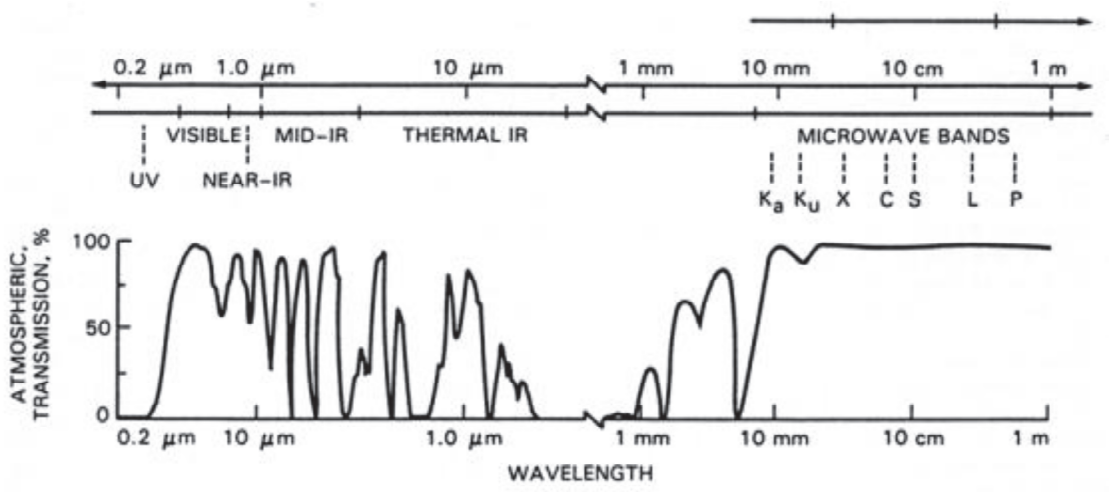

Fig. 2-2 Electromagnetic waves spectrum and relation between wavelength and the atmospheric transmission percentage

The early radar imaging is named as the Side Looking Aperture Radar (SLAR) or Real Aperture Radar (RAR). The continuously moving beam from the antenna used for scanning the scene along the flight path or along orbit (Bamler, 2000). Radar imaging acquisition is based on the time and distance calculation between object and the antenna. There are two kinds of resolution for radar imaging, the range resolution which is related to the scanning system in speed of light and azimuth resolution that related to the flight path direction. The SLAR system's azimuth resolution is highly depend on the antenna length, for example to get azimuth resolution of the order of a few meters, the antenna length should be several kilometers which is unrealistic (Bamler, 2000). Due to the long antenna that could not be mounted in satellite, the SAR system was invented to make good resolution imaging radar with short antenna feasible.

In SAR system, when spacecraft with SAR antenna moves along its path, the radar transmits pulses in repetition in certain frequency and receives the pulses from earth object (Patel et al. 2010). Thus, the antenna receives the pulses coherently (Bamler, 2000) and the object can be scanned several times during the acquisition process. The SAR system configuration that emulates the SLAR system with the short antenna can be seen in Fig. 2-3 based on (Richards, 2009).

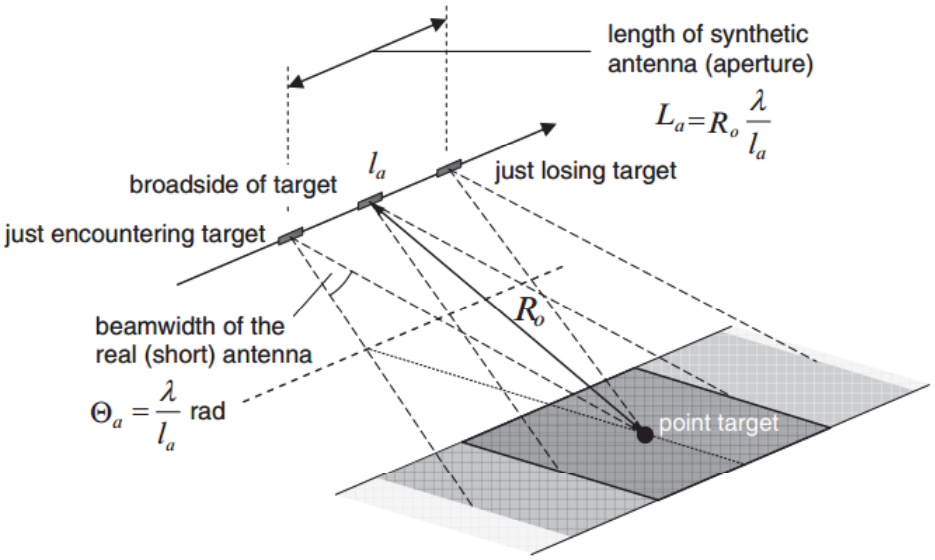

Fig. 2-3 The Synthetic Aperture Radar concept (Richards, 2009)

The microwave bands that usually used for SAR system are X, C, L, and P band. The ALOS PALSAR uses the L-band wavelength (~23 cm), Radarsat and ENVISAT use the C-band (5.6 cm) and X-band (3 cm) used by TerraSAR-X. Besides the wavelength, there are four common modes in SAR acquisition such as scan, stripmap, spotlight and inverse SAR (Patel et al., 2010). The characteristic of SAR is defined by using the orientation of transmitted and received pulses. The orientation of SAR is divided into horizontal (H) and vertical (V) directions. The combination between transmit and receive microwaves made four variations such as HH, HV,

VH, and VV which called as polarization. The first letter indicates the transmitted orientation and the second letter indicates the received orientation.

One of SAR system is ALOS PALSAR, a Japanese satellite which launched in 2006. The ALOS satellite stands for Advanced Land Observing Satellite (ALOS), meanwhile the PALSAR or Phased Array type L-band Synthetic Aperture Radar is one of three sensors and the only one sensor with microwave which carried by ALOS. There are several acquisition modes from ALOS PALSAR, fine beam mode, scanSAR, and the polarimetric mode. The fine beam mode can be divided into two according to the polarizations, the fine beam single (FBS) and fine beam dual (FBD). The FBS consists of HH or VV polarizations meanwhile the FBD consists of HH, HV or VV, VH polarizations. The ScanSAR mode is observing wide area with HH or VV polarizations.

The polarimetric mode consists of four polarizations data, the HH, HV, VH, and VV polarizations and often said as quad-polarizations (Quad-pol) data or full polarizations data. The ALOS-PALSAR ended its services on May 2011 after five years of exploration. The next generation of ALOS-PALSAR is ALOS-2/PALSAR-2 which was launched on May 2014. It has higher spatial resolution as well as higher temporal resolution.ALOS-2/PALSAR-2 has revisit time around 14 days. It is higher than previous ALOS/PALSAR with 46 days of revisit time. Besides the L-band wavelength, the other C-band wavelength named Sentinel-1 is used in this study. The Sentinel-1 SAR has higher temporal resolution than ALOS/PALSAR and ALOS2/PALSAR2 with 12 days repeat times. Similar to the ALOS/PALSAR, the Sentinel-1 provides the HH, HV, VH and VV polarization. The dual polarization of VH and VV will be used in this study.

Chapter 3
Application of ALOS PALSAR data for agriculture croplands classification in Central Java, Indonesia

3.1 Introduction

A tropical climate is beneficial for agriculture since it provides adequate sunlight and rainfall throughout the year. Indonesia, as one of the developing countries in Southeast Asia with a tropical environment, still depends on agriculture as a source of national income. The Indonesian statistics from 2010–2014 (Badan Pusat Statistik, 2015) indicate that the agricultural sectors contribute around 13.38% of the country's gross domestic product. These sectors are beneficial in terms of providing food resources and a large number of jobs for the country's rural inhabitants, especially in the most populated area in Indonesia, Java Island. Agriculture is also concentrated in Java due to its environmental conditions (Wahyunto et al. 2012) and demand for food consumption (Lavigne et al. 2008).

Java has various mountainous topographic conditions, including many active volcanoes that provide levels of elevation and fertile soil that are suitable for cultivating different crops. The decreasing flat area availability leads the agricultural fields to be small in scale and irregular shape to fit the hilly topography part. Intercropping systems are common in the upland fields, where cassava is cultivated along with other subsidiary crops; such as chili and vegetables. The topographic conditions and the intercropping system increase the complexity of the agricultural croplands in Java. These complex agricultural croplands in Java therefore require statistical as well as spatial analysis, when attempting to understand and monitor agricultural conditions.

Remote sensing technology can provide both spatial and statistical information regarding agricultural activities. Researchers endeavored to use remote sensing technology to monitor and map agricultural croplands in different areas, both spatially and temporally. These previous studies included optical sensor remote sensing for mapping and monitoring of paddy fields (Dong et al. 2015), crop identification (Serra and Pons 2008, Peña-Barragán et al. 2011), crop area estimation (Gallego et al. 2014), and vegetation index calculation for crop conditions (Yang et al. 2011). Optical remote sensing has also been widely used in Java for paddy monitoring (Uchida 2010, Xiao et al. 2005), monitoring of farmland loss (Partoyo and Shrestha 2013), and mapping of vegetable fields (Wikantika et al. 2002). Optical remote sensing has been confirmed as suitable for agricultural monitoring applications. However, the cloud cover in tropical areas limits the use of optical remote sensing. The synthetic aperture radar (SAR) system represents a reliable way to overcome this cloud problem.

Radar-based remote sensing, or SAR, is an active sensor system that transmits and receives microwaves

from an object, and is therefore independent of weather conditions. Previous studies have shown that the SAR system has potential for use with agricultural targets (Ferrazzoli 2002, Frate et al. 2003) in particular, the advantages of L-band are highly rated for crop and tree classification and crop mapping (Lee et al. 2001, Tian et al. 2010). ALOS PALSAR, as a SAR satellite with L-band wavelength, has also been used for crop classification, paddy identification, and crop extent estimation purposes (Zhang et al. 2011, Milisavljevic et al. 2012, Haldar et al. 2012) and is viewed as being capable of delivering sufficient and promising results in agricultural applications. However, the use of ALOS PALSAR has seldom been attempted in Java, where the land use/land cover is extremely complicated, or its use has been limited to the identification of paddy field areas (Shofiyati et al. 2011). Thus, ALOS PALSAR data are still interesting and have potential for use in agricultural croplands discrimination in Java. In this study, ALOS PALSAR data was applied to classify the land use/land cover in complex agricultural croplands in Central Java, Indonesia.

3.2 Study area and Data

3.2.1 Study area

The study area is located on an agriculture area in Central Java province, Indonesia, conterminous between the Klaten and Boyolali districts (Fig. 3-1). The area is around 50 km^2 within the geographic coordinates of $7^o32'55''$ - $7^o36'42''$ latitude south and $110^o32'39''$ - $110^o36'31''$ longitude east. The topographic location is on the eastern slopes of the Merapi, which is one of the most active volcanos in Indonesia.

The agriculture croplands in this area contain different sizes of field with various types of crops that make for quite a heterogeneous agricultural landscape. Four land cover classes are defined according to the condition of this study area, namely settlement, dry fields, mixed garden crops, and paddy fields. The settlement consists of land covered by small houses with yards, home gardens, or other artificial facilities. The dry fields are an agricultural area which is mostly located on the upper part of a slope with elevation around 500 to 600 meters. Some dry fields have also been identified inside the paddy field area.

The dry fields consist of various crop fields, such as maize, papaya, cassava, tobacco, and vegetables. Meanwhile mixed garden crops can be found in the northern and southern parts of the study area and at the same elevation as the dry fields. The cool temperature is the reason farmers mostly grow vegetables and tuberous roots (cassava) in this area. The main difference between mixed garden crops and dry fields is that the former are surrounded by dense perennial crops; while the latter are wide open without a canopy from other trees. The paddy fields are widely distributed in the lower part of the mountain slope with an elevation lower than 350 meters.

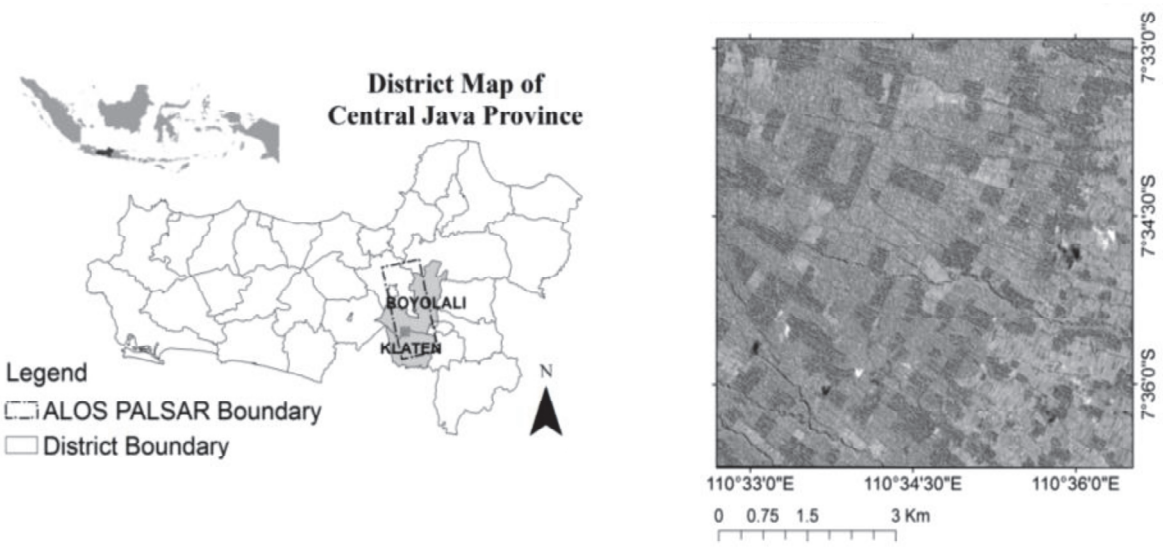

Fig. 3-1 Study area with the boundary of ALOS PALSAR data, and preview of WorldView-1 image

3.2.2 Data

PALSAR is an active microwave sensor system which is mounted on the ALOS satellite (DAICHI) operated by the Japan Aerospace Exploration Agency (JAXA). The sensor uses L-band wavelength with 1.27 GHz frequency and 23.6 cm wavelength, which gives PALSAR the ability to penetrate deeper into vegetated areas (Sandwell et al. 2008). We used ALOS PALSAR, full polarization mode taken on 9 April 2010 with a 21.5^{o} nadir angle (level 1.1). The full polarization mode has four polarizations: HH, HV, VH, and VV. The two letters in each abbreviation indicate transmission direction and receive direction in the horizontal (H) and vertical (V), respectively.

Besides ALOS PALSAR data, Worldview-1 satellite data with very high spatial resolution (0.5 m) was also used for the collection of training samples as well as the accuracy assessment. Worldview-1 image was acquired on 24 July 2010 and has minimal cloud cover and shadows. In addition, a field survey was conducted in August 2015 as complementary data collection for land use/cover conditions.

3.3 Methodology

3.3.1 Backscatter conversion process conversion

In general, the data processing consists of two main processes, backscatter intensity conversion and polarimetric decomposition. First, the Single Look Complex (SLC) of the full polarization mode data has to be converted into backscatter intensity in decibel unit (dB). The conversion process is done by using open-source software, Next ESA (European Space Agency) SAR Toolbox (NEST). This conversion is divided into four phases, namely multi-look, filtering, backscatter intensity conversion, and geocoding.

The multi-look factor for the range and azimuth of full polarization mode is 1 x 7 (Santoro et al. 2009). The speckle noise in data was reduced by using the Lee filter with a window size of 5. Then, the conversion of DN

into backscatter intensity is done based on the following formula (Shimada et al. 2009):

$$\sigma^0 = 10 \times \log_{10}\left[I^2 + Q^2\right] + \mathrm{CF} - 32 \qquad \text{(Eq. 3-1)}$$

where σ^o is the backscatter intensity in decibel unit, I and Q is the real and imaginary part of SLC, CF is the factor calibration is -83, the conversion factor A is 32.0 for the ALOS PALSAR 1.1 product.

The process of geocoding and topographic correction are performed using the digital elevation model (DEM) from ASTER GDEM with the Universal Transverse Mercator (UTM) zone 49 south projection, and WGS 1984 as datum projection and nearest neighbor interpolation.

Four basic operations of arithmetic such as add, subtract, multiply, and divide were employed to extract new parameters, after obtaining the backscatter intensity. This method was often applied to the SAR data for land use and land cover classification (Lonnqvist et al. 2010, Mishra et al. 2011, Zhang et al. 2011). The backscatter intensity is largely depends on the material and structure of the targets. Therefore, additional parameters that extracted from arithmetic operations are important to increase the probability of useful parameters for discriminating the agricultural fields.

In addition to the arithmetic operations, we also calculated the Normalized Difference Polarization Index (NDPI) for the backscatter intensity, which is written as follows (Mishra and Singh, 2011):

$$\mathbf{NDPI} = \frac{\sigma^o_{VV} - \sigma^o_{HH}}{\sigma^o_{VV} + \sigma^o_{HH}} \qquad \text{(Eq. 3-2)}$$

where σ^o is the backscatter intensity of VV and HH polarizations in linear units. The NDPI parameter is useful for interpreting the surface object roughness. In this study, there are two kinds of modified NDPI formulas, NDPI_H, which uses horizontal transmission (HH-HV/HH+HV), and NDPI_V, which uses vertical transmission (VV-VH/VV+VH), both in linear units.

3.3.2 Polarimetric decomposition

The polarimetric scattering mechanisms are also useful for discriminating objects besides the backscatter intensity (Adams et al. 2013). The polarimetric scattering mechanisms can be modeled by using polarimetric decomposition. In this study, incoherent decompositions, which are based on coherency and covariance matrix modeling such as Freeman and Durden polarimetric decomposition (Freeman and Durden 1998) and Yamaguchi 4 component polarimetric decomposition (Yamaguchi et al. 2005), were used.

Freeman and Durden decomposition (FD) is a model for fitting simple backscatter mechanisms of polarimetric SAR data by using three scattering components: volume scattering, odd bounce scattering, and double bounce scattering. This polarimetric decomposition has been proved to match very well with datasets obtained in tropical rain forest sites that contain a variety of land cover types (Freeman and Durden 1998). The FD is devised for modeling the scattering mechanism without ground truth; however, this decomposition will be used for maximum likelihood classification based on known points as ground truth.

The Yamaguchi 4 components (Y4) have four types of scattering: odd scattering, volume scattering, double bounce scattering, and helix scattering (Yamaguchi et al. 2005). In the study area, various artificial objects are mixed with the agricultural croplands, thus Y4 is used to examine whether this polarimetric decomposition is able to differentiate the agricultural croplands from the settlement area.

The FD and Y4 are generated by using POLSARPro (Polarimetric SAR Data Processing and Educational Tool) software with processing as follows: multi-look with 1:7 for range and azimuth, filter process by using Lee Sigma filter with window size of 5; and polarimetric decomposition generation with matrix coherence as the input. The geocode process uses open source software, ASF Mapready version 3.1 with similar parameters set in the backscatter geocode process.

3.3.3 Maximum likelihood classification

Maximum likelihood classification (MLC), a supervised classification method, was applied for discriminating four land cover classes. Those classes consist of settlement, paddy field, dry fields, and mixed garden crops. Supervised classification requires training samples for each category. In this study, the training samples were derived from visual interpretation of the Worldview-1 image. The training samples consist of 25 polygons (1036 pixels) for the settlement class, 18 polygons (355 pixels) for the paddy class, 37 polygons (954 pixels) for the dry fields class, and 25 polygons (985 pixels) for the mixed garden crops class. Accuracy assessment is employed with 784 points which are derived from 250m mesh grid on the WorldView-1 image.

3.4 Results and discussion

3.4.1 Backscatter intensity classification

Thirty-three new parameters were extracted from the combination of four polarizations, consist of 12 parameters from the add and subtract operation, 6 parameters from the multiply operation, 12 parameters from the divide operation, and 3 parameters of NDPI, NDPI_V, and NDPI _H. The thirty-three parameters and the four backscatter intensity (HH, HV, VH, VV) can be combined to generate around 77 data. However, generating 77 data are time-consuming process and ineffective method. Therefore, the four backscatter intensities (HH, HV, VH, VV) classification was performed to obtain brief information as well as to be the standard of the classification results.

The HH, HV, VH, VV classification (Fig. 3-2(a)) yielded 67.09% overall accuracy (OA) and kappa coefficient (KC) 0.523. The misclassifications were found between the dry field class and the paddy or mixed garden crops class, and between the settlement class and the mixed garden crops class. Regarding these findings, the separability index will be applied to obtain the useful parameters for separating the classes.

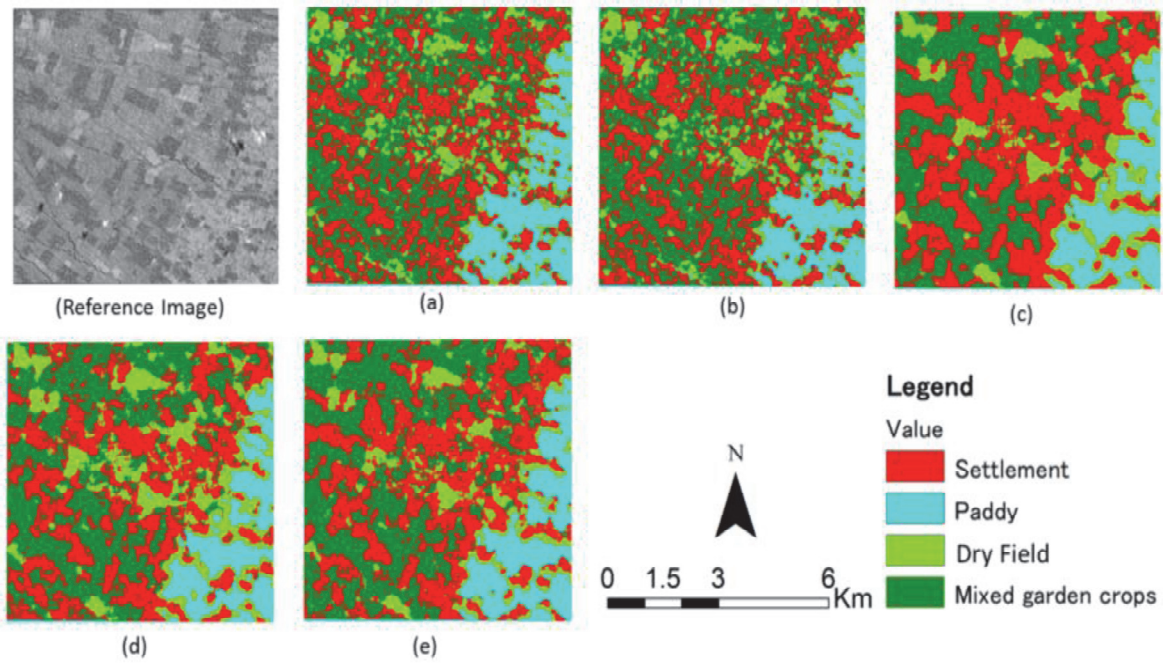

Fig. 3-2 Classification result of (a) HH, HV, VH, VV, (b) VH,VV,HH+HV, (c) Freeman and Durden decomposition, (d) Yamaguchi 4 component decomposition, and (e) the integration of HH,HV,VH,VV,FD,HH+HV

The separability index (SI) is the ratio of the subtraction of average pixel value to total standard deviations, between class A and class B in absolute value (Wu et al. 2011). In this study, the SI is calculated based on pixels value within the polygons of training samples. The SI value should be above 0.8 to be categorized as a useful parameter for separating the two classes (Wu et al. 2011). There are four kinds of separability indices tested in this study, namely dry field and settlement (D-S), dry field and paddy field (D-P), dry field and mixed garden crops (D-M), and settlement and mixed garden crops (S-M). Fig. 3-3 shows the trend of SI from ten selected parameters with the highest average of four SI value.

Overall, the separability index of S-M is below 0.8 and is the lowest average compared to the other SI value. It implies that the settlement class and the mixed garden crops class have similar backscattering characteristics. However the NDPI_V and VV-VH parameters presented the possibility of separating settlement and mixed garden crops with SI value for S-M 0.75 and 0.73 respectively; but could not separate the dry field and paddy. Ten selected parameters and HH, HV, VH, VV were combined to generate twenty data combinations. The combinations consist of three and five layers compositions. The three layers composition data produced from two backscatter intensity and one parameter. Meanwhile, the five layers composition data produced from four backscatter intensity and one parameter.

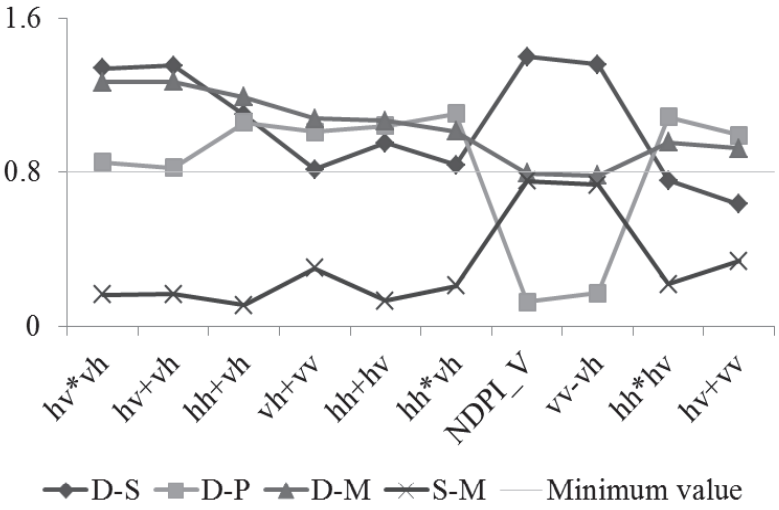

Fig. 3-3 Separability index value of D-S, D-P, D-M, S-M, from 10 selected parameters

Table 3-1 Combinations of backscatter intensity

No.	Polarization compositions	OA (%)	KC	No.	Polarization compositions	OA (%)	KC
1	HH,HV,**VH+VV**	60.84	0.441	11	HH,HV,VH,VV, **HH*HV**	66.45	0.508
2	HH,HV,VH,VV, **VH+VV**	64.67	0.469	12	HH,HV,**VV-VH**	66.58	0.514
3	HV,VV,**HH*VH**	65.18	0.495	13	HH,HV,VH,VV, **HV*VH**	66.58	0.512
4	HHVH,**HV+VV**	65.18	0.495	14	HH,HV,VH,VV	67.09	0.523
5	HH,HV,VH,VV, **NDPI_V**	65.43	0.503	15	HH,VV,**HV+VH**	67.35	0.527
6	HH,HV,**NDPI_V**	65.56	0.502	16	HH,HV,VH,VV, **HH+HV**	67.35	0.524
7	HV,VV,**HH+VH**	66.07	0.508	17	HH,VV,**HV*VH**	67.47	0.528
8	HH,HV,VH,VV, **HH*VH**	66.07	0.5	18	HH,HV,VH,VV, **HH+VH**	67.86	0.531
9	HH,HV,VH,VV, **HV+VH**	66.2	0.507	19	VH,VV, **HH*HV**	68.11	0.537
10	HH,HV,VH,VV, **VV-VH**	66.45	0.518	20	VH,VV,**HH+HV**	68.62	0.546

OA: Overall accuracy; KC: Kappa Coefficient

Table 3-1 shows the configuration of 20 combinations along with the OA and kappa coefficient achieved from the MLC process. The HH+HV parameter has the lowest standard deviation for separability index of D-S, D-P, and D-M (0.060) compared to other parameters. The low standard deviation means that the data are

reliable. Therefore, in the Table 3-1, the combination with HH+HV parameter consistently presented higher accuracy than the classification result of HH, HV, VH and VV. The VH, VV, and HH+HV combination emphasized that HH+HV is useful parameter for separating the D-S, D-P, and D-M, and important for increasing the classification accuracy. Classification results of VH, VV, and HH+HV can be seen in Fig. 3-2(b).

3.4.2 Polarimetric decomposition classification

The classification based on Freeman and Durden ((Fig. 3-2 (c)) and Yamaguchi 4-component polarimetric decomposition ((Fig. 3-2 (d)) delivered better OA and KC than the full polarization backscatter classification. The FD yielded overall accuracy and kappa coefficient 68.49% and 0.533, meanwhile the Yamaguchi 4-component yielded 67.47% and 0.533. The additional helix of the Y4 was not able to distinguish the settlement area or building objects from the agricultural classes (paddy, dry fields, mixed garden crops) very well. The perennial crops border or inside the settlement area are considered to influence the ability of helix components. However, if the helix component is excluded from the classification, the result is insignificantly improved (67.86% and 0.538).

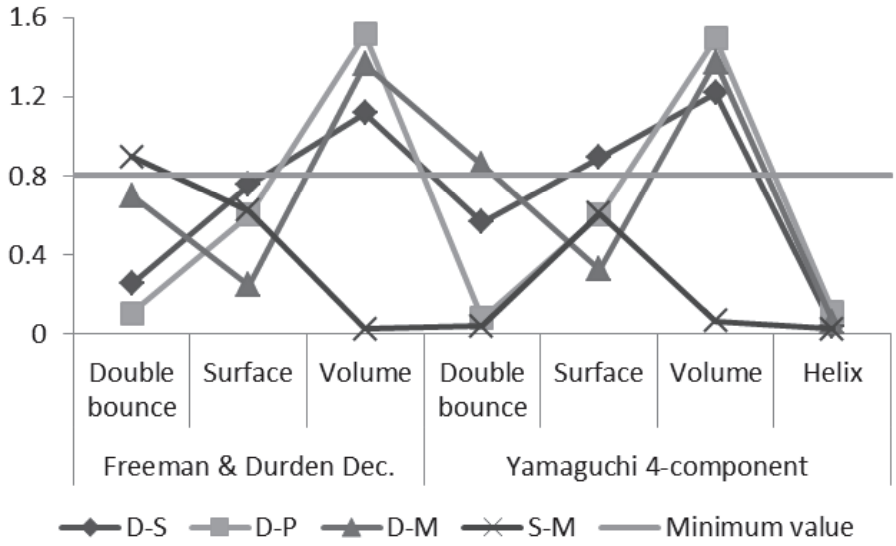

Fig. 3-4 Separability index value of D-S, D-P, D-M, and S-M from Freeman & Durden decomposition and Yamaguchi-4 component decomposition

By using the SI method, the double bounce scattering mechanism of FD is identified as having the capability to discriminate between the settlement and mixed garden crops, but being incapable of separating the dry fields from the other classes (Fig. 3-4). The double bounce scattering of the settlement area is related to the scatter interaction between the ground and the walls of the houses or the interaction on the roof. Meanwhile, the double bounce of the mixed garden crops areas is related to the scattering interaction between trees and short-crop

vegetation. The main difference is the double bounce scattering of the settlement area is more stable than the double bounce scattering of the mixed garden crops area. In contrast, volume scattering is an important component for discriminating the types of agricultural fields. This is because the morphology of vegetation of paddy, dry fields, and mixed garden crops reflects different canopy layer scatter mechanisms. In this study, the mixed garden crops class has the most volume scattering and the paddy field class has the least volume scattering.

3.4.3 Integrated classification of backscatter and polarimetric decomposition

From the previous results, the backscatter intensities and polarimetric decomposition were found to be useful for discriminating agricultural objects. In this study, we explored backscatter intensity and polarimetric decomposition integration for agricultural croplands classification as well, because this kind of integration has rarely been performed. Five integrations between backscatter intensity and polarimetric decomposition were generated and classified (Fig. 3-2(e)). The overall accuracy and kappa coefficient for these data integrations can be seen in Fig. 3-5.

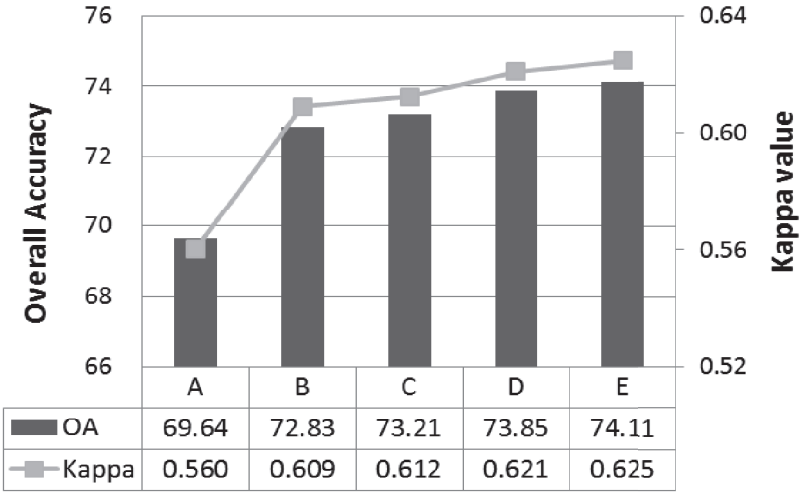

	A	B	C	D	E
OA	69.64	72.83	73.21	73.85	74.11
Kappa	0.560	0.609	0.612	0.621	0.625

Fig. 3-5 The integration of backscatter and polarimetric decomposition classification results: (a) HH+HV,FD, (b) HH,HV,VH,VV,FD,Y4, (c) VH,VV,HH+HV,FD, (d) HH,HV,VH,VV,FD, (e) HH,HV,VH,VV, HH+HV, FD

The integration between HH+HV and FD consisted only of 4 layers and yielded slightly higher accuracy than the HH, HV, VH,VV classification, which is also consisted of four bands. The MLC calculated the mean and standard deviation from the training samples and applied the probability density function before assigning a class to each pixel (Mishra et al. 2011). The integration of VH, VV, HH+HV, and FD also show higher accuracy (73.21%) compared to the VH, VV and HH+HV with 68.62% accuracy. Therefore, the integration of HH+HV and FD gave better distribution for classification than only backscatter intensity.

Table 3-2 Accuracy assessment of HH, HV, VH, VV, HH+HV, and Freeman & Durden decomposition

Class	Producer's accuracy (%)	User's accuracy (%)
Settlement	78.87	70.61
Paddy	91.46	70.75
Dry field	58.49	60.78
Mixed garden crops	70.99	83.93
Overall Accuracy and Kappa coefficient : 74.11% and 0.625		

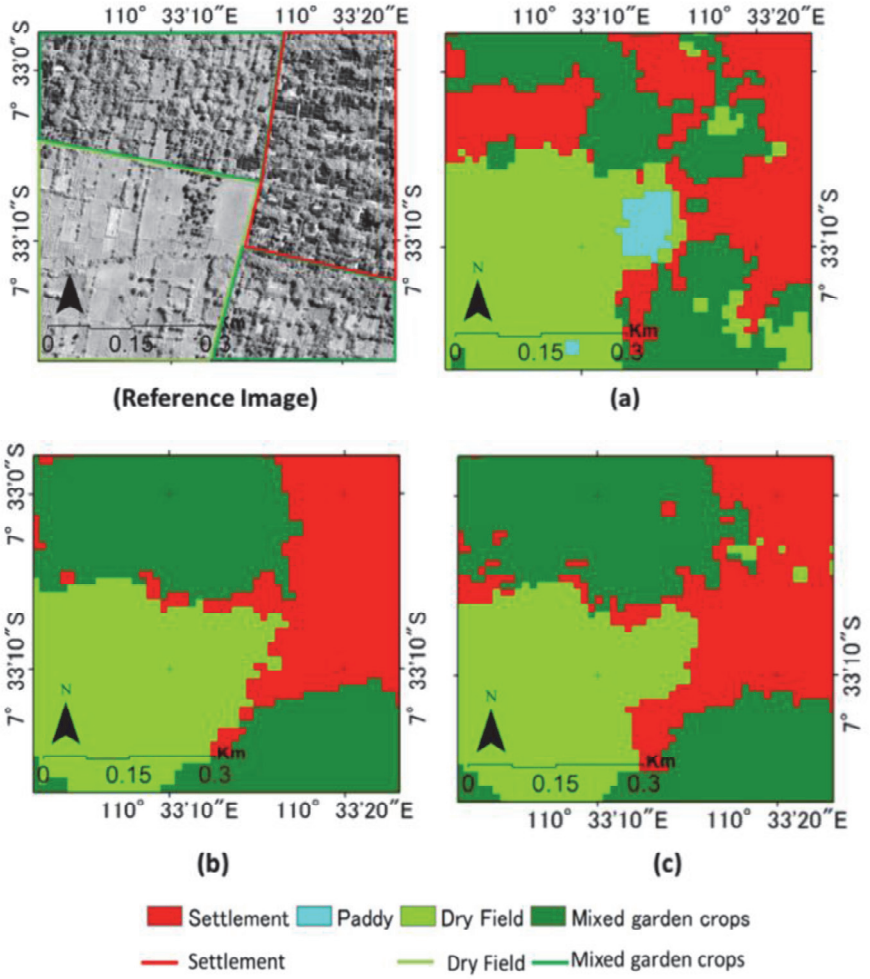

Fig. 3-6 Comparison of agricultural croplands classification by using (a) VH,VV,HH+HV, (b) FD polarimetric decomposition and (c) the integration of HH,HV,VH,VV, HH+HV and FD.

Moreover, by applying the HH, HV, VH, VV, HH+HV, and FD; the OA and KC of the classification result (Fig. 3-5 (e)) was significantly increased (74.11%, 0.6247). The Table 3-2 shows the accuracy assessment of the integration classification result. This finding proved that discriminating complex agricultural croplands can

be done by using full polarization mode of ALOS PALSAR.The good classification results of integrating the backscatter intensity (HH, HV, VH, VV), HH+HV, and FD can be explained by two factors. First, the polarimetric decomposition components were able to complement the interpretation of natural scattering characteristic that the backscatter intensity could not provide. Second, the HH+HV parameter made a valuable contribution to generating a good backscatter intensity distribution of the maximum likelihood classifier for separating the four classes.

Fig. 3-6 presents a comparison of agricultural area classification by using (a) VH, VV, and the HH+HV, (b) FD polarimetric decomposition, and (c) the integration of HH, HV, HV, VV, HH+HV and FD. The Fig. 3-6 (a) shows that the backscatter intensities are sensitive to the water condition in the agriculture area, therefore the dry field area is classified as paddy field, due to low backscatter intensity in dry field area. The backscatter intensity is unable to separate the mixed garden crops with settlement area. In contrast, the polarimetric decomposition (Fig. 3-6 (b)) and the integration between HH, HV, VH, VV, HH+HV, and polarimetric decomposition (Fig. 3-6 (c)) is able to separate paddy and dry field and also the settlement and mixed garden crops.

3.5 Conclusions

Full polarization mode (HH, HV, VH, and VV) of ALOS PALSAR was examined for classification of agricultural croplands, and it was confirmed empirically as being beneficial for discriminating complex agricultural croplands such as in Central Java, Indonesia. Full polarization mode was also very useful for generating parameters and for generating polarimetric decompositions. Calculation of the separability index allowed evaluation of the HH+HV as the most useful and suitable parameter in this study. The Freeman and Durden polarimetric decomposition model was identified to give higher accuracy in discriminating agricultural croplands when compared with the Yamaguchi 4 components.

Overall, the integration between backscatter intensities (HH, HV, VH, VV, and HH+HV) and the three components of the Freeman and Durden decomposition significantly improved the overall accuracy and kappa coefficient (74.11% and 0.6247, respectively). This fact implies that the integration of the backscatter intensity and polarimetric decomposition methods was able to compensate for the weakness of each component in discriminating complex agricultural croplands. This study introduces a preliminary method for discriminating agricultural croplands using ALOS PALSAR data. We believe that the methodology of PALSAR data integration established in this study can be also applied using ALOS PALSAR-2 data.

Chapter 4
Application of Sentinel-1 data for classifying croplands using Google Earth Engine

4.1 Introduction

The agricultural sector is important for the Indonesian economy. According to the Indonesian statistics, the agricultural sectors contributed approximately 9.9% of Indonesia's gross domestic product in 2017. Many people living in rural areas depend on agricultural activities for their main source of income. One of the prominent agricultural areas on Java Island is found in the upper Solo basin of the Central Java Province. This area has rich and fertile soil with enough water discharge to make agricultural activities viable. However, the dense populations of Java and its uneven road structure force the agricultural fields to be small in size and complex in shape. The agricultural parcels size in Indonesia is around 0.3 Ha per household (Agus and Manikmas 2003). Most of the farmers in this area manage and cultivate croplands depending on the meteorological and topographic conditions. It is common to have paddy fields in flat areas and upland fields in hilly areas. Paddy is the main crop for this agricultural sector as it is consumed by the majority of Indonesian people and requires an abundant amount of water in the early stage of cultivation, which is complemented by the heavy rainfalls. Beyond rainfall, the water for paddy cultivation is also sourced through irrigation. The intercropping method is often practiced to increase the farmers' income. Therefore, it is common to find different cropping patterns in these agricultural fields throughout the year.

The Indonesian government has monitored agricultural croplands using direct field survey and remote sensing technology. A direct field survey is time consuming and requires surveyors. Satellite remote sensing consists of optical sensor data and synthetic aperture radar (SAR) data and provides wide range spatial and temporal data. Optical remote sensing is susceptible to the atmospheric conditions, especially during the tropical monsoon season. The SAR satellite offers active remote sensing is capable to penetrate the atmospheric conditions and provides cloud cover free data.

Recently, satellite remote sensing data has drastically improved in terms of temporal and spatial resolution used to produce the large satellite images. Developing countries or communities with limited budgets could have difficulty accessing these satellite images. However, the advanced technology of cloud-based computing provides an efficient and low cost alternative for processing these images. The Google Earth Engine (GEE) is one of the cloud-based geospatial platforms that provides numerous collections of geospatial datasets and algorithms to process the satellite images. It offers flexibility to the users for conducting research related to satellite images and geospatial data. Users are able to process these datasets as long as an internet connection is available. In recent years, GEE has been used for many remote sensing applications, such as land cover change

(Sidhu et al. 2018), cropland mapping (Xiong et al. 2017), and crop classification analysis using huge amounts of multi-temporal data, (Shelestov et al. 2017) because of its simplicity and user friendly interface.

There are several types of SAR wavelengths used in microwave remote sensing, such as X-band (2.5–4 cm), C-band (4–8 cm), and L-band (15–30 cm). Besides penetration through cloud, the SAR images could detect the moisture condition as well as the canopy or surface structure. Therefore, SAR data is advantageous for monitoring agriculture even in tropical areas (Nelson et al. 2014). One of the SAR satellite images provided by GEE is the C-band SAR of Sentinel-1. The C-band wavelength is shorter than the L-band wavelength, and the C-band wavelength could not penetrate deeper than the L-band wavelength. Sentinel-1 data has been applied in several studies for hydrological dynamic in wetland area (Cazals et al. 2016) as well as for agricultural applications, such as mapping rice planted areas (Clauss et al. 2017; Tian et al. 2018), temporal behavior of crops (Veloso et al. 2017), and rice growth monitoring (Torbick et al. 2017).

The L-band SAR, ALOS/PALSAR, is often used for agricultural cropland classification, such as paddy field identification (Zhang et al. 2011), and the classification of abandoned paddy fields (Yusoff et al. 2016). The L-band SAR, ALOS/PALSAR-2, is used for classifying agricultural croplands (Mirelva & Nagasawa, 2018). However, the L-band SAR has a longer revisit time than the C-band SAR. This creates the need to consider the agricultural fields' cropping patterns before selecting the satellite images to fit the cropping pattern of agricultural fields. Sentinel-1 offers high temporal images that are useful for understanding the cropping pattern, especially in complex agriculture croplands with uncertain cropping patterns.

Recently, Ghazaryan et al. (2018) reported the effectiveness of Sentinel-1 and GEE for identifying the cereal cropping system in one of regions in continental Europe. However, few studies have used Sentinel-1 and GEE in the Asian region, specifically the areas with a tropical monsoon climate. In the present study, the combination of Sentinel-1 data and GEE was implemented to identify small, mixed agricultural crop fields in the tropical Asian region. The complex agricultural cropland in the Central Java Province (an area of approximately 112 km2) was selected because of its irregular cropping patterns, various types of cropland, and the other surrounding land covers, such as woodland and settlement. This study aimed to understand the characteristics of Sentinel-1 when classifying two cropping patterns of paddy fields and other land use or land cover types, as well as the classification performed in GEE.

4.2 Materials and methods

4.2.1 Study Area

The study area is located on the southeastern slopes of the Merapi volcano in the Klaten Regency of Central Java in Indonesia. The area is in the boundary of the following coordinates: 7º 37' 10.7"-7º 42' 56.8" South Latitude and 110º 29' 31.89"- 110º 35' 17.02" East Longitude. The study area coverage appears as a red square on the map and the Pleiades image, taken in 2015, was used for information on the land use and the

land cover in the study area as can be seen in Fig. 4-1. The altitude varies from 200-600 meters above sea level.

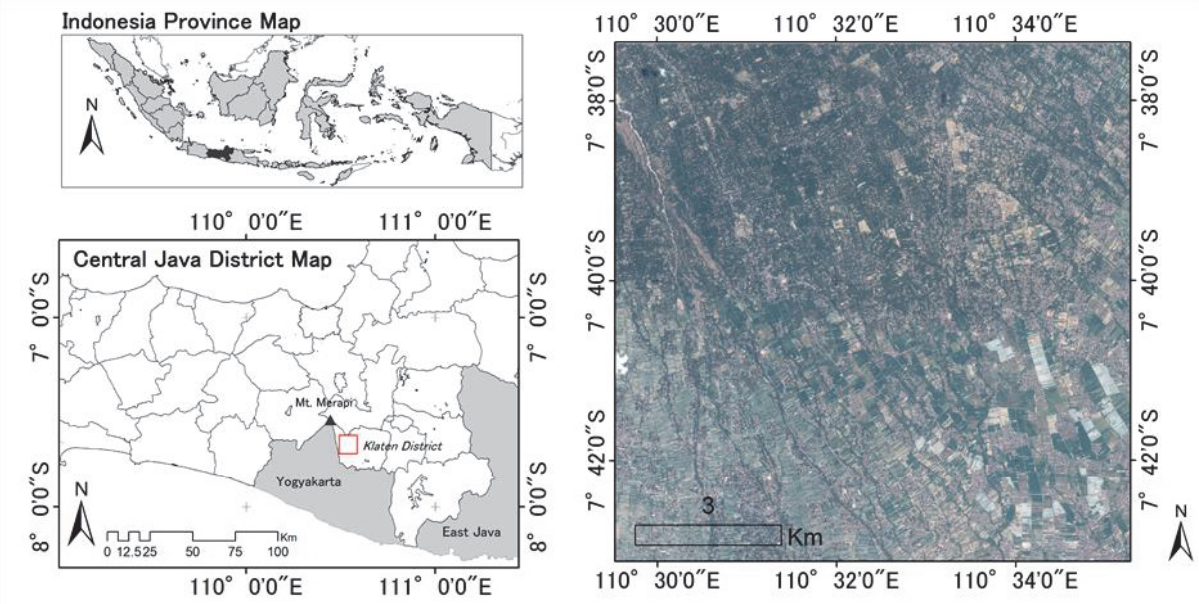

Fig. 4-1 Study area coverage with Pleiades image taken on 2015

The Merapi volcano is one of the most active volcanoes on the island of Java. Therefore, the soil is nutrient-rich which is beneficial for agricultural activities. Most people who live in this area work as farmers or sharecroppers and depend on agricultural production for their livelihood. In general, land usage can be divided into northern and southern sections. The northern area has a higher altitude and is mainly covered by settlement, woodland, and upland fields. The southern area is relatively flat and is generally covered by settlement and agricultural fields, such as paddy and tobacco fields.

4.2.2 Datasets

The study materials consisted of 56 satellite images of dual polarization of C-band SAR Sentinel-1 taken in 2017, the 49 satellite optical images of Sentinel-2 collected in 2017 and the Pleiades image taken on August 26, 2015. Only the Sentinel-1 and Sentinel-2 were acquired from the GEE data collection. Sentinel-1 has two polarization types, VH and VV polarization. VH polarization transmits microwaves in a vertical direction and receives scatter from the surface in a horizontal direction. VV polarization transmits and receives the microwaves in a vertical direction. The Sentinel-1 and Sentinel-2 have a 10 meter resolution and the Pleiades image has 0.6 meter resolution. Table 4-1 shows the availability of acquisition dates for both Sentinel-1 and Sentinel-2.

Table 4-1 Sentinel-1 and Sentinel-2 acquisition date

	Date of acquisition			Date of acquisition	
Month	Sentinel-1	Sentinel-2	Month	Sentinel-1	Sentinel-2
January	3, 27	9, 19, 29	July	2, 6, 14, 18, 26, 30	13, 18, 28
February	8, 20, 24	8, 18, 28	August	7, 11, 19, 23, 31	2, 7, 12, 17, 22, 27
March	4, 8, 16, 20, 28	10, 20	September	4,12, 16, 24, 28	1, 6, 11, 16, 21
April	1, 9, 13, 21, 25	9, 19, 29	October	6, 10, 18, 22, 30	1, 6, 11, 21, 26, 31
May	3, 7, 15, 19, 27, 31	9, 19, 29	November	3, 11, 15, 23, 27	5, 10, 15, 20, 25, 30
June	8, 12, 20, 24	8, 18, 28	December	5, 9, 17, 21, 29	5,10, 15,20, 25, 30

4.2.3 Methodology

The methodology can be separated into two parts, pre-processing and the classification process. The Sentinel-1 was downloaded and processed in GEE, except for the speckle noise filtering process which was processed in Sentinel Application Platform (SNAP) software (SNAP software). The classification process was done in GEE by using the random forest classifier. The methodology details are described in the following sections and the framework of methodology can be found in Fig. 4-2.

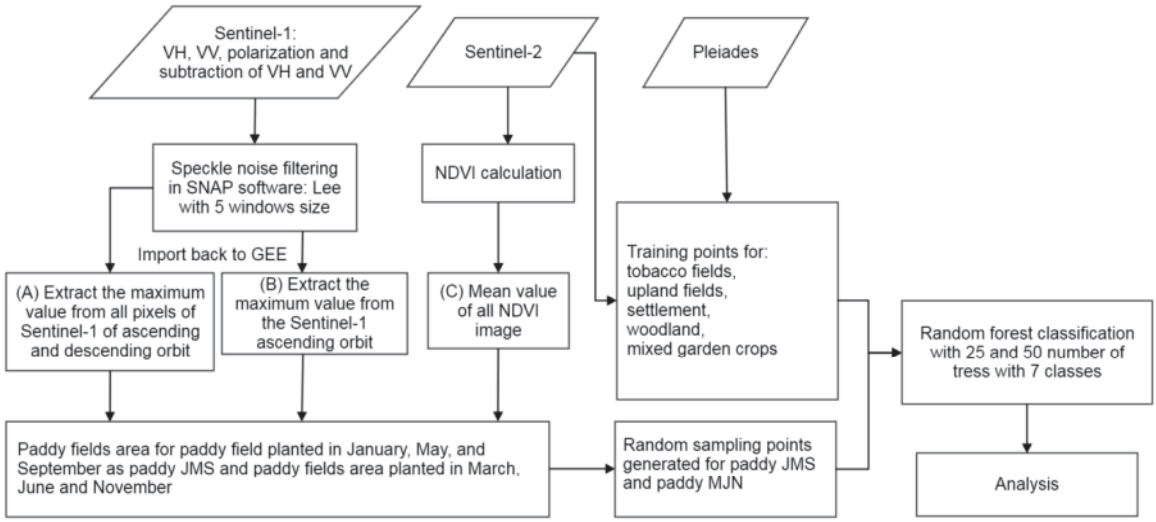

Fig. 4-2 Overall framework for cropland classifying in GEE

4.2.3.1 Data pre-processing

GEE data collections provide satellite remote sensing data, including Sentinel data. The Sentinel-1 data used SAR system which capable to penetrate cloud coverage. In addition, it has high temporal data which is useful to be used for monitoring agricultural condition in Indonesia. In GEE, to get one year of data, the Sentinel-1 was filtered by setting a boundary area similar to the study area and the date range from January 1 to December 31, 2017. The Sentinel-1 data from GEE data collection was already pre-processed using the

Sentinel-1 Toolbox, a software for SAR satellite data processing from ESA (European Space Agency). The pre-processing steps are thermal noise removal, radiometric calibration, and terrain correction by using SRTM 30 or ASTER DEM. The ASTER DEM is used for the area located above 60 degrees of latitude, or when the SRTM is unavailable. Thus the SRTM was used in this study. However, the speckle noise reduction process was not yet performed because GEE has no algorithm to execute this process. The speckle noise reduction is important because the radar data is often affected by the coherent summation of the signals that scattered from ground (Saxena & Rathore 2013). Therefore, the speckle noise reduction in Sentinel-1 was processed outside the GEE environment by using the SNAP software.

In order to reduce the speckle noise using SNAP software, the data collection of Sentinel-1 was clipped using the boundary of the study area and downloaded from GEE to the user's local drive. Then, a Lee filter with a 5 window size was used to reduce the speckle noise in the study area. After the speckle noise reduction, the VH and VV polarizations images were stacked and re-uploaded to the GEE as an asset for the further process. Besides the Sentinel-1 data, the subtraction between VH and VV polarization (VH-VV) for each image were also calculated. The speckle noise process was applied to the subtraction of VH and VV polarization with similar steps.

Sentinel-2 images are often affected by clouds; therefore, the cloud removal process for Sentinel-2 was processed in GEE. In general, the cloud removal process consists of cloud and shadow removal. Cirrus clouds were removed by subtracting the bands in each image with the cirrus band or the tenth band of Sentinel-2. The cloud area with a greater thickness than cirrus was selected with the rule condition if the reflectance value in red band, green band, and blue band are greater than 1700. Meanwhile, the shadow was removed based on the calculation of green (B3), blue (B2), and red edge (B8A) bands. The area identified as a shadow if the red edge reflectance value is between 900 and 1800, and the division of blue and green band is greater than 1.2. These calculations were modified from the automatic cloud and shadow detection for optical satellite imagery (Parmes et al. 2017). Then, the normalized difference vegetation index (NDVI) was calculated from the ratio of the near infrared band (B8) and the red band (B4).

4.2.3.2 Classification process

The GEE provides several types of supervised and unsupervised classification algorithms. In this study, the supervised classification named "random forest" was chosen as the classifier. The random forest algorithm, in simple terms, can be defined as a forest made of several decision or predictor trees. Each tree depends on the value of the random sample independently, with equal distribution for the entire tree in the forest (Breiman, 2001). The study area is divided into classes named upland fields, paddy, tobacco fields, settlement, woodland, and mixed garden crops. The training and accuracy assessment points for settlement, woodland, upland fields and mixed garden crops classes were selected based on the Pleiades image, with the assumption that the land

use and land covers change of these classes was minimum and could be neglected. The class of tobacco fields was selected from the Sentinel-2 optical images. Meanwhile, the sample points and accuracy assessment points for the paddy fields were selected based on Sentinel-1 data.

The field survey conducted on August 2017 presented the paddy fields area in diverse stages. It was common to have some area in the early cultivation stage and the other area in the harvest stage. The steps for selecting the sample point for these paddy classes were as follows:

(1) The woodland in the northern area and settlement areas are masked out. The average NDVI of Sentinel-2 in 2017 is calculated and a value greater than 0.63 is used as a woodland mask. The settlement mask for the average value of NDVI is less than 0.38, and the average VV band is greater than -3.8 dB. On the other hand, the slope area is masked out with the value less than -9 dB from the maximum VV polarization in one year.

(2) The early stages for paddy fields, like transplanting, are crucial for detecting paddies using the SAR remote sensing, because this stage requires a lot of water. The 39 points from the transplanting stage during the field survey on August 2017 was selected for calculating the average value of the backscatter coefficient. Thus, in this study, the area identified as paddy if the backscatter coefficient of each image is between -31 to -17.4852 dB (from the average value calculation). This step changes images into Boolean data, with 0 as false and 1 as true (fulfill the rule conditions).

(3) Sentinel-1 images were divided into six groups according to the image acquisition month: January to February as (a), March to April as (b), May to June as (c), July to August as (d), September to October as (e), and November to December as (f). The total value was changed into Boolean values by applying a rule greater than 1 for the January to February group, and greater than 2 for the other groups. These rules are generated because the image acquisition in January and February are less than in other months.

(4) The paddy fields were often cultivated two or three times a year. Therefore, paddy fields were separated into two types, paddy planted in January, May, or September, and named Paddy-JMS, and paddy planted in March, July, and November, named Paddy-MJN class. The area with the value equaling 2 or 3 from the total of (a), (c), and (e) groups indicate Paddy-JMS, and the area with the value equaling 2 or 3 from the total of (b), (d) and (f) groups indicate Paddy-MJN. The value equaling 1 indicates that the area was rarely cultivated as paddy fields and more likely to contain other croplands, such as maize, cassava, or other vegetable crops. Therefore, the area equaling 1 was omitted.

(5) Following that, the images of the Paddy-JMS and Paddy-MJN area were converted into vector polygons. Both the vector polygons were used to generate 90 random points.

The classification was run in GEE with the proportion around 70% sample points and 30% accuracy assessment points for all classes, which is described on Table 4-2. The random forest classifier was set with two numbers of trees equal to 25 and 50. There are four sets combination of Sentinel-1 polarization images (VH and VV) and the VH-VV polarization used for classifications. Table 4-3 describes the detail of four sets of polarization combinations for the classification. Thus, there were eight classifications generated in this study.

Table 4-2 Detail description of sample and accuracy assessment points

Class Name	Sample points	Accuracy assessment points	Total Points
Upland fields	73	31	104
Paddy-JMS	62	28	90
Paddy-MJN	63	27	90
Tobacco fields	40	16	56
Woodland	70	28	98
Settlement	72	29	101
Mixed garden crops	65	27	92
Total Points	445	186	631

Table 4-3 Polarization combination for the classification process

Polarization Combination Name		Description of polarization combination	Number of images
25	50		
A_25	A_50	VH and VV polarization	112
B_25	B_50	VH, VV, subtraction of VH and VV	168
C_25	C_50	VH, VV, subtraction of VH and VV taken on January to February, May to June and September to October	75
D_25	D_50	VH, VV, subtraction of VH and VV taken on March to April, July to August and November to December	91

4.3 Results and Discussion

4.3.1 Sentinel-1 and Sentinel-2 data pre-processing

Fig. 4-3 shows the Sentinel-1 image before and after the speckle filtering process for an image taken on January 3, 2017. The RGB in Fig. 4-3 is set with VV, VH, and VH-VV polarizations band composite to analyze the effect of speckle filtering. The backscatter coefficient became lower and the salt-pepper noise was decreased after the speckle filtering process, as can be seen in Fig. 4-3(b). In addition, the boundary between northern and southern area became clearer compared to the image before the speckle filtering process. The VV, VH, and VH-VV polarizations band composite follows (Cazals et al. 2016). In (Cazals et al. 2016) study shown

that the VV, VH, and VH-VV polarization band composite capable to differentiate the flooded area with non-flooded area. In Fig. 4-3 (b), the dark blue color shows low backscatter coefficient and indicates areas with higher moisture conditions, such as from land irrigation or agricultural activities for paddy field cultivation.

The cloud cover in Sentinel-2 can be eliminated by the cloud removal method. However, pixel value content similar to spectral value characteristics were identified as clouds or shadows and masked out in this process. The shadow removal is more difficult than the cloud cover removal due to its similarity with the water area and dense vegetation. Even though there is no large water body in the study area, the shadow can still be found in some part of the study area. Due to the high percentage of cloud coverage in several Sentinel-2 images, the Sentinel-2 was reduced from 49 images to 20 images.

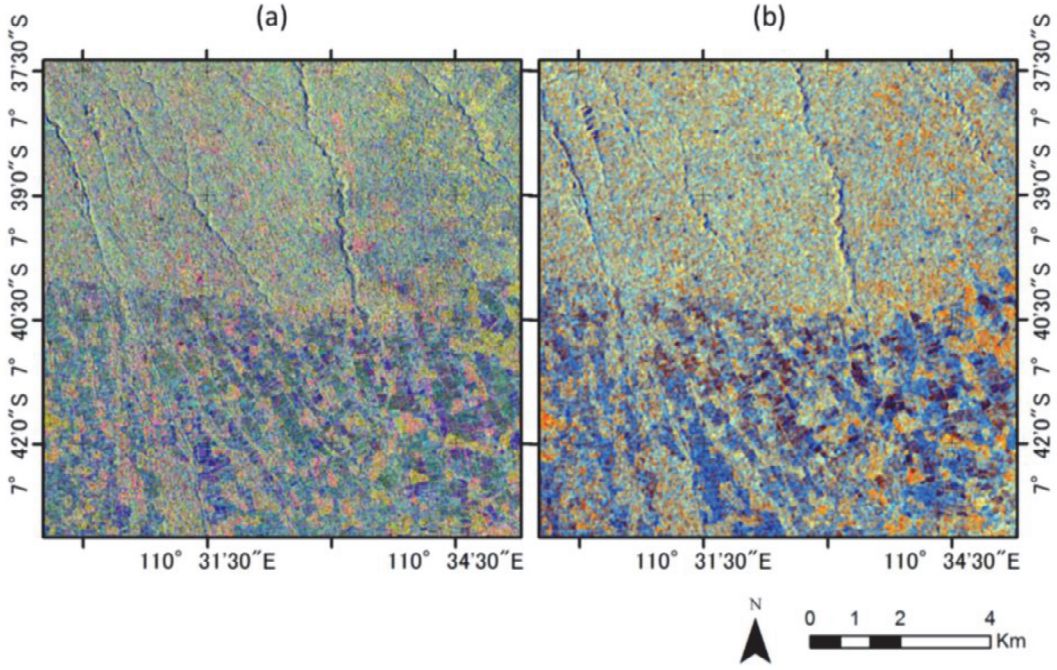

Fig. 4-3 The Sentinel-1 image taken on 3 January 2017, (a) before speckle filtering process and (b) after speckle filtering process

4.3.2 Paddy fields area identification

The pixel area coverage of Paddy-JMS and Paddy-MJN were calculated in GEE. The total area identified as Paddy-JMS and Paddy-MJN is approximately 415.83 Hectare and 548.78 Hectare, respectively. Fig. 4-4 shows the area identified as Paddy-JMS in magenta and Paddy-MJN in cyan. The majority of paddy fields are identified in the southern part of study area. However, some bare or open fields in the northern part are also identified as Paddy-JMS or Paddy-MJN. These areas often inundated during rainfall and cause the moisture conditions to be higher than their surroundings. The backscatter coefficient became low which was misidentified as paddy fields.

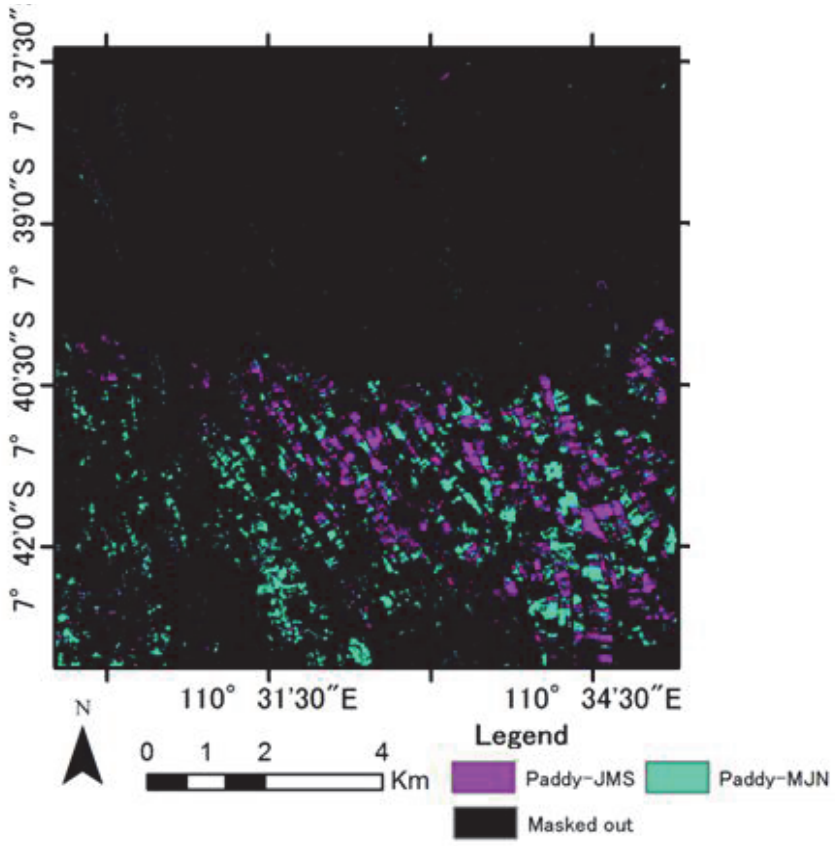

Fig. 4-4 The distribution of Paddy-JMS and Paddy-MJN identification

The average of temporal backscatter coefficient and NDVI from Paddy-JMS and Paddy-MJN areas were calculated in GEE, which are shown in Fig. 4-5. After cloud removal, there are five days that the Sentinel-1 and Sentinel-2 acquired the same satellite image: June 8, July 18, August 7, October 6, and December 5. In order to simplify the visual presentation of the graph in Fig. 4-5, only three dates were marked in black vertical lines. In general, the backscatter coefficient and NDVI value have similar temporal patterns.

The fluctuating patterns of the backscatter coefficient in Fig. 4-5 of Paddy-JMS occur from May to July. This phenomenon occurred because the Sentinel-1 images have two types of orbit modes—ascending and descending—that have different backscatter coefficients. The area identified as paddy fields has a low backscatter coefficient and NDVI value at the starting time of paddy cultivation for both cropping patterns. The low backscatter coefficient was influenced by the structure of the paddy growing stages. The backscatter coefficient is low during the preparation of paddy field cultivation. For the Paddy-JMS, cultivation occurs in January, from May to June, and from September to October. The backscatter coefficient increases until the mature stage and then starts to decrease near harvest time. The similar backscatter coefficients characteristic shows by the paddy cultivated in March, July and November.

However, the changes in backscatter coefficient trends came later compared to the NDVI value trend at around 20 days, which is the peak of the NDVI value in May for the Paddy-MJN, and the peak of the NDVI

value in June for the Paddy-JMS. The NDVI value was derived from the optical remote sensing, meaning it is more sensitive to the greenness of the surface object. In comparison, the backscatter coefficient is more sensitive to surface structures conditions. As pointed by (Yang et al. 2008), the paddy growth parameters such as plant height, water content and plant structure are the most responsible for backscatter coefficient. Therefore, the backscatter coefficient remained high because the area was covered by the mature stage of paddy field, and the NDVI started to have a lower value because the greenness of paddy was fading. By contrast, the backscatter coefficient started to decrease, similar to NDVI value, immediately after the mature stage of paddy fields.

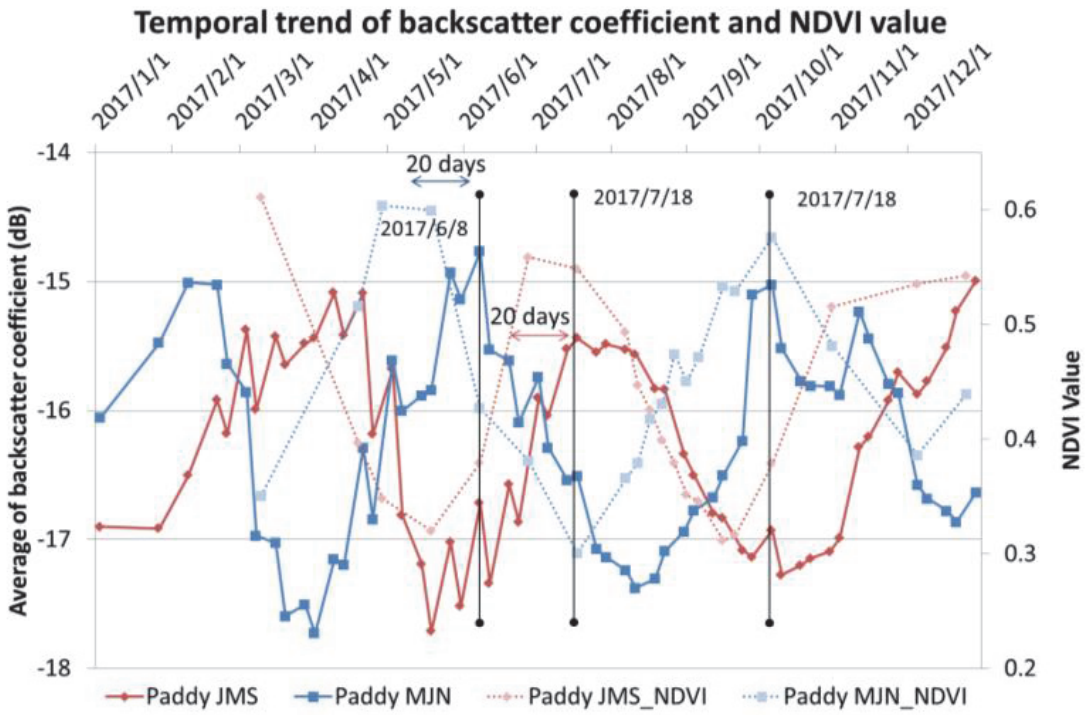

Fig. 4-5 The average of VH polarization backscatter coefficient and NDVI value from paddy JMS and paddy

4.3.3 Classification result

Random forest with 50 trees gave a higher classification accuracy with an average above 70% than the random forest with 25 trees, as can be seen in Fig. 5-6 (a). The highest classification accuracy was obtained using a combination B_50, with 76.88% of the overall accuracy and 0.728 of the kappa value. The classification of D_25 gave the lowest accuracy, with 65.05% and 0.588 for overall accuracy and the kappa value, respectively. These results present that the additional bands from the subtraction of VH and VV polarizations increased both the overall accuracy and the kappa value, as can be seen in high accuracy for the classification of the B_25 and B_50 polarization band combination.

Amongst all classes, both of producer's and user's accuracy of mixed garden crops classes remained below 60%. The average accuracy of the mixed garden crops class from 8 classifications is 35.18% and 46.61%, for

the producer's and the user's accuracy, respectively. The Fig. 4-6 (b) shows the producer's and user's accuracy classifications using random forest with 50 trees. The mixed garden crops class was often misclassified as an upland field class and a woodland class. The location of mixed garden crops is near the upland fields and is similar to upland fields but covered with tree canopy. It is because the C-band used for Sentinel-1 could not penetrate the dense canopy and received only the backscatter of the surface canopy. In the previous study (Mirelva & Nagasawa, 2018), mixed garden crops could be identified and classified better in L-band SAR, because the L-band could penetrate the canopy. Therefore, the mixed garden crops class tended to have lower accuracy and was misclassified as woodland class in C-band Sentinel-1.

Settlement and woodland class have a minimum temporal change which influenced the stability of the backscatter coefficient in their surface area. Therefore, the accuracy of both classes is higher than other agricultural classes. The Paddy-JMS and Paddy-MJN have an acceptable producer's and user's accuracy above 65% for all classifications.

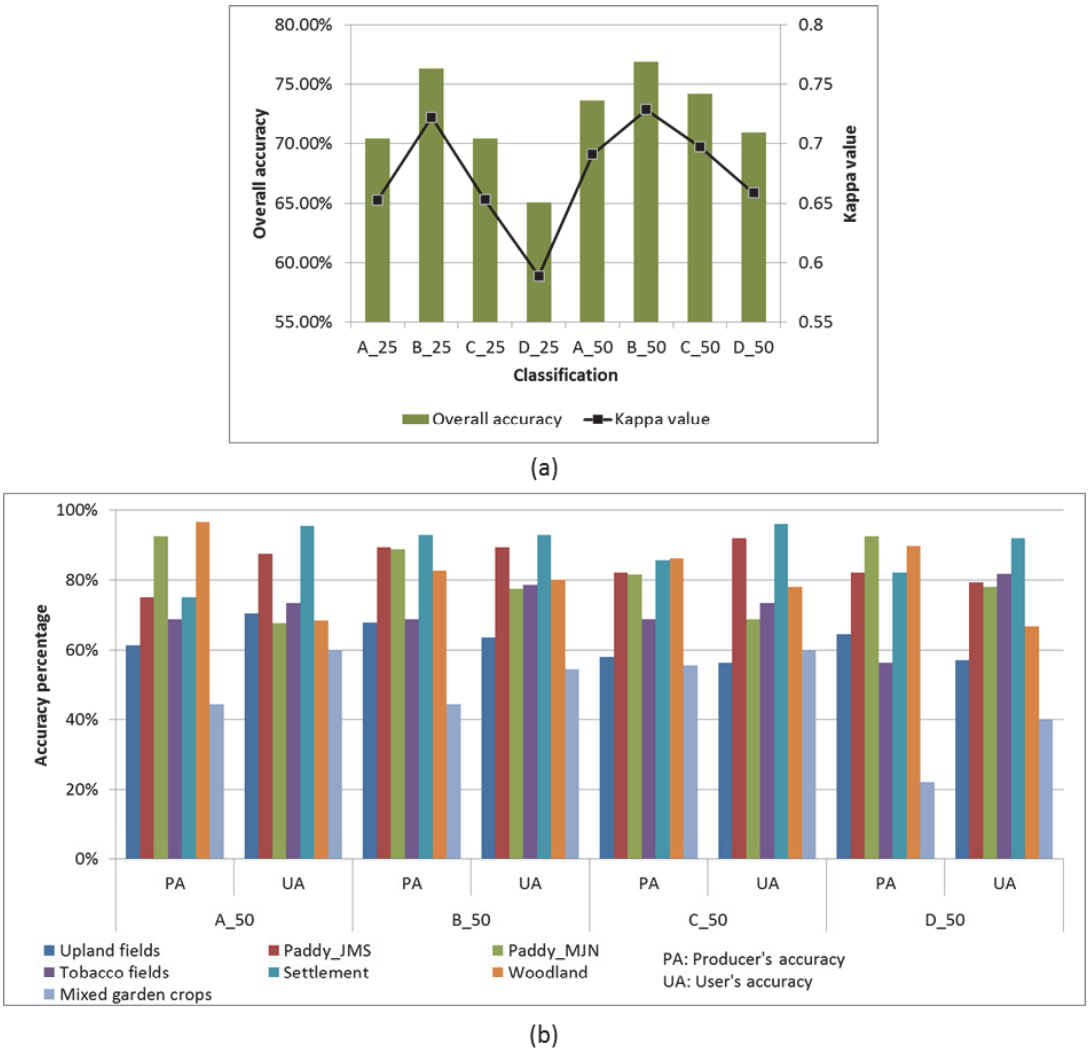

Fig. 4-6 (a) The overall accuracy and kappa value of classification result and (b) the producer's and user's accuracy of all classes from random forest 50 classification

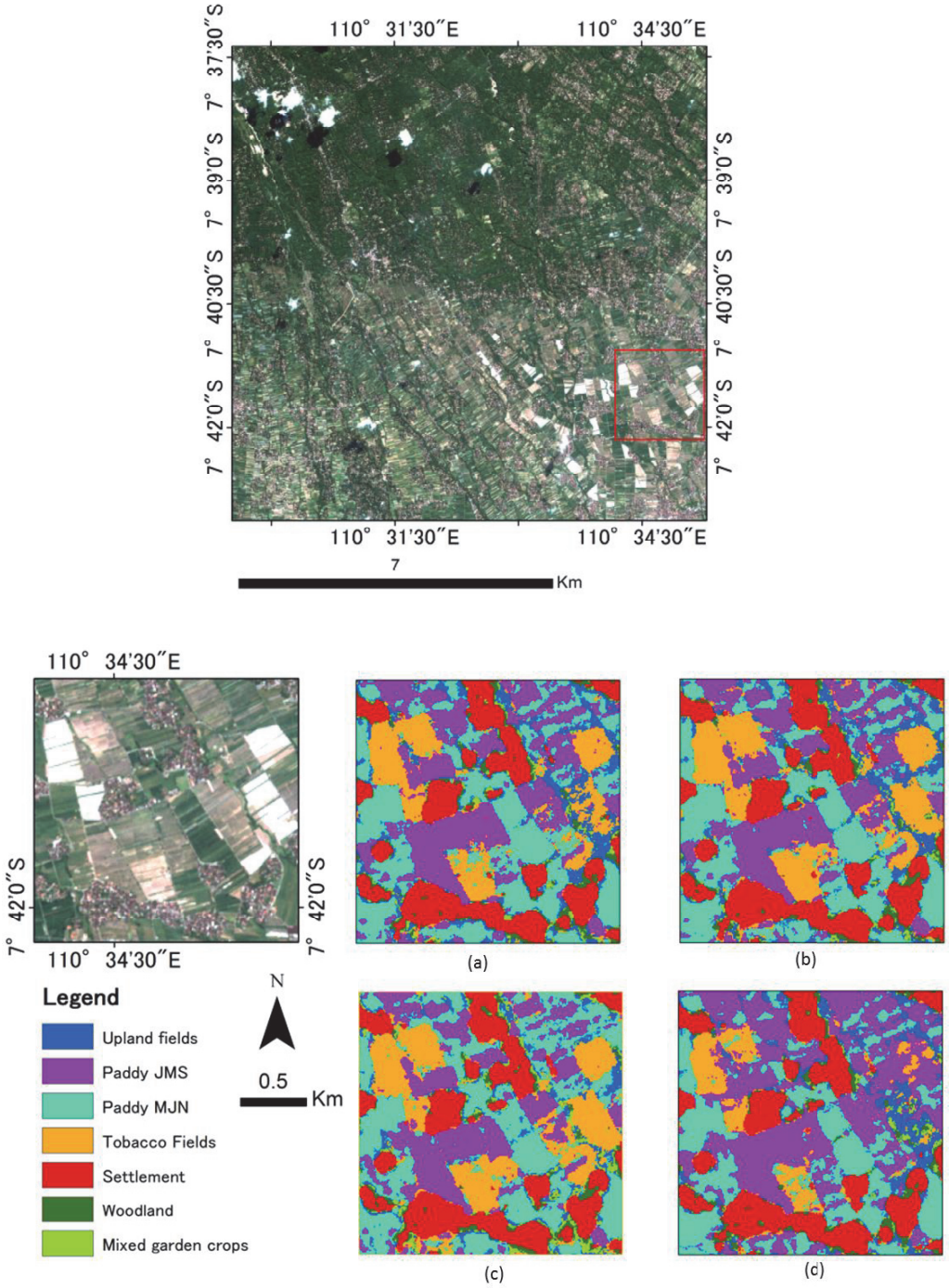

Fig. 4-7 The image of Sentinel-2 taken on 19 May 2017 and classification result for (a) A_50, (b) B_50, (c) C_50 and (d) D_50 with experimental part shows in red square

In Fig. 4-7, the experimental part of study area sized 4 km^2 of land uses and land covers consisting of settlements, paddy fields, and tobacco fields, which was selected to evaluate the classification results. The Sentinel-2 was taken on May 19, 2017, with band 4, band 3, and band 2 as RGB composite image. Some areas of the Paddy-JMS and the Paddy-MJN class were misclassified as tobacco fields because the tobacco fields were planted in the paddy field area during the dry season. The visual interpretation of Sentinel-2 indicates that

the plantation of tobacco fields started in the middle of May 2017 and finished around the end of September 2017. As a result, the net cover for tobacco plantation was removed and the area became paddy fields in October. Therefore, the tobacco fields were correctly identified in A_50, B_50, and C_50. However, in D_50, some areas, which were identified with a yellow circle, were classified as the paddy fields and upland fields because the fields were cultivated after harvesting the tobacco fields.

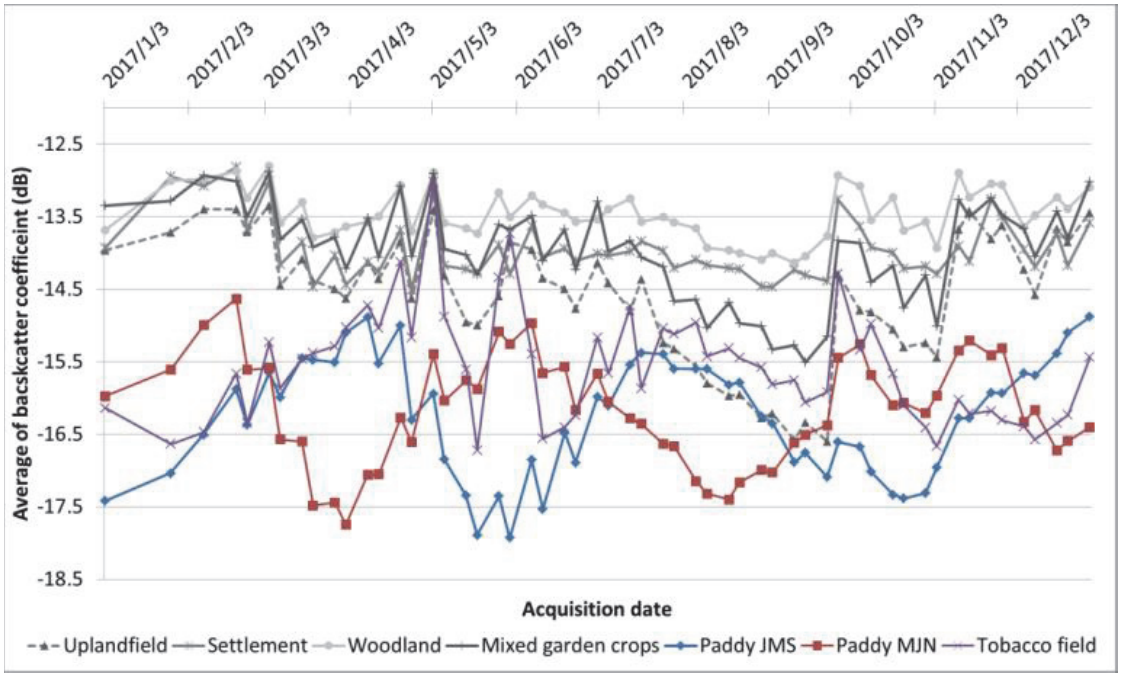

Fig. 4-8 The average of VH polarization backscatter coefficient for all classes

Fig. 4-8 shows the average of VH polarization backscatter coefficient for all classes. In VH polarization, the Paddy-JMS, the Paddy-MJN, and the tobacco fields class have a lower average backscatter coefficient than other classes. A study conducted by (Tian et al. 2018) confirmed that the backscatter coefficient of paddy fields was lower than the backscatter coefficient of other land covers. The backscatter coefficient of tobacco fields reached the highest backscatter coefficient on May 3, 2017, and May 30, 2017, which are almost equal to other classes, such as woodland, settlement, upland fields, and mixed garden crops. The low moisture from land preparation for tobacco fields affected the low moisture in the soil, which shows in high backscatter coefficient. The backscatter coefficient of tobacco fields is relatively low, around -16 dB during wet season in January and December after the harvest of tobacco field. Therefore, the tobacco fields were often misclassified as paddy fields. The other classes, such as woodland and settlement, have the most stable VH polarization. In this study, the complex agricultural area and two paddy fields cropping pattern can be identified and classified using Sentinel-1 in GEE.

4.4 Conclusion

The temporal microwave satellite images, such as Sentinel-1, could contain a large amount of data, and require a lot of storage for processing. However, GEE provides cloud-based storage for processing satellite images, including Sentinel-1. In this study, the Sentinel-1 data assisted with Sentinel-2 were successfully classified for the complex agricultural area in GEE platform. The threshold of backscatter coefficient less than -17.4852 dB and greater than -31 dB generated a paddy fields area. As a result, the cropping pattern of paddy fields was calculated based on how many times paddy fields were cultivated. In this study, the cropping patterns were separated into two types, Paddy-JMS (paddy planted in January, May, and September) and Paddy-MJN (paddy planted in March, July, and November). The average producer's and user's accuracy for both paddy fields was above 65%. A comparison of the backscatter coefficient and NDVI value of these paddy fields classes shows the backscatter coefficient was more sensitive to the surface structure, which led to the shifting time between the backscatter coefficient and NDVI. The random forest with 50 trees gave higher accuracy than the random forest with 25 trees, especially accuracy for the dataset with less polarization band combination. The combination band of VH, VV, and the subtraction of VH and VV polarization classified with the random forest with 50 number of trees obtained the highest overall accuracy and kappa value as 76.88% and 0.728, respectively. In this study, the Sentinel-1 was found to be very useful for agricultural croplands, especially paddy fields with different cropping patterns. The Sentinel-2 provides NDVI and the images for selected sample points and accuracy assessment points. As a result, the processing of Sentinel-1 and Sentinel-2 using GEE could successfully be applied in the agricultural croplands classification in tropical areas.

Chapter 5
Identification and classification of complex agricultural Croplands using multi-temporal ALOS-2/PALSAR-2 data: a case study in Central Java, Indonesia

5.1 Introduction

Indonesia, like many Southeast Asian countries, depends on agriculture as one of national income sources, as well as for economic growth and fulfilling the country's consumption needs. According to Statistics Indonesia's 2014 report, the agricultural sector (including forestry and fishery) contributed 13.38% of Indonesia's gross domestic product. Moreover, a substantial 32% of Indonesians in rural areas work in the agricultural sector. The agriculture croplands are mainly located on Java Island, where smallholding farmers cultivate agricultural cropland near volcanos due to the fertile soil available.

The small-scale cultivated fields on Java typically follow the terrain contour. In general, horticultural crops are planted in upland areas, which range from flat to hilly, while paddy fields are mostly found in flat areas at lower altitudes. Agricultural parcels in Indonesia are small, around 0.3 ha per household (Agus & Manikmas 2003), with many farmers often being sharecroppers who do not own their fields. Farmers have limited access to technology and are highly dependent on the seasonal weather for maintaining their crops. The intercropping method is usually applied to increase farmers' incomes. As such, it is uncommon to find distinctive cropping patterns and types on adjacent agricultural croplands. These conditions increase the complexity of monitoring complex agricultural cropland on Java Island.

The Indonesian government monitors agricultural areas on Java Island by using direct field surveys and the remote sensing technology. There are two kinds of remote sensing technology: optical and radar-based remote sensing. The optical remote sensing satellite captures the spectral value of the earth's surface via sunlight reflectance and provides high temporal data. Atmospheric conditions, such as clouds, limit the usage of optical data, while the radar-based remote sensing capability is unaffected. The satellite sensor for radar-based remote sensing, also known as synthetic aperture radar (SAR), transmits specific wavelengths and receives the scatter from the earth's surface. Common wavelengths for SAR sensors are the X-band (2.5-4 cm), C-band (4-8 cm) and L-band (15-30 cm). SAR sensors using longer wavelengths penetrate deeper vegetation cover than those using shorter ones, as well as provide temporal data day and night and overcome the limitations caused by cloud cover, which often occurs in tropical areas.

In recent years, many researchers have monitored agriculture using SAR data because of their sensitivity to the moist conditions and surface roughness of the areas monitored. Paddy fields are frequently monitored by a SAR because the inundation stage of the early planting season is useful as a key factor, which allows the SAR

to distinguish between paddy fields from other crops and land uses. Some studies have used SAR for paddy field identification and mapping (Y. Zhang, Wang, & Q. Zhang, 2011; Nelson et al. 2014), paddy field monitoring (Torbick et al. 2017), and paddy yield estimation (Inoue, Sakaiya, & Wang, 2014). Other studies have shown SAR to be highly effective in classifying whether a paddy is abandoned or not, identifying rubber and oil palm agricultural land (Yusoff et al. 2016), classifying crops (Tian et al. 2010), and separating tall vegetation from short vegetation (Mishra, Singh, & Yamaguchi, 2011).

The Advanced Land Observing Satellite 2 (ALOS-2) was launched on May 24, 2014. Mounted on the ALOS-2 is the second-generation Phased Array Type L-band Synthetic Aperture Radar (PALSAR-2) sensor (Kankaku, Suzuki, & Osawa, 2013). The number of agricultural monitoring applications using SAR in Indonesia is still limited, especially when involving ALOS-2/PALSAR-2. This study aimed to analyze the ability and emphasize the advantages of multi-temporal ALOS-2/PALSAR-2 data for identifying complex agricultural croplands and classifying other land uses near agricultural cropland. Furthermore, this study was carried out to investigate the useful backscatter characteristics of temporal PALSAR-2 data for separating out the paddy field planting stages.

5.2 Materials and methods

5.2.1 Study area

The study area covered 112 km^2 of the Klaten Regency in Indonesia's Central Java Province, within the following geographic coordinates: $7^o 37' 10.7''$ - $7^o 42' 56.8''$ south latitude and $110^o 29' 31.89''$ -$110^o 35' 17.02''$ east longitude (Fig. 5-1). It is located on the southeastern slopes of Java's most active volcano, Mount Merapi, with elevations of 200-600 m.

Despite frequent volcanic eruptions, people continue to live and work in this hazardous area because of the strong relationship between the Javanese people and the mountain (Lavigne et al. 2008). They view Mount Merapi as a sacred living thing, which provides abundant natural resources (Nofrita & Krol, 2014; Mei et al. 2013), given that the fertile soil resulting from the eruptions is highly beneficial to their agricultural activities. Therefore, many households depend on the agricultural sector and work as farmers or sharecroppers. Land use in the study area generally consists of woodland, settlements, paddy fields, upland fields, tobacco fields and mixed garden crops. The distribution of land covers differs in the northern and southern parts according to topographic conditions. The hilly northern part has woodlands, upland fields and mixed garden crops, while paddy fields, tobacco fields and some upland fields are located in the flat or gently sloping areas of the southern part. The settlements are spread across both southern and northern parts of the study area.

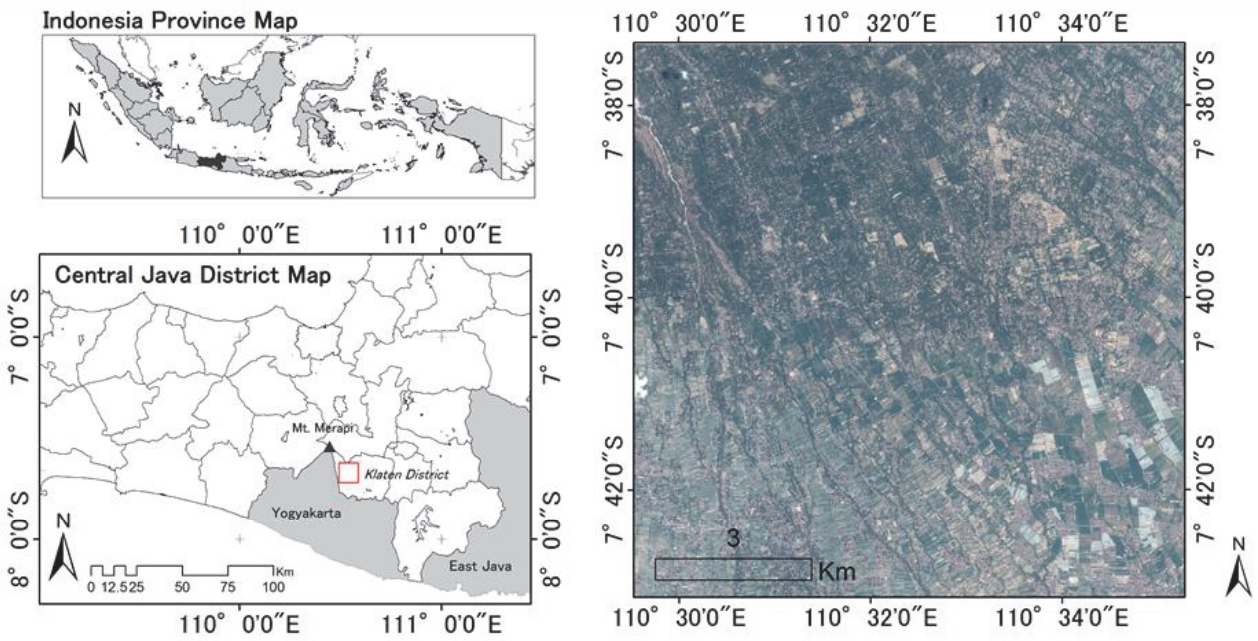

Fig. 5-1 Location of study area and coverage of Pleiades

5.2.2 Remotely sensed data

ALOS-2/PALSAR-2 is provided by the Japan Aerospace Exploration Agency (JAXA) and delivers higher resolution SAR images than its predecessor, ALOS/PALSAR (Rosenqvist et al. 2014). This study used multi-temporal dual polarization and full polarization data in the highly sensitive mode with a 6.85 m resolution as the primary data. The dual polarization of PALSAR-2 consisted of HH and HV polarizations and the full polarization consisted of HH, HV, VH and VV polarizations. The first letter of polarization indicates the transmission direction, while the second letter indicates the received direction. H stands for horizontal and V for vertical direction. The complementary data are from Pleiades and the Landsat 8 Operational Land Imager (OLI), which hereafter will be referred to as Landsat 8.

Table 5-1 Acquisition description of primary and complementary data used in this study

Primary data	Acquisition date in yyyy.mm.dd	Complementary data	Acquisition date in yyyy.mm.dd	
ALOS-2/PALSAR-2: Level 1.1		Pleiades Image	2015.08.26	
	2015.01.30		2015.01.05	2015.07.16
- Dual polarization	2015.07.03		2015.02.22	2015.08.01
(HH & HV polarizations)	2015.09.11	Landsat 8 Images	2015.03.26	2015.09.02
- Full polarization		(12 images)	2015.05.13	2015.09.18
(HH, HV, VH, and VV polarizations)	2015.05.17		2015.05.29	2015.10.04
			2015.06.14	2015.10.20

Pleiades is an ortho-rectified multi-spectral imagery satellite with a 0.5 m spatial resolution, while Landsat 8 is a multispectral image satellite with a 30 m spatial resolution. These complementary data were used for a preliminary study of the land use and cropping patterns in the study area. In addition, Pleiades was used for the base image in the georeference process. Table 5-1 describes the detailed acquisition of primary and complementary data used in this study. The date acquisition description in the yyyy.mm.dd format will be used hereafter. The field survey was performed twice, on March 25, 2017, and August 24-25, 2017, in order to validate the land use and cropping patterns in the study area.

5.2.3 ALOS-2/PALSAR-2 Preprocessing and Landsat-8 Preprocessing

Sentinels Application Platform (SNAP) software from the European Space Agency (ESA) provides the tools for processing Sentinel-1 satellite data, as well as other satellite data, such as from PALSAR-2. The preprocessing steps are (i) calibration, (ii) multi-look with a 1:2 ratio for azimuth and range (JAXA, 2014), (iii) co-registration, (iv) speckle filtering for reducing the noise in SAR data, (v) geocoded processing and (vi) backscatter coefficient calculation.

All PALSAR-2 data were stacked and co-registered together by using the Shuttle Radar Topographic Mission digital elevation model (SRTM DEM). The single product speckle filter was applied based on the Lee speckle filtering method with a window size of 5 × 5. The PALSAR-2 data were geocoded to the Universal Transverse Mercator (UTM) projection 49S with World Geodetic System 1984 (WGS84) datum. The topographic effect was corrected using the SRTM DEM. The results of the geocoded images formed a subset based on study area coverage and were confirmed to have a perfect fit with the Pleiades image. The backscatter coefficient in decibel units (dB) was then calculated using this formula (JAXA, 2017) where the Cf and A are calibration factors with a value of -83 and 32 dB, respectively.

$$Backscatter\ coefficient\ =\ 10\ \times\ Log10(polarization)+\ Cf\ -A \qquad \text{(Eq. 5-1)}$$

Landsat 8 data were processed using ERDAS Imagine 9.2 software. The preprocessing steps were (i) conversion from a digital number to a reflectance value with sun angle correction (USGS, 2014), (ii) the study area subset and (iii) the cloud removal process. The Iterative Self-Organizing Data Analysis Technique (ISODATA) method (Helmer & Ruefenacht, 2005) was used for removing cloud cover from the study area. Then, cloud-free Landsat 8 data were examined to observe the growing stage of the agricultural cropland between the acquisition dates of the PALSAR-2 data.

5.2.4 Sample point collection and classification method

Sample points, consisting of training and accuracy assessment points, were randomly selected by using a

combination of visual interpretations from PALSAR-2, Pleiades and Landsat 8 data. PALSAR-2 data are sensitive to water. Therefore, the red-green-blue (RGB) channel composite was set with a backscatter coefficient of HH, HV and HV-HH polarizations and used to separate the paddy fields in the early growing stage (inundated phase) from those in the late stage (generative phase). A previous study (Cazals et al. 2016) showed that the RGB composite of VV, VH and VH-VV Sentinel-1 data was useful for identifying the moisture condition of wetland areas. In this study, a similar approach was implemented using HH, HV and HV-HH polarizations instead of VV, VH and VH-VV, for identifying paddy fields. Other land uses, such as tobacco fields, settlements, woodland upland fields and mixed garden crops, were identified and selected based on visual interpretations in the Pleiades and Landsat 8 data. After collecting the sample points for all land use, the points were divided into training points (70%) and accuracy assessment points (30%). The supervised classification method, known as maximum likelihood classification, was used for the classification process. The accuracy assessment of remote sensing classification results can be estimated by calculating the error matrix, which consists of producer accuracy and user accuracy for each class, overall accuracy and the kappa coefficient as total accuracy (Congalton, 1991). Producer accuracy is related to the proportion of correctly classified reference samples, while user accuracy is related to sample or training points that are correctly classified (Mas et al. 2014). Overall accuracy and the kappa coefficient are related to classification accuracy in general.

5.3 Results and Discussion

5.3.1 ALOS-2/PALSAR-2 backscatter coefficient

Fig. 5-2 shows the backscatter coefficient of PALSAR-2 polarizations. The brightness of the backscatter coefficient could be used to identify the surface roughness condition and/or water content in the study area. In general, HV polarization has a lower average value than HH polarization, which affects the image brightness intensity color. The bright color in HH polarization indicates a rougher surface condition and less water content. It also has a higher backscatter coefficient than the darker color. Bareland and concrete buildings will have a stronger backscatter coefficient than water body areas, which give a weak or almost no backscatter. Therefore, the water body or high water content area appeared darker.

In Fig. 5-2, there were temporal changes in the southern part as indicated by the color variation in HH polarizations of the PALSAR-2 backscatter coefficient. The cropping activities in the paddy fields, tobacco fields and upland fields in the southern part of the study area affect the backscatter coefficient value. Paddy fields require large amounts of water in the early planting stage. Therefore, the paddy fields scatter different backscatter coefficient strengths between the inundated and harvested periods. The HH polarization for January 30, 2015, in the southwestern part appeared very bright compared to other acquisition dates because the surface was rough and lacked water content or was very dry. This is an indication that the fields were being prepared for

other agricultural activities or just harvested. Thus, the backscatter coefficient is very strong. The tobacco fields and upland fields have varied backscatter coefficients during the growing stages. The northern part of the study area was mostly covered by woodland and mixed garden crops, which were surrounded by perennial trees and indicated less temporal change compared to the upland fields, thereby affecting the brightness of the backscatter coefficient in terms of appearing consistent.

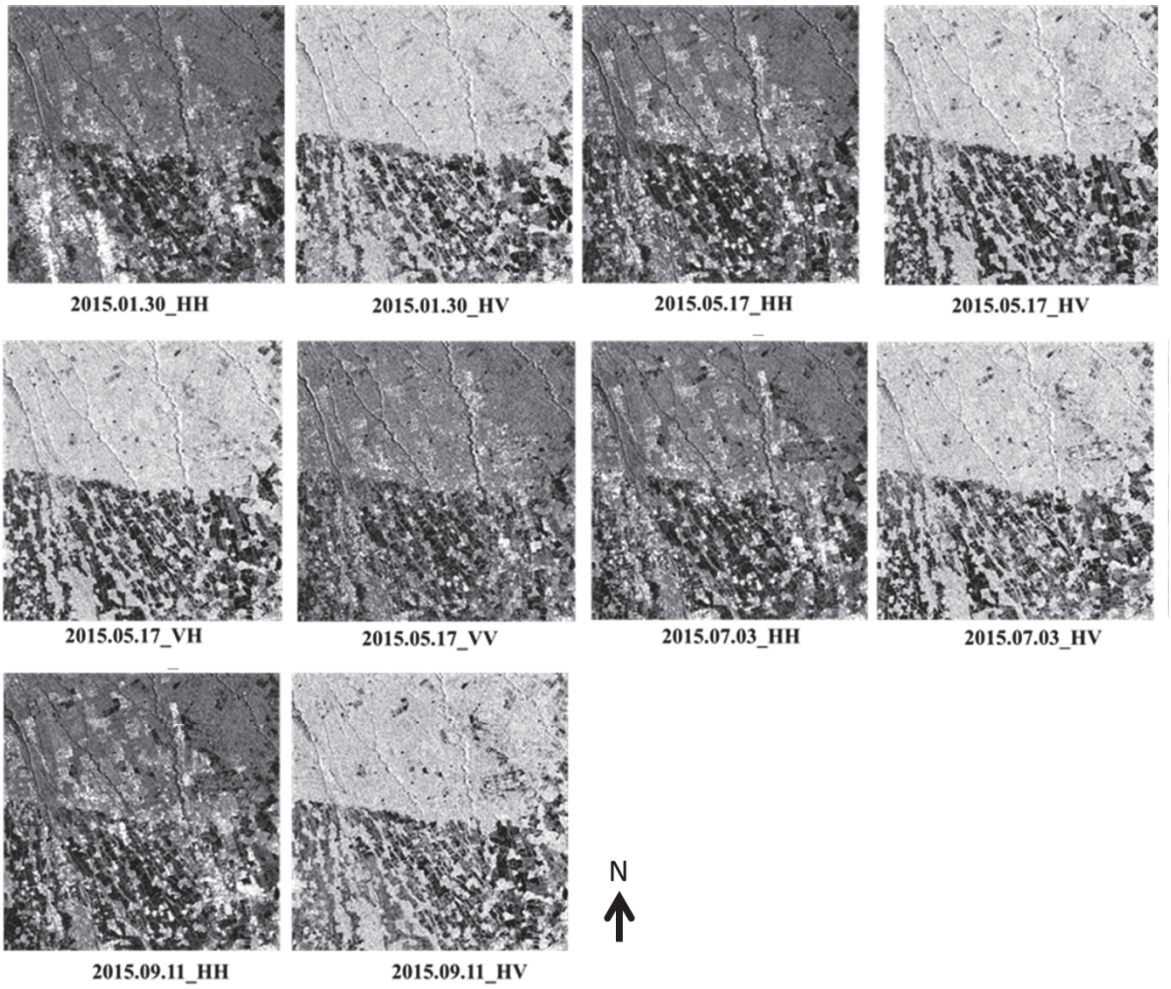

Fig. 5-2 Backscatter coefficient of PALSAR-2 polarizations

Based on the field survey, it was found that paddy field irrigations in this study area are not equally distributed. These irrigation conditions influence the paddy fields' cropping patterns in the southwestern and southeastern parts of the study area. Therefore, the paddy fields in this study are divided into two classes: paddy-I and paddy-II. The paddy-I class was made up of paddy fields with adequate irrigation, which were cultivated either three times a year or five times in two years. The paddy-II class was rain-fed and cultivated as paddy fields in the wet season and changed to upland fields in the dry season. In this study, the RGB composite of HH, HV and HV-HH polarizations was used for the separation of these paddy fields' cropping patterns. Fig.

5-3 shows the RGB composite of HH, HV, HV-HH polarizations for each PALSAR-2 data. The low backscatter coefficient areas, which appeared as dark blue, were interpreted as being inundated or in an early vegetative stage. These areas are categorized as paddy-I. Meanwhile, the paddy fields in a late growing stage, or those being prepared for a change of crop, showed more roughness and a higher backscatter coefficient. They appeared as bright orange on the RGB composite and categorized as paddy-II.

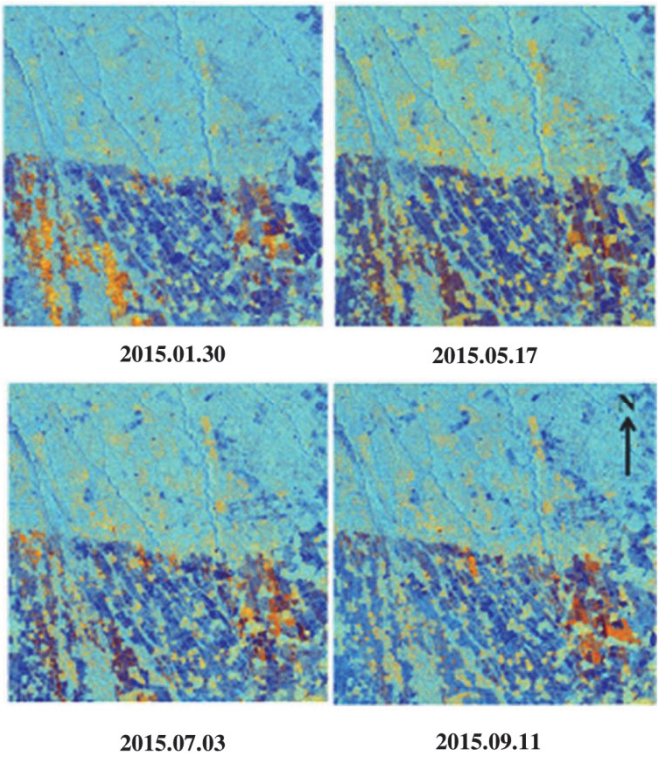

Fig. 5-3 RGB composite of HH, HV, VH-VV of ALOS-2/PALSAR-2 taken on January 30th, May 17th, July 3rd, and September 11th

5.3.2 Landsat 8 preprocessing result

The cloud-free Landsat 8 data in a true-color composite (reflectance bands of 4, 3 and 2) are shown in Fig. 5-4. The temporal changes in cropping patterns could be visually identified. For example, the tobacco fields appeared as a bright white area on the Landsat 8 data for the period from March 26 to September 2, 2015, because of the shade nets used for pest prevention. The tobacco plants in this area took about six months from first planting to harvest. After harvesting, several tobacco shade nets were removed as can be seen in the Pleiades data (Fig. 5-1).

Besides the tobacco fields, the other cropland cropping activities could be identified as well. In the 2015.03.26 image (Fig. 5-4), the southern part was in a dry condition but the vegetation coverage was identified

in images for previous (2015.02.22) and later months (2015.05.13 and 2015.06.14). Therefore, other land use classes, except paddy fields, were selected by using visual interpretations of Pleiades and Landsat 8 data with the following descriptions: (i) woodland comprising several trees or non-agricultural tall vegetation, (ii) a settlement comprising housing and nearby home gardens, (iii) upland fields with an open field for growing cassava, maize and horticultural crops, and (iv) an area where mixed garden crops are cultivated, which has similar characteristics to upland fields, but is located near perennial trees or non-agricultural tall vegetation.

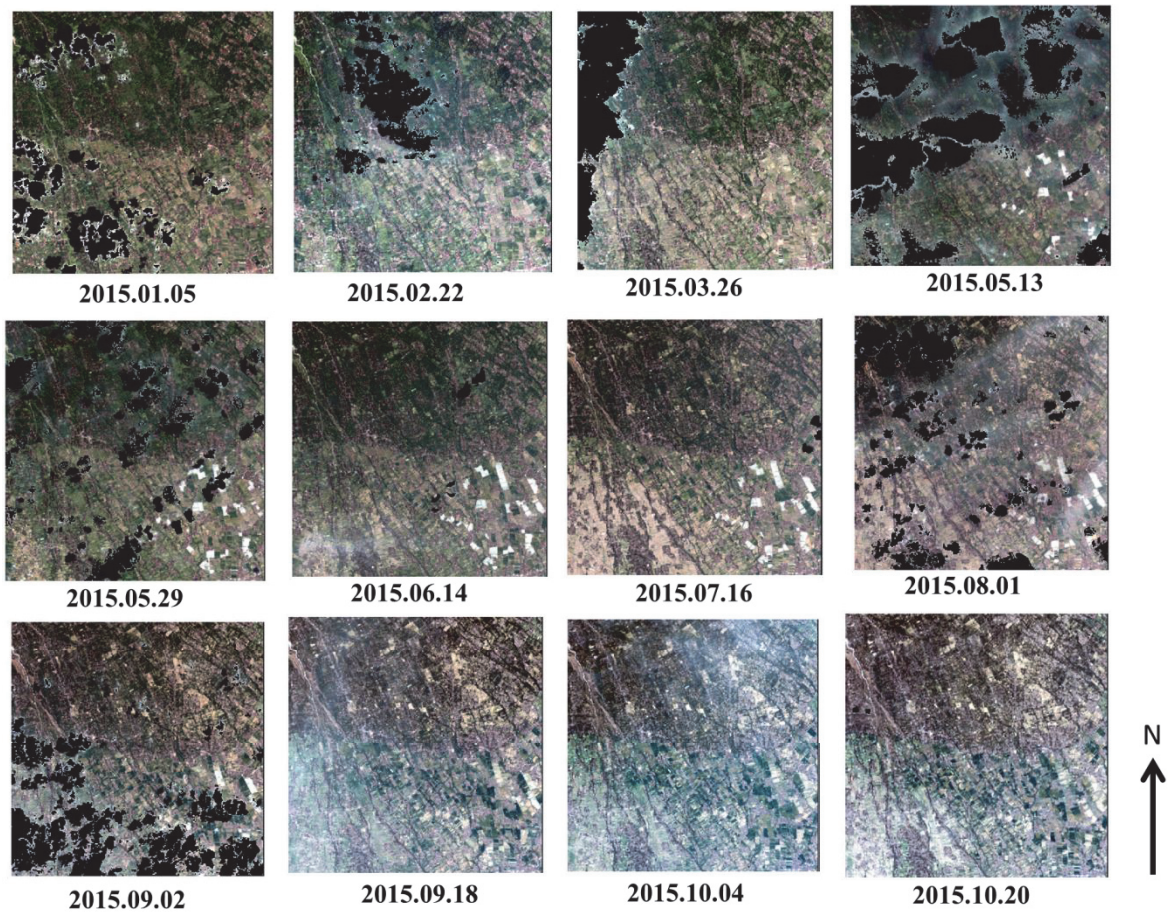

Fig. 5-4 The cloud-free Landsat 8 data in true color composite (reflectance bands of 4,3,2)

5.3.3 Training points analysis and classification result

In total, there were seven land use classes, namely: paddy-I, paddy-II, woodland, settlements, upland fields, tobacco fields and mixed garden crops. Table 5-2 shows the training points and accuracy assessment points collected from the analysis of the PALSAR-2 backscatter coefficient and the visual interpretation of Landsat 8 and Pleiades data. The temporal combination column in Table 5-2 was obtained and randomly selected based on combined paddy-I and paddy-II sample point classes from each acquisition date. These sample points were especially applied with regard to the combination of multi-temporal classification process. The other classes

were assumed to have minimum land use change; therefore, the temporal classification process will be used the same set of sample points. The combination and polarization band compositions for the classification process are described in the Table 5-3.

Table 5-2 Training points and accuracy assessment points

Class Name			Temporal combination	
	TP	AAP	TP	AAP
Paddy-I				
2015.01.30 (0130)	74	33		
2015.05.17 (0517)	70	30	119	50
2015.07.03 (0703)	71	31		
2015.09.11 (0911)	56	24		
Paddy-II				
2015.01.30 (0130)	70	30		
2015.05.17 (0517)	73	30	117	50
2015.07.03 (0703)	56	24		
2015.09.11 (0911)	35	15		
Upland fields	78	33	78	33
Tobacco Fields	55	23	55	23
Woodland	90	38	90	38
Settlement	85	36	85	36
Mixed garden crops	89	37	89	37

Note. TP means training points, AAP means accuracy assessment points.

Table 5-3 Polarization composition for classification process

Combination name	Polarization composition description	Number of bands
0130_A	2015.01.30 (HH, HV)	2
0130_B	2015.01.30 (HH, HV, HV-HH)	3
0517_A	2015.05.17 (HH, HV)	2
0517_B	2015.05.17 (HH, HV, HV-HH)	3
0517_C	2015.05.17 (HH, HV, VH, VV)	4
0517_D	2015.05.17 (HH, HV, VH, VV, HV-HH)	5
0703_A	2015.07.03 (HH, HV)	2
0703_B	2015.07.03 (HH, HV, HV-HH)	3
0911_A	2015.09.11 (HH, HV)	2

0911_B	2015.09.11 (HH, HV, HV-HH)	3
Temp_comb_1	2015.01.30 (HH, HV) 2015.05.17 (HH, HV) 2015.07.03 (HH, HV) 2015.09.11 (HH, HV)	8
Temp_comb_2	2015.01.30 (HH, HV, HV-HH) 2015.05.17 (HH, HV, HV-HH) 2015.07.03 (HH, HV, HV-HH) 2015.09.11 (HH, HV, HV-HH)	12
Temp_comb_3	2015.01.30 (HH, HV) 2015.05.17 (HH, HV,VH, VV) 2015.07.03 (HH, HV) 2015.09.11 (HH, HV)	10
Temp_comb_4	2015.01.30 (HH, HV, HV-HH) 2015.05.17 (HH, HV,VH, VV, HV-HH) 2015.07.03 (HH, HV, HV-HH) 2015.09.11 (HH, HV, HV-HH)	14

5.3.4 ALOS-2/PALSAR-2 backscatter coefficient characteristics

Fig. 5-5 shows the averages of the training points of land use classes based on the backscatter coefficient from HH and HV polarizations from each PALSAR-2 data. Fig. 5-5 (a) and 5(b) shows the averages of training points for woodland, settlements, upland fields, tobacco fields and mixed garden crops. The HH and HV polarizations of the paddy-I and paddy-II classes from each acquisition date were shown in Fig. 5-5 (c) and 5(d) respectively. In Fig. 5-5 (a), the settlement class showed the highest HH polarization backscatter coefficient around -5 dB to -3 dB. It can be seen in Fig. 5-5 (b) that the HV polarization backscatter coefficient of settlement and woodland classes was almost identical and higher than the other classes. The HV polarization value for these classes was around -14 dB to -12 dB. The dense vegetation and the home gardens close to the settlement areas influenced the HV polarization behavior. The HV polarization for settlement appeared similar to the woodland area. The mixed garden crops also have higher HV polarization backscatter coefficient than upland fields and tobacco fields. Thus, the HV polarization was found to be more sensitive to buildings and tall or dense vegetation.

In Fig. 5-5 (c), the HH polarization of the paddy-I class has a lower backscatter coefficient and more repeated patterns than the paddy-II class. This backscatter coefficient pattern was similar to the paddy field pattern presented in the study from Zhang et al. (2009). The dynamic pattern of the backscatter coefficient from the

paddy-I class was influenced by the moisture conditions, which changed during the paddy growing stages. As can be seen in Fig. 5-5 (c), the HH polarization of paddy-I class shows two graphs involving opposite temporal patterns. The first pattern consists of the paddy-I class from the acquisitions from January 30 (paddy I_0130) and July 3 (paddy I_0703), 2015. The second pattern concerns acquisitions from May 17 (paddy I_0517) and September 11 (paddy I_0911), 2015. However, all of the backscatter coefficients from the PALSAR-2 acquisition dates were low, with a value below -15 dB. Thus, the sample points were selected in the same stage of the paddy fields. Paddy I_0130 in Fig. 5-5 (c) represents the repetition of paddy cultivation in this study area.

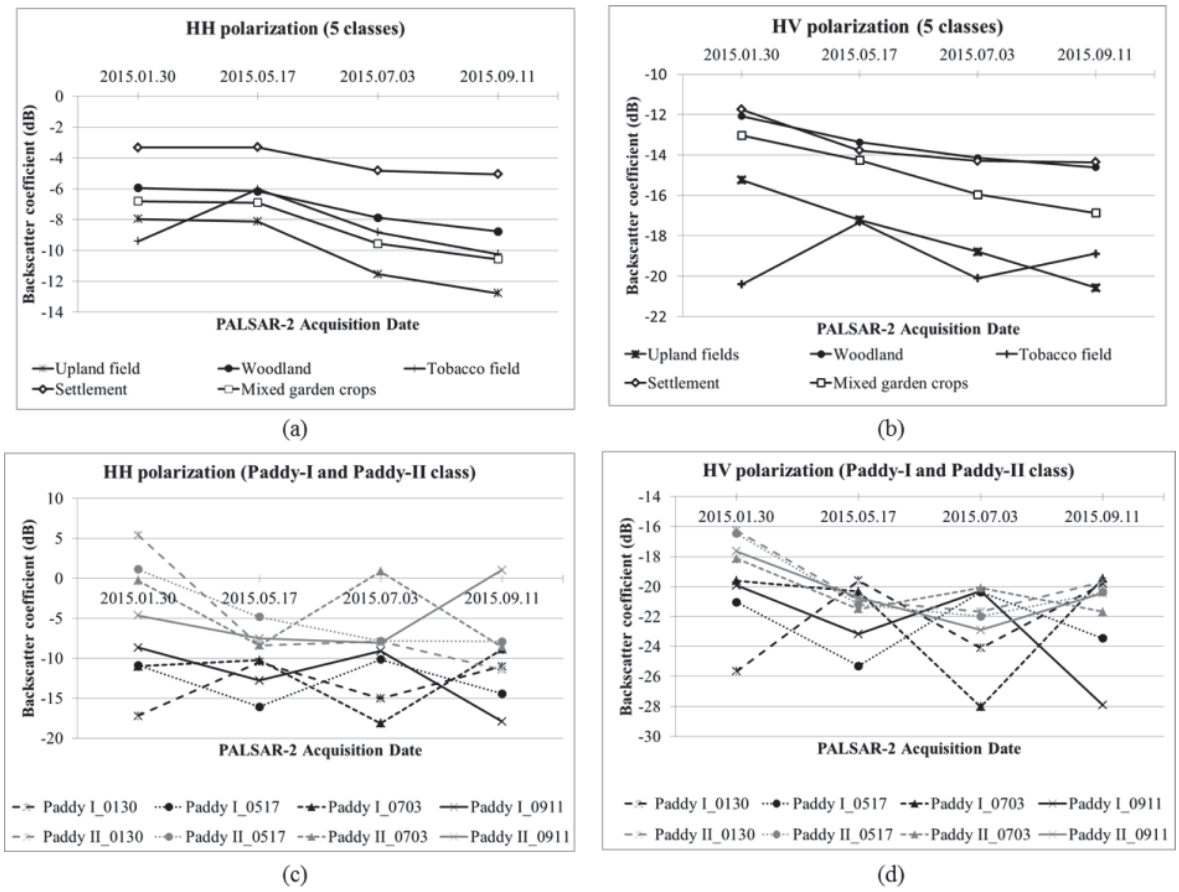

Fig. 5-5 Averages of training points based on HH and HV polarization from each PALSAR-2 data: (a) and (b) for woodland, settlement, upland fields, tobacco fields, mixed-garden-crops classes; (c) and (d) for paddy-1 and paddy-II classes

The backscatter coefficient of paddy I_0517 and paddy I_0703 also increased from the backscatter coefficient in the acquisition date. Thus, the backscatter coefficient of HH polarization from the paddy-I class revealed the paddy fields' characteristics. In contrast to the paddy-I class, the HH polarization backscatter coefficient of the paddy-II class, as can be seen in Fig. 5-5 (c), showed an inconsistent temporal change and a high backscatter coefficient. The high backscatter coefficient is related to low moisture conditions or a rough

surface, such as that in the dry condition area. In Fig. 5-5 (d), the HV polarization backscatter coefficient value of the paddy II_0130, paddy II_0517, paddy II_0703 and paddy II_0911 classes were around -22 dB to -16 dB, that is, the same range as the upland fields class. This result was expected because the paddy-II class fields became upland fields when there was minimum water availability.

5.3.5 Classification result analysis

Table 5-4 shows the overall accuracy and kappa coefficient values obtained from the classification process. In general, the classification result based on a single PALSAR-2 acquisition date was lower compared to the classification result for multi-temporal combinations. The 0911_A gave the highest accuracy amongst other single acquisition data sets, with an overall accuracy of 71.35% and a kappa coefficient of 0.66. The classification result of 0911 is higher than other single date acquisition data because the dates of acquisition for the Pleiades and PALSAR-2 data taken on September 9, 2015, involve a short time gap and affect the sample points, which are based on visual interpretations of Pleiades data. In this study, PALSAR-2 data taken on May 17, 2015, are the only full polarization data.

Table 5-4 The overall accuracy and kappa coefficient of classification result

Combination name	Number of bands	Overall accuracy (%)	Kappa coefficient
0130_A	2	64.37	0.582
0130_B	3	63.91	0.577
0517_A	2	65.63	0.596
0517_B	3	62.99	0.567
0517_C	4	66.07	0.603
0517_D	5	67.4	0.619
0703_A	2	66.21	0.603
0703_B	3	64.41	0.585
0911_A	2	71.35	0.66
0911_B	3	70.98	0.655
Temp_comb_1	8	85.02	0.824
Temp_comb_2	12	76.4	0.724
Temp_comb_3	10	80.6	0.775
Temp_comb_4	14	73.03	0.685

The full polarization of PALSAR-2 data (0517_C) showed higher accuracy than the 0517_A classification, which consists of two polarizations, HH and HV. The additional polarization of HV-HH decreases the classification accuracy for 0130_B, 0517_B, 0703_B and 0911 _B, as can be seen in Table 4. However, the addition of the HV-HH polarization causes an increase in the classification result of the full polarization data

(0517_D). In Table 5-4, the classification of multi-temporal combinations shows a high level of accuracy. Temp_comb_1 obtained the highest accuracy with an overall accuracy of 85.02% and a kappa coefficient value of 0.824. The additional band in temp_comb_2 and temp_comb_4 was not able to improve the accuracy. Therefore, higher classification accuracy can be achieved by using the multi-temporal combination of HH and HV polarizations.

Fig. 5-6 shows producer accuracy and user accuracy in all classes for the temp_comb_1, 0130_A, 0517_A and 0911_A classification results. These classification results were chosen in order to compare the accuracy of all classes. According to Fig. 5-6, the paddy-I and paddy-II classes displayed higher producer and user accuracy compared to other classes.

In the single date acquisition, as can be seen in Fig. 5-6, the producer and user accuracy of paddy-I and paddy-II classes were typically above 90%, with some obtaining 100% accuracy. These results confirmed that the selection based on the RGB composite of PALSAR-2 data is effective in increasing paddy field accuracy. However, the temporal combination of dual polarizations could increase producer or user accuracy in all classes, except the paddy-I and paddy-II classes. The sample points for multi-temporal classification were randomly selected from the sample points for single acquisition date classification. Thus, the producer and user accuracy of multi-temporal classification was lower than the single date classification result. In contrast with the paddy-I and paddy-II classes, the multi-temporal backscatter could have increased the probability of separating woodland, settlements, upland fields, tobacco fields and mixed garden crops classes.

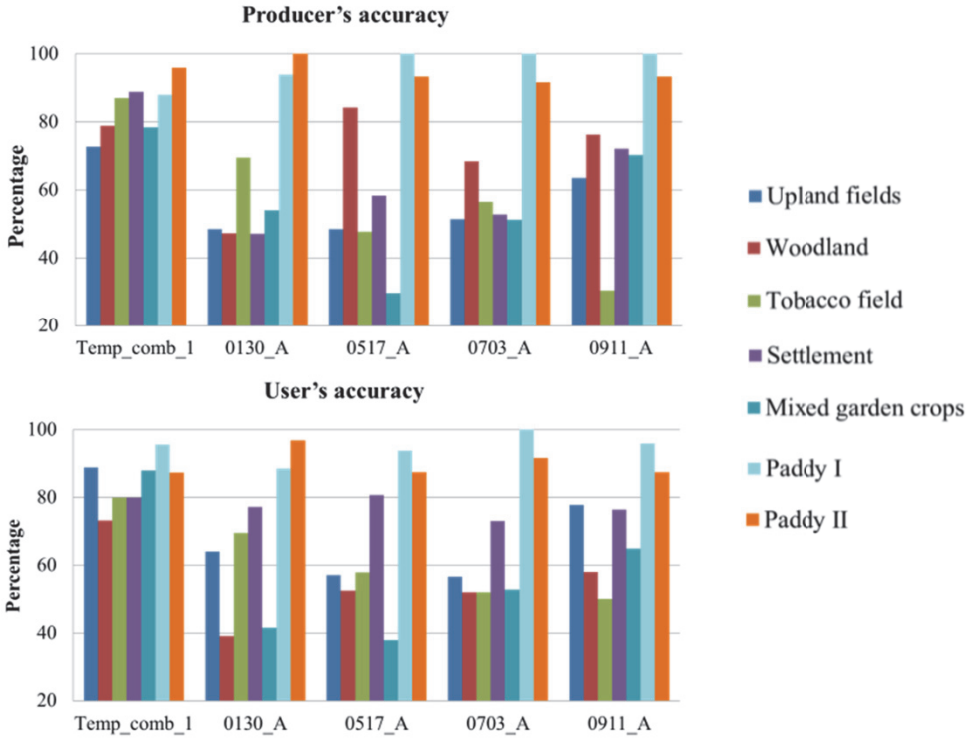

Fig. 5-6 Producer's accuracy and user's accuracy of temp_comb_1, 0130_A, 0517_A and 0911_A classification result

Fig. 5-7 shows the agriculture cropland classification results by using single date acquisition data (0130_A, 0517_A, 0703_A and 0911_A) and the multi-temporal combination (temp_comb_1). These classification results were chosen as the most representative comparison between single acquisition and multi-temporal classification results. The southern part was mostly classified as tobacco fields, as can be seen in Fig. 5-7(a), and upland fields, as can be seen in Fig. 5-7 (b), (c), and (d). The settlement areas were misclassified as woodland or mixed garden crops. Therefore, producer and user accuracy for these classes was very low. The paddy-II class was used for classifying the area with cropping patterns of paddy fields in the rainy season and upland fields in the dry season.

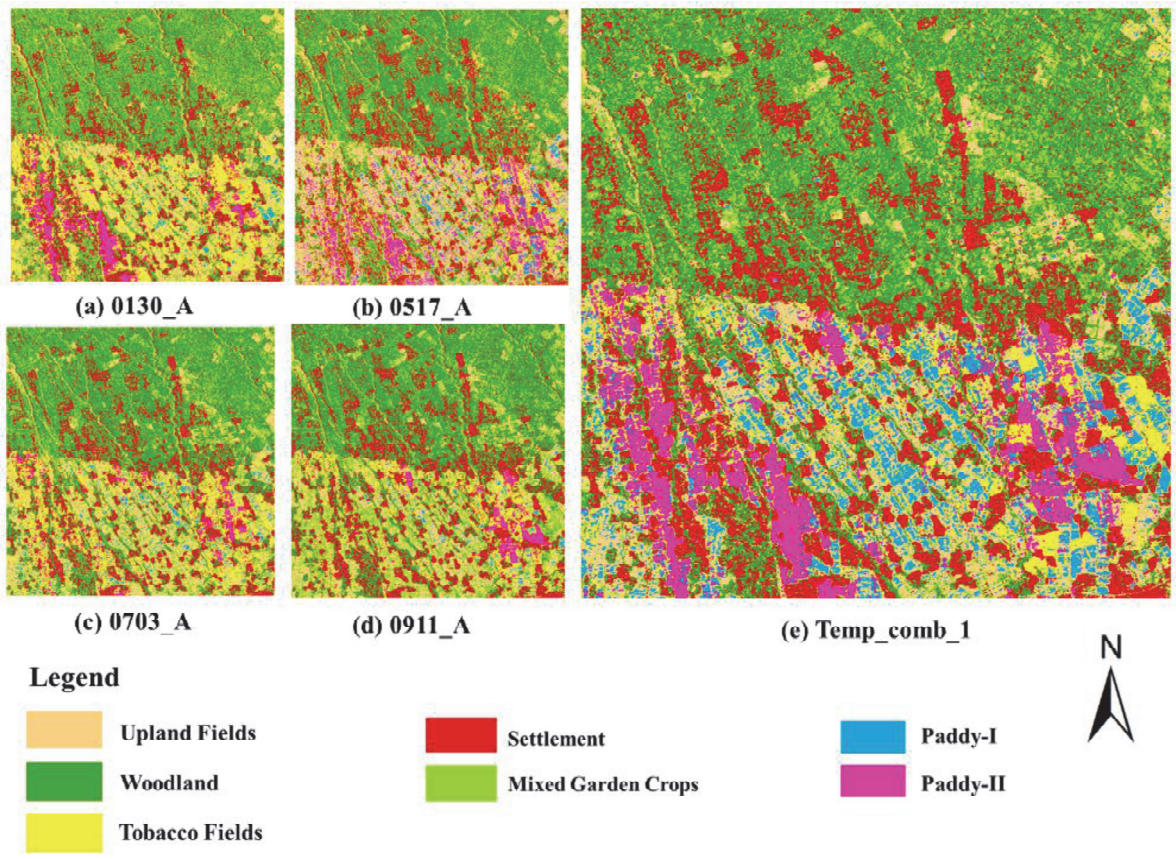

Fig. 5-7 The classification result of (a) 0130_A, (b) 0517_A, (c) 0703_A, (d) 0911_A, and (e) temp_comb_1

In Fig. 5-7(a), the area was classified as paddy-II, spreading out in the eastern part, while decreasing in the next acquisition time period (Fig. 5-7 (c)-(d)). The paddy-I class was identified in smaller areas, compared to the paddy-II class, because the planting time for paddy fields was not coordinated, as it was decided by each farmer. However, by combining the multi-temporal dual polarization data (Fig. 5-7(e)), the paddy-I and paddy-II areas became larger and easier to identify, even though the producer and user accuracies decreased. The coverage upland fields and mixed garden crops also decreased, which corresponds to higher accuracy. This

result is similar to that reported in a study revealing that temporal SAR data are useful for classifying paddy fields (Zhang, Wang, & Zhang, 2011). Therefore, the backscatter coefficient was found to be useful for separating the cropping patterns of paddy fields. Moreover, the highly accurate classification of complex agricultural croplands could be achieved by using a multi-temporal combination of dual polarization PALSAR-2 data.

5.4 Conclusion

This study shows the potential of PALSAR-2 multi-temporal data in examining complex agricultural croplands. In this study, the RGB composite of HH, HV and HV-HH and multi-temporal PALSAR-2 data were used and found to be very useful when identifying and classifying the particulars of complex agricultural croplands. The RGB composite of HH, HV and HV-HH supported the selection of sample points needed to separate two types of paddy field: the all-year paddy (paddy-I) and paddy upland field (paddy-II) cropping patterns, which are often found in this study area. By using this RGB composite, producer accuracy and user accuracy for paddy-I and paddy-II were very high compared to other land use classes. This study also achieved an overall accuracy of 85.02% and a kappa coefficient of 0.824 by using the multi-temporal combination of HH and HV polarization from four temporal data taken between January and September 2015. This multi-temporal combination was effective for classifying the agricultural croplands, which could increase overall accuracy by about 10%, compared to the average of single date acquisition classification results. Moreover, these temporal combination data increased the producer and user accuracy of other land use classes, such as woodland, upland fields, tobacco fields, settlements and mixed garden crops up to 70%. This study successfully demonstrated PALSAR-2's ability to identify and classify complex agricultural croplands.

Chapter 6
General discussion and recommendation

6.1 General discussion

The aim of this study was to explore the identification of agricultural croplands by using synthetic aperture radar. The research was conducted by selecting suitable complex agricultural croplands as study area and developed methodology for classifying the agricultural croplands by using single date imagery and multi-temporal imageries of SAR. The agricultural croplands in Central Java fulfilled two characteristics which is suitable as study area for this research. The first characteristic is various cropland types, such as rice, horticulture croplands, and tobacco, are grown in small fields size by the smallholder famers. The second characteristic is the location of agricultural croplands is close to other land use types such as settlement and woodland area. The SAR imagery is sensitive to the backscatter of various objects. Therefore, the area consists of both agricultural croplands and non-agricultural croplands will be valuable to gather more information about SAR capabilities. The optical remote sensing imageries and field survey were also utilized as the complementary data to provide description the distribution of land use and land cover types. The research was further divided into more specific objectives in order to obtain satisfactory method for identifying complex agricultural croplands.

The first objective is *to examine the characteristic of complex agriculture cropland that can be identified by using active remote sensing data.* The agriculture croplands such as paddy fields have specific phenology which is inundated phase at the beginning of cultivation. The inundated phase can be detected as low backscatter coefficient in SAR imagery. The dry field and non-agricultural like settlement was detected as higher backscatter coefficient. Based on these hypotheses, the full polarization was selected to obtain more characteristic of backscatter coefficient which leads to the second objective, *to explore the ability of ALOS/PALSAR full polarization mode for classifying agricultural croplands.*

There were thirty-three new parameters generated from the combination of four polarizations from one full polarization image. In addition to these parameters, the full polarization was generated into two types of decomposition, the Freeman and Durden decomposition and Yamaguchi 4 components decomposition. These parameters were evaluated by using separability index for separating the land use types. Several combinations from polarization of ALOS/PALSAR and the new parameters were classified by using the Maximum Likelihood Classification method. The result shows for full polarization (HH, HV, VH, and VV) achieved 60.84% and 0.441 for overall classification and kappa respectively. Meanwhile, the integration between backscatter coefficients (HH, HV, VH, VV, and HH+HV) and the three components of the Freeman and Durden decomposition significantly improved the overall accuracy and kappa coefficient (74.11% and 0.6247,

respectively). This fact implies that the integration of the full polarization and polarimetric decomposition of Freeman and Durden methods was able to compensate for the weakness of each component in discriminating complex agricultural croplands. Based on the classification result, the dry fields and paddy fields become bare land before the cultivation or after the harvest. These stages lead to the misclassification between both classes. On the other hand, mixed garden crop was surrounding with tree canopy that produced unique backscatter. Consequently, the mixed garden crop could be distinguished from other croplands class. The settlement class is recognized from the building structures that reflect stronger backscatter compared to other classes.

The third objective is *to perform classifying and mapping of Sentinel-1 by using the cloud based system of GEE.* In the fifth chapter, the multi-temporal imageries of Sentinel-1 taken on 2017 were applied in the similar study to the ALOS2/PALSAR2 study area. Compared to the previous chapters, it has fifty-six imageries with two types of polarization, the VH and VV polarizations. In this study, the Sentinel-1 data assisted with Sentinel-2 were successfully classified for the complex agricultural area in GEE platform. The threshold of backscatter coefficient less than -17.4852 dB and greater than -31 dB generated a paddy fields area. The detail cropping pattern of paddy fields became possible with the high multi-temporal of Sentinel-1 and the optical of Sentinel-2. A comparison of the backscatter coefficient and NDVI value derived from the Sentinel-2 of these paddy fields classes shows the backscatter coefficient was more sensitive to the surface structure, which led to the shifting time between the backscatter coefficient and NDVI. The combination band of VH, VV, and the subtraction of VH and VV polarization classified with the random forest with 50 number of trees obtained the highest overall accuracy and kappa value as 76.88% and 0.728, respectively. The accuracy of agricultural croplands classification from C-band wavelength is lower than the accuracy of the L-band wavelength. It is acceptable because the C-band wavelength is more sensitive to the canopy structure and could not penetrate deeper than the L-band which lead to lower accuracy.

The knowledge derived from the first study was then continued by utilizing the multi-temporal of ALOS2/PALSAR2. The four and fifth objective was designed *to investigate the multi-temporal of ALOS-2/PALSAR-2 for identifying and classifying the agricultural croplands* as well as *to analyze the influence of sample points selection based on the backscatter value characteristic for classification process.* The new study area with more complex agricultural cropland and more classes were selected to attain those objectives. Three dual polarizations mode imageries of ALOS2/PALSAR2 were assigned together with one full polarization mode imagery. The paddy field was separated into two types the paddy-I with irrigation system and paddy-II with rain-fed system. The sample points for both paddy fields classes were selected from the backscatter coefficient condition. The integrated between this new point selection method and the multi-temporal imagery gained higher classification result compared to the first study. The overall accuracy of 85.02% and a kappa coefficient of 0.824 were achieved by using the multi-temporal combination of HH and

HV polarization from four temporal data taken between January and September 2015. The multi-temporal data of ALOS2/PALSAR2 with only HH and HV polarization from all imageries were favorable in increasing the classification accuracy. The image combination with VH and VV polarization achieved lower accuracy compared to the combination of HH and HV polarizations. This fact shows that increase in number of bands was not a guarantee to get satisfactory accuracy for ALOS2/PALSAR2. However, multi-temporal combination was effective for classifying the agricultural croplands. The combination could increase overall accuracy by about 10%, compared to the average of single date acquisition classification results.

Based on the results of this study, the agricultural cropland classification and mapping could be achieved by using single full polarization of ALOS/PALSAR, multi-temporal of dual and full polarization of ALOS2/PALSAR2, and multi-temporal of dual polarization of Sentinel-1. There are several important notes to be discussed especially from the results obtained in this study: (1) the similarity and dissimilarity of L-band and C-band SAR capability in term of identifying agricultural croplands, (2) the complexity of agricultural croplands and its relation to the L-band and C-band SAR characteristic, and (3) the advantage and disadvantaged of the cloud based system in identifying and classifying agricultural croplands.

The C-band and L-band has similarity in sensitivity to the water content or moisture in earth's surface. The dissimilarity between both C-band and L-band is the acquisition time frequency and the strength of penetration. The C-band and L-band SAR are affected by the moisture condition such as in the paddy fields area especially during the early stage of paddy plantation. The water column in paddy field is beneficial for separating the paddy field with other agricultural cropland classes. Thus, the water content on soil affect the backscatter coefficient C-band and L-band SAR become lower which often assumed as the paddy fields. The complex agricultural croplands in Central Java characterized with the high perennial tree surrounding the agricultural fields and have the various cropping types in close by each other. The C-band has shorter wavelength than L-band therefore it is less capable to differentiate the structure of the perennial tree and the croplands. However, the acquisition of C-band is more frequent than L-band that can compromise the seasonal pattern of agricultural croplands.

The integration between the cloud based system and the SAR data was possible and could improve the time process in classification and mapping. However, the cloud based system for processing SAR data, like other methodology, will have advantage and disadvantage. The processing satellite imagery without cloud based system need to obtain the imagery from the satellite image service provider and then the user will be able to use the satellite imagery. At this step, the file size of imageries, especially SAR imageries, could be huge. It will be inconvenient for study with small target area because the user need to generate the satellite imagery using the similar boundary with target area. The cloud based system provides the tools for user to select the provided satellite imageries as well as to crop the satellite imagery by using the boundary of study area, even

before obtaining the satellite imagery. The process is easier and more efficient. However, the availability of satellite imageries in cloud based system is limited to free of charge satellite imageries. The L-band SAR such as ALOS/PALSAR and ALOS2/PALSAR2 were not provided in the cloud based system. Besides the availability of satellite imageries, the main pre-processing for SAR imageries, for example the speckle noise filtering, have to be performed in other software outside the GEE. Despite the advantages of cloud based system, there are three important things to be noted: (i) the processing of satellite imageries took short time in GEE, but the download process from cloud server to the user computer hardware requires more time, (ii) the users is recommend to have other commercial remote sensing and GIS processing software, and (iii) there is limitation between user interaction with the GEE windows.

This study has been to be useful in establishing the methodology for classifying complex agricultural croplands by using C-band and L-band SAR imageries. The methodology for choosing sample points and applying in cloud-based processing to get the most effective and efficient classification were also demonstrated in this study.

6.2 Recommendation

In establishing and updating the land use and land covers of complex agricultural croplands in tropical area, the two types of SAR imageries were used to compensate the cloud cover. The L-band is more capable in separating the area which often covers or surrounding by the tree branches. Meanwhile the high temporal of C-band SAR is more useful for understanding the cropping pattern of paddy fields. These two SAR wavelengths were processing separately. However, the possibility to combine these wavelengths to get higher accuracy for land use and land cover mapping in agricultural croplands is high. Hence the combination is encouraged to be done in the next study. In this study, the selection of sample points by using the backscatter coefficient, especially for the paddy fields, and based on the visual interpretation for other agricultural croplands. Even though the other land use and land cover types has relatively similar backscatter coefficient, the sample points by using backscatter coefficient is applicable by increasing the number of backscatter coefficient parameters from both C-band and L-band. Thus, the same method could be applied on other land use and land cover agricultural croplands area with less dynamic cropping pattern than paddy field area, in order to give higher accuracy. The recent technology of cloud based system processing could increase the time processing of satellite imageries as well as decrease the necessity of high performance processing hardware. Therefore, the methodology of the croplands identification in cloud based system could be implemented in larger area scale such as regency or province. Hopefully, this could be benefit for updating the existing land use and land cover map for the other agricultural croplands area.

Bibliography

Abidin, H. Z. & Badan Informasi Geospasial, Staf. (2018). Teknologi Geospasial Presisi dan Pemanfaatannya di Indonesia. 10.13140/RG.2.2.23845.35042.

Adams, J. R., Rowlandson, T. L., McKeown, S. J., Berg, A. A., McNairn, H., and Sweeny, S. J. (2013). Evaluating the Cloude-Pottier and Freeman-Durden scattering decompositions for distinguishing between unharvested and post-harvested agricultural fields. *Canadian Journal Remote Sensing*, 39, pp. 1-10.

Agus, F., & Manikmas, M. O. A.. (2003). *Environmental roles of agriculture in Indonesia.* Presented at the 25th Conference of the International Association of Agricultural Economists, Durban, South Africa. Retrieved from ftp://193.43.36.92/es/esa/roa/pdf/2_Environment/Environment_IndonesiaNA.pdf

Badan Pusat Statistik. (2014). Statistik Komuter Jabodetabek 2014. Jakarta: BPS - Statistics Indonesia.

Badan Pusat Statistik. (2015). Pendapatan Nasional Indonesia 2010-2014 (National Income of Indonesia 2010-2014). Jakarta: BPS - Statistics Indonesia.

Badan Standardisasi Nasional. (1999). Spesifikasi teknis peta rupabumi skala 1:10000. Retrieved from http://big.go.id/assets/download/sni/SNI/SNI%2019-6502.1-2000_image.pdf

Baghdadi, N., Boyer, N., Todoroff, P., El Hajj, M., and Begue, A. (2008). Potential of SAR sensors TerraSAR-X, ASAR/ENVISAT and PALSAR/ALOS for monitoring sugarcane crops on Reunion Island. *Remote Sensing of Environment*, 113(8), pp. 1724-1738.

Bamler, R. (2000). Principles of Synthetic Aperture Radar. *Surveys in Geophysics*, 21(2), pp. 147-157.

Berens, D. (2006). Introduction to Synthetic Aperture Radar (SAR). In: Advanced Radar Signal and Data processing, Educational Notes RTO-EN-SET-086. Neulilly-sur-seinem, France: RTO, pp. 3-1 - 3-14.

Canada Center for Remote Sensing, (2014). *Fundamentals of Remote sensing.* Canada: Canada Center for Remote Sensing.

Cazals, C., Rapinel, S., Frison, P.-L., Bonis, A., Mercier, G., Mallet, C., Corgne, S., and Rudant, J.-P. (2016). Mapping and characterization of hydrological dynamics in a coastal marsh using high temporal tesolution Sentinel-1A images. *Remote Sensing,* 8(7), p.570. https://doi.org/10.3390/rs8070570

Clauss, K., Ottinger, M., and Kuenzer, C. (2017). Mapping rice areas with Sentinel-1 time series and superpixel segmentation. *International Journal of Remote Sensing,* 39(5), pp. 1399–1420.

Congalton, R.. (1991). A Review of Assessing The Accuracy of Classifications of Remotely Sensed. *Remote Sensing of Environment,* 37(1), pp. 35-46.

Daldjoeni, N. (1984). Pranatamangsa, the Javanese agricultural calendar - its bioclimatic and socio-cultural functions in developing rural life. *The Environmentalist,* 4, pp. 15-18.

European Space Agency. (2011). Polarimetry Tutorial. [Online], Available at: http://earth.eo.esa.int/polsarpro/Manuals/4_Polarimetric_Decompositions.pdf, [Accessed 12 May 2016].

European Space Agency. (2011). Polarimetry Tutorial. [Online] Available at:

http://earth.eo.esa.int/polsarpro/tutorial.html, [Accessed 18 June 2014].

Ferrazzoli, P. (2002). SAR for agriculture: advances, problems and prospects. In Proceeding of the third International Symposium, 'retrieval of Bio- and Geophysical Parameters from SAR data for land applications', held in Sheffield, U.K., on 11-14 September 2001, ESA SP Publication 475, pp. 47-56.

Firman, T. (2016). The urbanisation of Java, 2000–2010: towards 'the island of mega-urban regions', *Asian Population Studies*, https://doi.org/10.1080/17441730.2016.1247587

Frate, F. D., Schiavon, G., Solimini, D., Borgeaud, M., Hoekman, D. H., and Vissers, M. A. M. (2003). Crop classification using multiconfiguration C-band SAR data. *IEEE Transactions on Geoscience and Remote Sensing*, 41, pp. 1611-1619.

Freeman, A. and Durden, S. (1998). A three-component scattering model for polarimetric SAR data. *IEEE Transactions on Geoscience Remote Sensing*, 36, pp. 963-976.

Gallego, F. J., Kussul, N., Skakun, S., Kravchenko, O., Shelestov, A., and Kussul, O. (2014). Efficiency assessment of using satellite data for crop area estimation in Ukraine. *International Journal of Applied Earth Observation and Geoinformation*, 29, pp. 22-30.

Ghazaryan, G., Dubovyk, O., Löw, F., Lavreniuk, M., Kolotii, A., Schellberg, J., and Kussul, N. (2018). A rule-based approach for crop identification using multi-temporal and multi-sensor phenological metrics. *European Journal of Remote Sensing*, 51(1), 511-524, https://doi.org/10.1080/22797254.2018.1455540.

Haldar, D., Das, A., Mohan, S., Pal, O., Hooda, R. S., and Chakraborty, M. (2012). Assessment of L-band SAR data at different polarization combinations for crop and other landuse classification. *Progress in Electromagnetic Research B*, 36, pp. 303-321.

Hamada, J., Yamanaka, M. D., Matsumoto, J., Fukao, S., and Sribimawati, T. (2002). Spatial and Temporal variations of the Rainy Season over Indonesia and their Link to ENSO. *Journal of the Meteorological Society of Japan*, 80(2), pp. 285-310.

Helmer, E. H., and Ruefenahct, B. (2005). Cloud-free satellite image mosaics with regression trees and histogram matching. *Photogrammetric Engineering and Remote Sensing*, 71(9), 1079-1089. https://doi.org/10.14358/ PERS.71.9.1079

Inoue, Y., Kurosu, T., Maeno, H., Uratsuka, S., Kozu, T., Dabrowska-Zielinska, K., and Qi, J. (2002). Season-long daily measurements of multifrequency (Ka, Ku, X, C, and L) and full-polarization backscatter signatures over paddy rice field and their relationship with biological variables. *Remote Sensing of Environment,* Vol. 81 (2–3), pp.194-204.

Inoue, Y., Sakaiya, E., and Wang, C. (2014). Potential of X-Band images from high-resolution satellite SAR sensors to assess growth and yield in paddy rice. *Remote Sensing*, 6(17), 5995-6019. https://doi.org/ 10.3390/rs6075995

JAXA (Japan Aerospace Exploration Agency). (2014). ALOS-2/PALSAR-2 Level 1.1/1.5/2.1/3.1 CEOS SAR Product Format Description. Retrieved from http://www.eorc.jaxa.jp/ALOS-2/en/doc/fdata/PALSAR-2_xx_Format_CEOS_E_r.pdf

JAXA (Japan Aerospace Exploration Agency). (2017). Calibration result of ALOS-2/PALSAR-2 JAXA standard products. Retrieved from http://www.eorc.jaxa.jp/ALOS-2/en/calval/calval_index.htm

Jones, H. G., & Vaughan, R. A. (2010). Remote sensing of vegetation: Principles, techniques, and applications. Oxford: Oxford University Press.

Kankaku, Y., Suzuki, S., and Osawa, Y. (2013). ALOS-2 mission and development status. Geoscience & Remote Sensing Symposium, 2014 (pp. 2396-2399). Melbourne, Australia: IEEE. https://doi.org/10.1109/IGARSS. 2013.6723302

Lavigne, F., Coster, B. D., Juvin, N., Flohic, F., Gaillard, J-C., Texier, P., Morin, J., and Sartohadi, J. (2008). People's behaviour in the face of volcanic hazards: Perspectives from Javanese communities, Indonesia. *Journal of Volcanology and Geothermal Research*, 172(3-4), pp. 273-287.

Lee, J.-S. and Pottier, E. (2009). Polarimetric Radar Imaging from Basics to Applications. Florida: CRC Press.

Lillesand, T., Kiefer, M. and Chipman, J. (2008). Remote sensing and Image Interpretation Sixth ed.USA. s.l.:John Willey & Sons, Inc.

Lonnqvist, A., Rauste, Y., Molinier, M. and Hame, T. (2010). Polarimetric SAR data in land cover mapping in Boreal Zone. *IEEE Transacations on Geoscience and Remote Sensing*, 48(10), pp. 3652-3662.

Mas, J. F., Vega, A. P., Ghilardi, A., Martinez, S., Carrillo, J. O. L., and Vega, E. (2014). A suite of tools for assessing thematic map accuracy. *Geography Journal*, 2014(10), 1-10. https://doi.org/10.1155/2014/372349

McNairn, H., Shang, J., Jiao, S. and Champagne, C. (2009). The contribution of ALOS PALSAR multipolarization and polarimetric data to crop classification. I*EEE Transcations Geoscience and Remote sensing*, 47(12), pp. 3981-3992.

Mei, E. T. W., Lavigne, F., Picquout, A., Bélizal, E. D., Brunstein, D., Grancher, D., Sartohadi, J., Cholik, N., and Vidal, C. (2013). *Lessons learned from the 2010 evacuations at Merapi volcano*. Journal of Volcanology and Geothermal Research, 261, 348-365. https://doi.org/10.1016/j.jvolgeores.2013.03.010

Milisavljevic, N., Holecz, F., Bloch, I., Closson, D., and Collivignarelli, F. (2012). Estimation of Crop Extent Using Multi-Temporal Palsar Data. Geoscience and Remote Sensing Symposium (IGARSS), 2012 IEEE International, pp. 5943-5946.

Mirelva, P. R. and Nagasawa, R. (2018). Identification and Classification of Complex Agricultural Croplands Using Multi-Temporal ALOS-2/PALSAR-2 Data: A Case Study in Central Java, Indonesia. *Journal of Agricultural Science*, Vol. 10(2), 58-70.https://doi.org/10.5539/jas.v10n2p58

Mishra, P. and Singh, D. (2011). Role of polarimetric indices based on statistical measures to identify vairous land cover classes in ALOS PALSAR data. Synthetic Aperture Radar (APSAR), 2011 3rd International Asia-Pasific Conference, 26(30), pp. 1-4.

Mishra, P., Singh, D., and Yamaguchi, Y. (2011). Land cover classification of Palsar images by knowledge based decision tree classifier and supervised classifiers based on SAR observables. *Progress in Electromagnetics Research B*, 30, pp. 47-70.

Naylor, R., Falcon, W., Wada, N., and Rochberg, D. (2002). Using El Nino Southern Oscillation climate data to improve food policy planning in Indonesia. *Buletin of Indonesian Economic studies*, 38, pp. 75-91.

Nelson, A., Setiyono, T., Rala, A.B., Quicho, E.D., Raviz, J.V., Abonete, P.J., Maunahan, A.A., Garcia, C.A., Bhatti, H.Z.M.; Villano, L.S., Thongbai, P., Holecz, F., Barbieri, M., Collivignarelli, F., Gatti, L., Quilang, E.J.P., Mabalay, M.R.O.; Mabalot, P.E.; Barroga, M.I.; Bacong, A.P.; Detoito, N.T.; Berja, G.B.; Varquez, F., Wahyunto, Kuntjoro, D., Murdiyati, S.R., Pazhanivelan, S., Kannan, P., Mary, P.C.N., Subramanian, E., Rakwatin, P., Intrman, A., Setapayak, T., Lertna, S., Minh, V.Q., Tuan, V.Q., Duong, T.H., Quyen, N.H., Van Kham, D., Hin, S., Veasna, T., Yadav, M. , Chin, C., Ninh, N.H. (2014). Towards an Operational SAR-Based Rice Monitoring System in Asia: Examples from 13 Demonstration Sites across Asia in the RIICE Project. *Remote Sensing*, 6(11), pp. 10773-10812.

Nofrita, S., and Krol, B. G. C. M. B. (2014). The Livelihood Analysis in Merapi Prone Area after 2010 Eruption. *Indonesian Journal of Geography*, 46(2), pp. 195-207. https://doi.org/10.22146/ijg.5790

Parmes, E., Rauste, Y., Molinier, M., Andersson, K., and Seitsonen, L. (2017). Automatic Cloud and Shadow Detection in Optical Satellite Imagery Without Using Thermal Bands—Application to Suomi NPP VIIRS Images over Fennoscandia. *Remote Sensing*, 9(8), 806; doi:10.3390/rs9080806

Partoyo, and Shrestha, R. P. (2013). Monitoring farmland loss and projecting the future land use of an urbanized watershed in Yogyakarta, Indonesia. *Journal of Land Use Science*, 8, pp. 59-84.

Patel, V. M., Easley, G. R., Healy Jr., D. M. and Chellapa, R. (2010). Compressed Synthetic Aperture Radar. *IEEE Jornal of Selected Topics in Signal Processing*, 4(2), pp. 244-254.

Peña-Barragán, J. M., Ngugi, M. K., Plant, R. E., and Six, J. (2011). Object-based crop identification using multiple vegetation indices, textural features and crop phenology. *Remote Sensing of Environment*, 115, pp. 1301-1316.

Richards, J. A. (2009). *Remote Sensing with Imaging Radar.* New York: Springer .

Rosenqvist, A., Shimada, M., Suzuki, S., Ohgushi, F., Tadono, T., Watanabe, M., Tsuzuku, K., Watanabe, T., Kamijo, S., and Aoki, E. (2014). Operational performance of the ALOS global systematic acquisition strategy and observation plans for ALOS-2 PALSAR-2. *Remote Sensing of Environment*, 155, pp. 3-12. https://doi.org/10.1016/j.rse.2014.04.011

Sandwell, D. T., Myer, D., Mellors, R., Shimada, M., Brooks, B., and Foster, J. (2008). Accuracy and resolution of ALOS Interferometry: vector deformation maps of the father's day intrusion at Kilauea. *IEEE Transactions on Geoscience and Remote Sensing*, 46, pp. 3524-3534.

Santoro, M., Fransson, J.E.S., Magnusson, M., Ulander, L.M.H., and Olsson, H. (2009). Signatures of ALOS PALSAR L-Band Backscatter in Swedish Forest. *IEEE Transactions on Geoscience and Remote Sensing*, Vol. 47(12), pp. 4001-4019.

Sarwani, M., Anda, M. and Shofiyati, R. (2015). Policy and Development of Agricultural land Resource Mapping in Indonesia: Experiences, Achievements and Impacts. [Online] Available at: http://www.slideshare.net/FAOoftheUN/policy-and-development-of-agricultural-land-resource-mapping-in-indonesia-experiences-achievements-and-impacts-by-muhrizal-sarwani-markus-anda-and-r

izatus-shofiyati [Accessed 16 May 2016].

Saxena, N., and Rathore N. (2013). A Review on Speckle Noise Filtering Techniques for SAR images. *International Journal of Advanced Research in Computer Science and Electrnoic Engineering(IJARCSEE),* 2(2), pp. 243-247

Serra, P., and Pons, X. (2008). Monitoring farmers' decisions on Mediterranean irrigated crops using satellite image time series. *International Journal of Remote Sensing*, 29, pp. 2293-2316.

Shelesto, A., Lavreniuk, M., Kussul, N., Novikov, A., and Skakun, S. (2017). Exploring Google Earth Engine Platform for Big Data Processing: Classification of Multi-Temporal Satellite Imagery for Crop Mapping. *Frontiers in Earth Science*, 5, https://doi.org/10.3389/feart.2017.00017

Shimada, M., Isoguchi, O. and Tadono, T. (2009). PALSAR Radiometric and Geometric Calibration. *IEEE Transactions on Geoscience and Remote Sensing*, 47(12), pp. 3915-3932.

Shofiyati, R., Ismullah, I. and Hakim, D. (2011). Identification of Paddy Planted Area Using ALOS PALSAR data. *Journal of Geographic Information System*, 3(4), pp. 351-356.

Sidhu, N., Pebesma, E., and Câmara, G. (2018). Using Google Earth Engine to detect land cover change: Singapore as a use case, E*uropean Journal of Remote Sensing*, 51(1), pp. 486-500, DOI: 10.1080/22797254.2018.1451782

SNAP Software, Brockmann Consult, Array Systems Computing and C-S. Available online: http://www.step.esa.int/main/toolboxes/snap/ (Last accessed on 10 April 2019).

Tian, H., Wu, M., Wang, L., and Niu, Z. (2018). Mapping early, middle and late rice extent using Sentinel-1A and Landsat-8 Data in the Poyang Lake Plain, China. *Sensors,* Vol. 18(1), https://doi.org/10.3390/s18010185

Tian, X., Chen, E., Li, Z., Su, Z. B., Ling, F., Bai, L., and Wang, F. (2010), Comparison of crop classification capabilities of spaceborne multi-parameter SAR data. In Geoscience and Remote Sensing Symposium (IGARSS2010), held in Honolulu, Hawaii, on 25-30 July 2010, IEEE International, pp. 359-362.

Torbick, N., Chowdhury, D., Salas, W., and Qi, J. (2017). Monitoring rice agriculture across Myanmar using time series sentinel-1 assisted by Landsat-8 and PALSAR-2. *Remote Sensing*, 9(2), 119. https://doi.org/ 10.3390/rs9020119

Uchida, S. (2010). Monitoring of planting paddy rice with complex cropping pattern in the tropical humid climate region using Landsat and Modis data a case of West Java, Indonesia. International Archives of the Photogrammetry, Remote Sensing and Spatial Information Science. 38, Part 8, pp.477-481.

USGS (U.S. Geological Survey). (2014). Landsat 8 data users handbook. USGS Earth Resources Observation and Science, Sioux Falls, South Dakota, USA. Retrieved from https://landsat.usgs.gov/sites/default/ files/documents/Landsat8DataUsersHandbook.pdf

USGS (U.S. Geological Survey). (2017). Product guide Landsat surface reflectance-derived spectral indices. USGS Earth Resources Observation and Science, Sioux Falls, South Dakota, USA. Retrieved from https://landsat.usgs.gov/sites/default/files/documents/si_product_guide.pdf

Veloso, A., Mermoz, S., Bouvet, A., Toan, T. L., Planells, M., Dejoux, J-F., and Ceschia, E. (2017). Understanding the temporal behavior of crops using Sentinel-1 and Sentinel-2-like data for agricultural applications. *Remote Sensing of Environment*, 199, pp. 415–426.

Verburg, P. H., Veldkamp, T. A., and Bouma, J. (1999). Land use change under conditions of high population pressure: the case of Java. *Global Environmental Change,* 9(4), pp: 303-312.

Wahyunto, K. D., Nugroho, K., and Sarwani, M. (2012). Agricultural Recovery Action for Area Affected by 2010 Merapi Volcano Eruption, Indonesia. *International Journal of Geoinformatics*, 8(4), pp. 41-48.

Widiatmaka, Ambarwulan, W., Setiawan, Y., and Walter, C. (2016). Assessing the suitability and availability of land for agriculture in Tuban Regency, East Java, Indonesia. *Applied and Environmental Soil Science*, Vol. 2016. https://doi.org/10.1155/2016/7302148.

Wikantika, K., Uchida, S., and Yamamoto, Y. (2002). Mapping vegetable area with spectral mixture analysis of the Landsat-ETM. In International Geoscience and Remote Sensing Symposium (IGARSS2002) held in Toronto, Canada, on 24-28 June 2002, IEEE International, Vol. 4, pp. 1965-1967.

Wu, F., Wang, C., Zhang, H., and Zhang, B. (2011). Rice Crop Monitoring in South China with RADARSAT-2 Quad-Polarization SAR Data. *IEEE Geoscience and Remote Sensing Letters*, 8(2), pp. 196-200.

Xiao, X., Boles, S., Frolking, S., Li, C., Babu, J. Y., Salas, W., and Moore III, B. (2005). Mapping paddy rice agriculture in South and Southeast Asia using multi-temporal MODIS image. *Remote sensing of Environment*, 100, pp. 95-113.

Xiong, J., Thenkabail, P. S., Gumma, M. K., Teluguntla, P., Poehnelt, J., Congalton, R. G., Yadav, K., and Thau, D. (2017). Automated cropland mapping of continental Africa using Google Earth Engine cloud computing. *ISPRS Journal of Photogrammetry and Remote Sensing.* 126, pp: 225-244, https://doi.org/10.1016/j.isprsjprs.2017.01.019

Yamaguchi, Y., Moriyama, T., Ishido, M. and Yamada, H. (2005). Four-Component Scattering Model for Polarimetric SAR Image Decomposition. *IEEE Transaction on Geoscience and Remote Sensing*, 43(8), pp. 1699-1706.

Yang, S., Shen, S., Li, B., Le Toan, T., and He, W. (2008). Rice Mapping and Monitoring Using ENVISAT ASAR Data. *IEEE Geoscience and Remote Sensing Letters,* 5(1), pp:108–112, https://doi:10.1109/lgrs.2007.912089

Yang, Z., Liping, D., Yu, G., and Chen, Z. (2011). Vegetation condition indices for crop vegetation condition monitoring. In Geoscience and Remote Sensing Symposium (IGARSS 2011), held in Vancouver, Canada, on 24-29 July 2011, IEEE International, pp. 3534-3537.

Yusoff, N. M., Muharam, F. M., Takeuchi, W., Darmawan, S., and Razak, M. H. A. (2016). Phenology and classification of abandoned land based on ALOS-1 and 2 PALSAR multi-temporal measurements. *International Journal of Digital Earth*, 10(2), pp. 155-174, https://doi.org/10.1080/17538947.2016.1216615

Zhang, Y., Wang , C., Chen , X. and Su, S. (2011). Support vector machine approach to identifying building using multi temporal ALOS/PALSAR data. *International Journal of Remote Sensing*, 32(23), pp. 7163-7177.

Zhang, Y., Wang, C., Wu, J., Qi, J., and Salas, W. A. (2009). Mapping paddy rice with multitemporal ALOS/PALSAR imagery in southeast China. *International Journal of Remote Sensing,* 30(23), 6301-6315. https://doi.org/10.1080/01431160902842391

Zhang, Y., Wang, C. and Zhang, Q. (2011). Identifying paddy fields with dual-polarization ALOS/PALSAR data. *Canadian Journal Remote Sensing*, 37(1), pp. 103-111.

List of Publications

Chapter 3

Author : Prima Rizky Mirelva, Ryota Nagasawa

Title : Application of ALOS PALSAR data for Agriculture Croplands Classification in Central Java, Indonesia

Journal : Journal of Japanese Agricultural System Society, Vol. 33, No.2, pp:27-36 10.14962/jass.33.2_27

Chapter 4

Author : Prima Rizky Mirelva, Ryota Nagasawa

Title : Application of Sentinel-1 data for classifying croplands using Google Earth Engine

Journal : International Journals of Geoinformatics (Accepted: April 2019)

Chapter 5

Author : Prima Rizky Mirelva, Ryota Nagasawa

Title : Identification and Classification of Complex Agricultural Croplands Using Multi-Temporal ALOS-2/PALSAR-2 Data: A Case Study in Central Java, Indonesia

Journal : Journal of Agricultural Science, Vol.10, No.2, pp: 58-70 10.5539/jas.v10n2p58

APPENDIX

Appendix 1 The agricultural condition of study area

(a)

(b)

(c)

(d)

(e)

(f)

Picture (a), (b), (c) are typical paddy field which often cultivated with other horticultural croplands. Picture (d) is typical upland field area. Picture (e) is tobacco fields and picture (f) is vegetable crops.

Appendix 2 The classification result of Central Java province by using random forest in Chapter 4

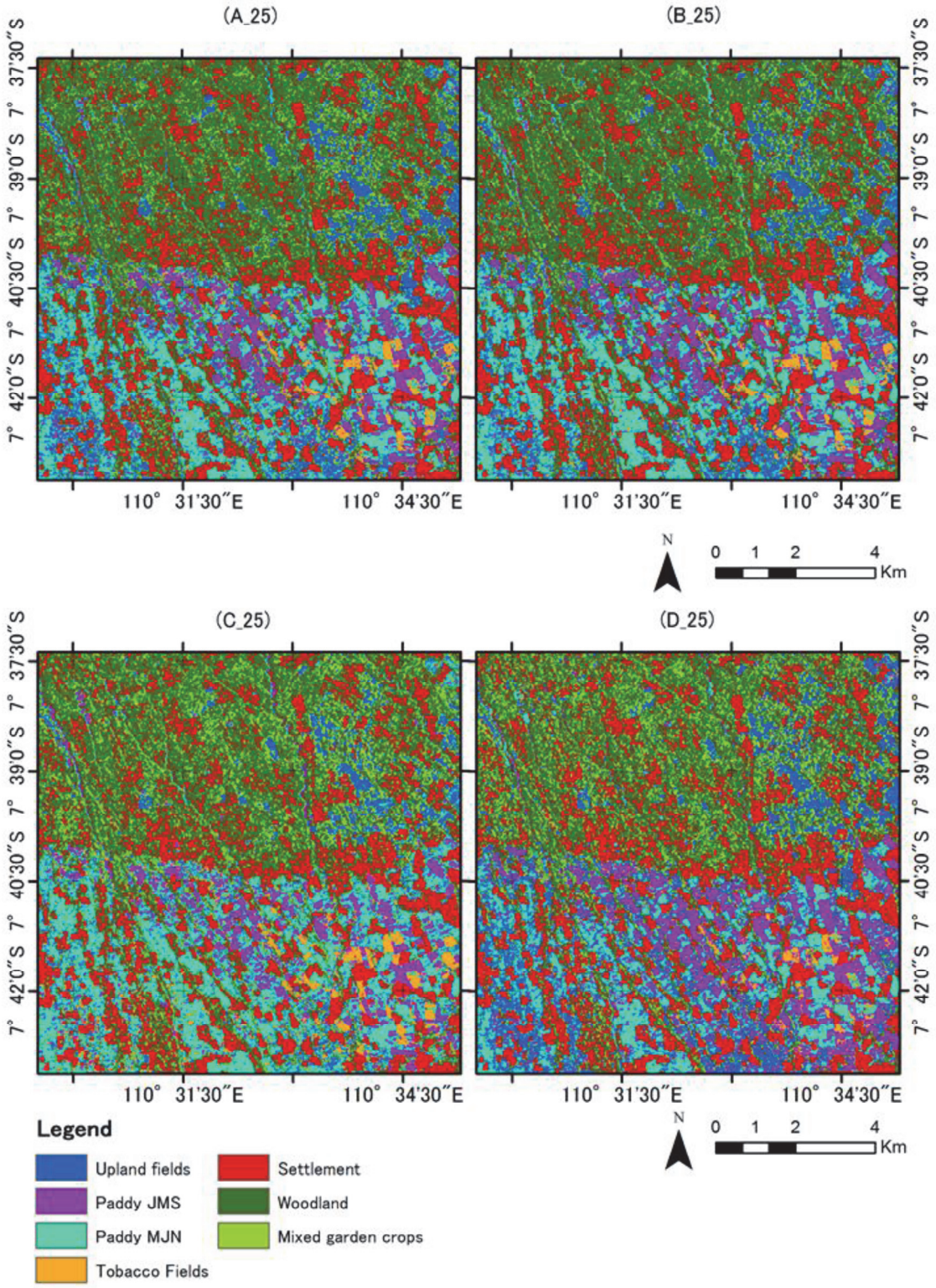

The classification result with 25 random forest

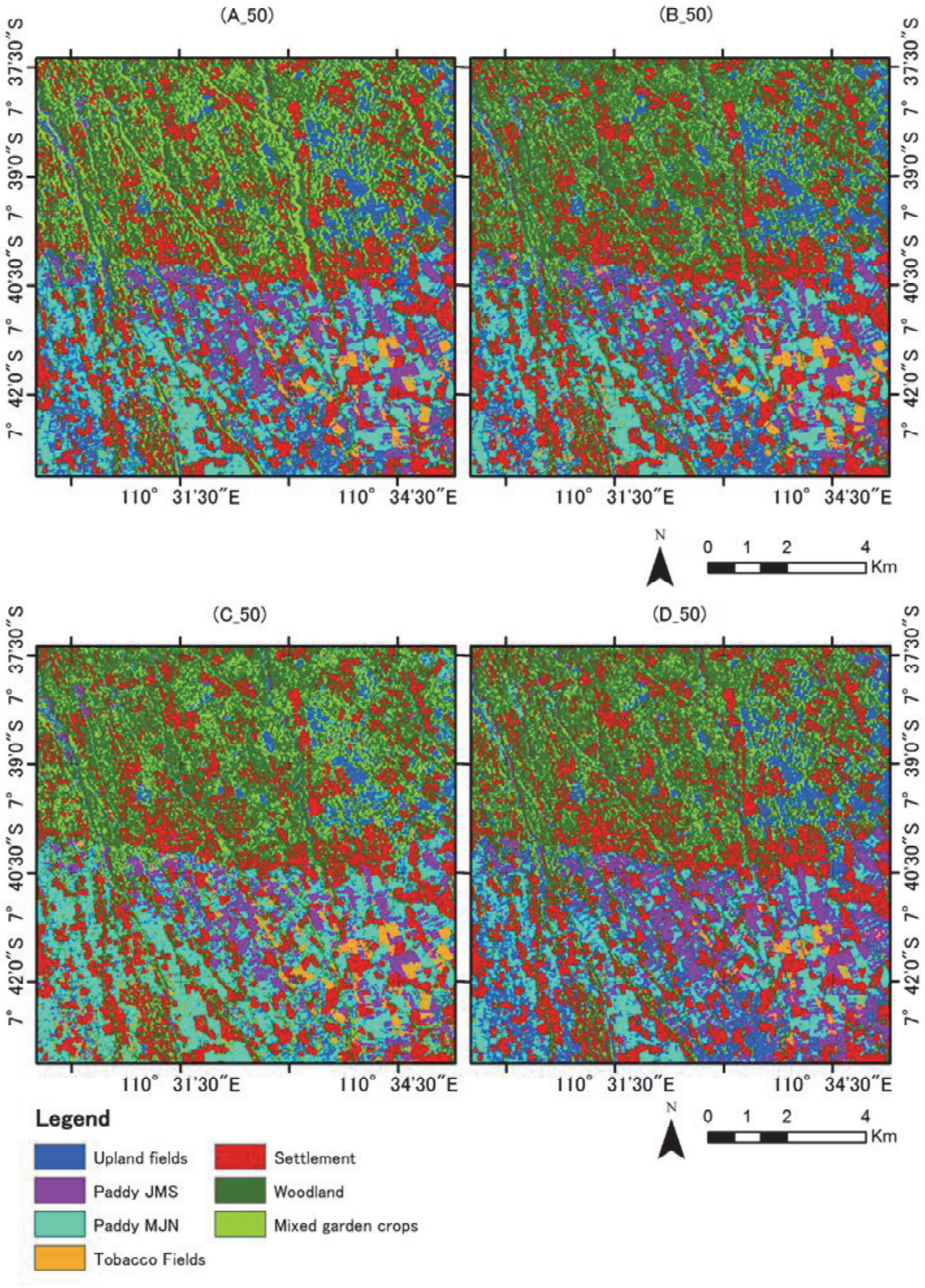

The classification result with 25 random forest

Appendix 3 The classification result of Central Java province in Chapter 5

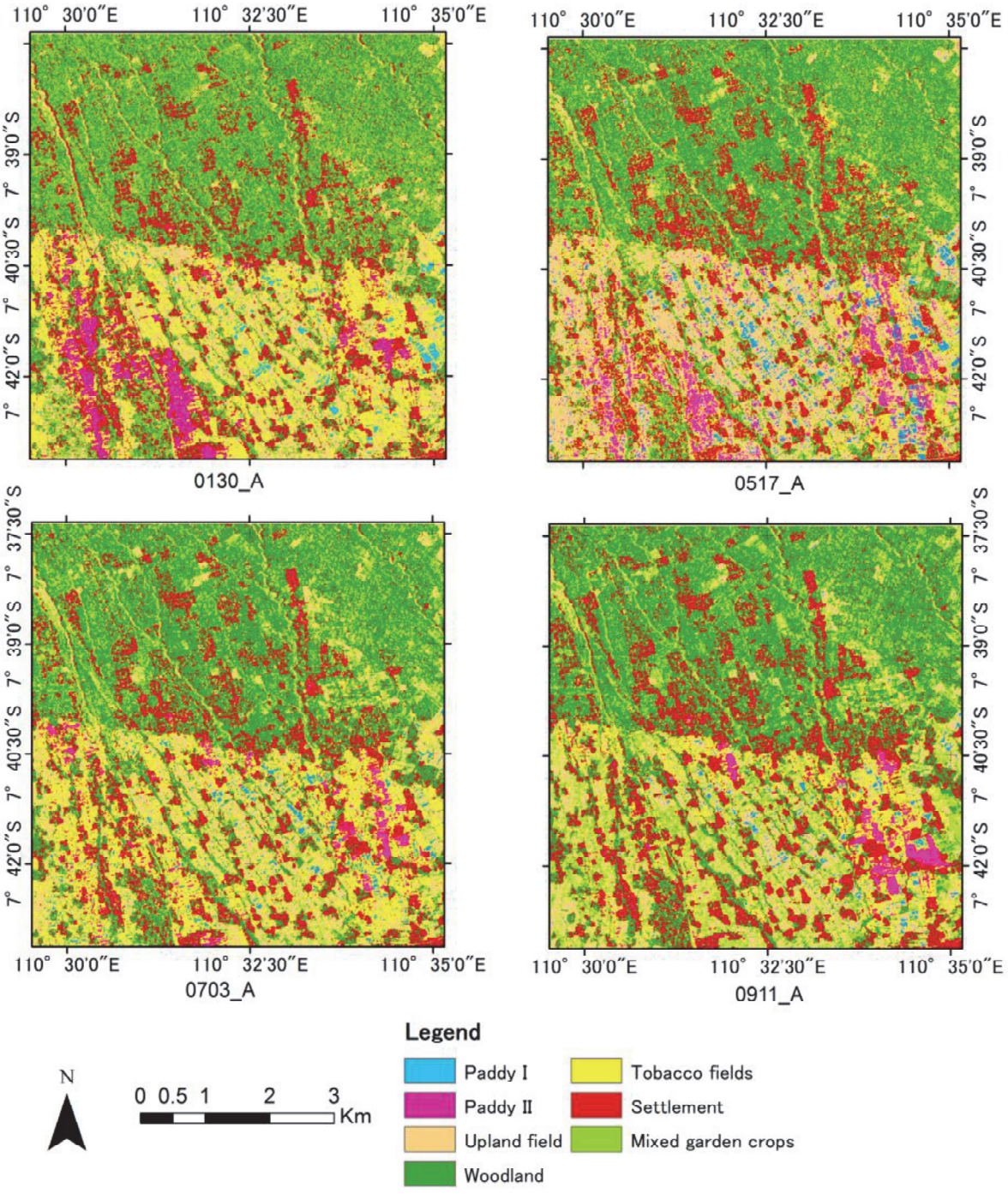

The classification result for 0130_A, 0517_A, 0703_A, and 0911_A

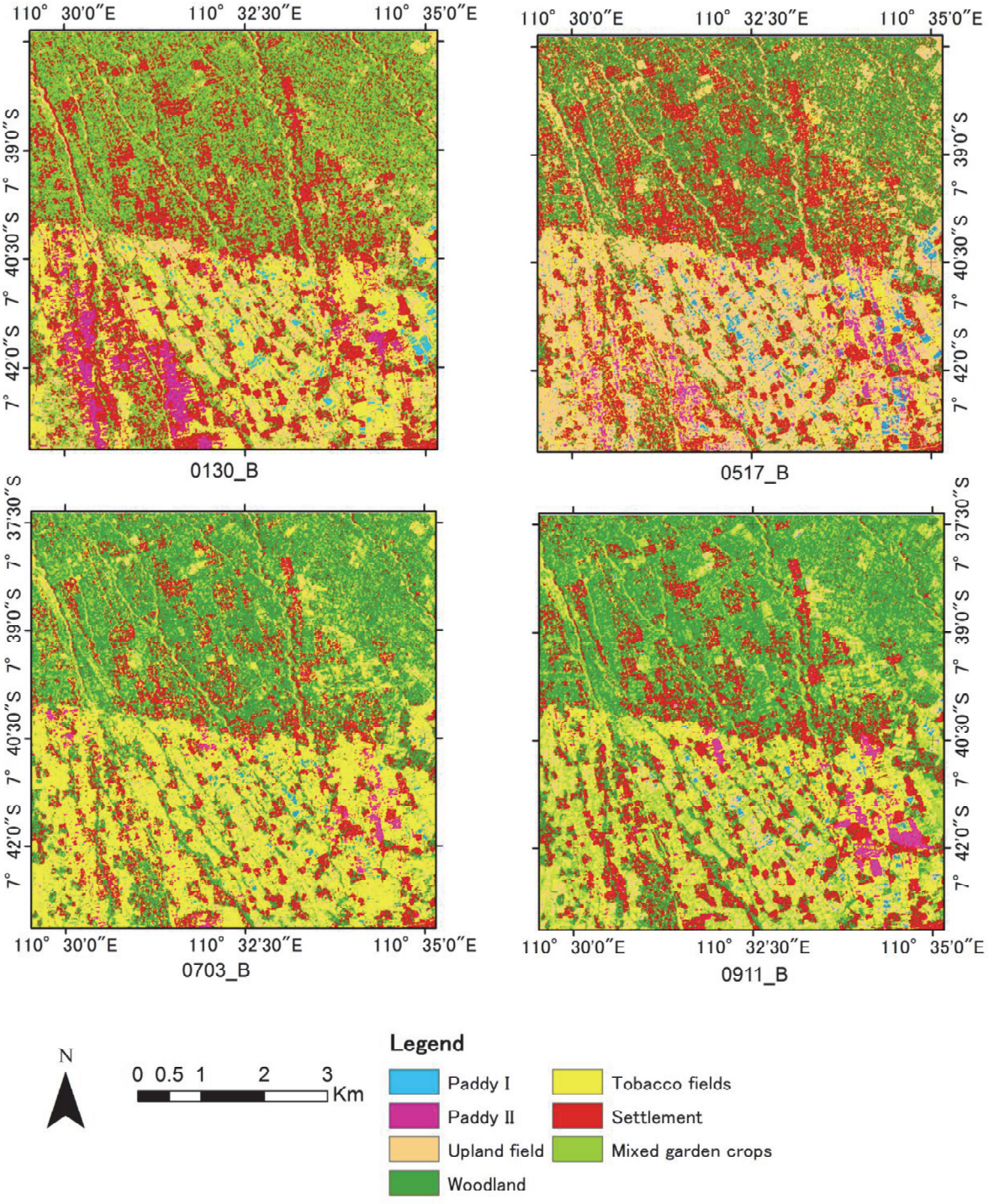

The classification result for 0130_B, 0517_B, 0703_B, and 0911_B

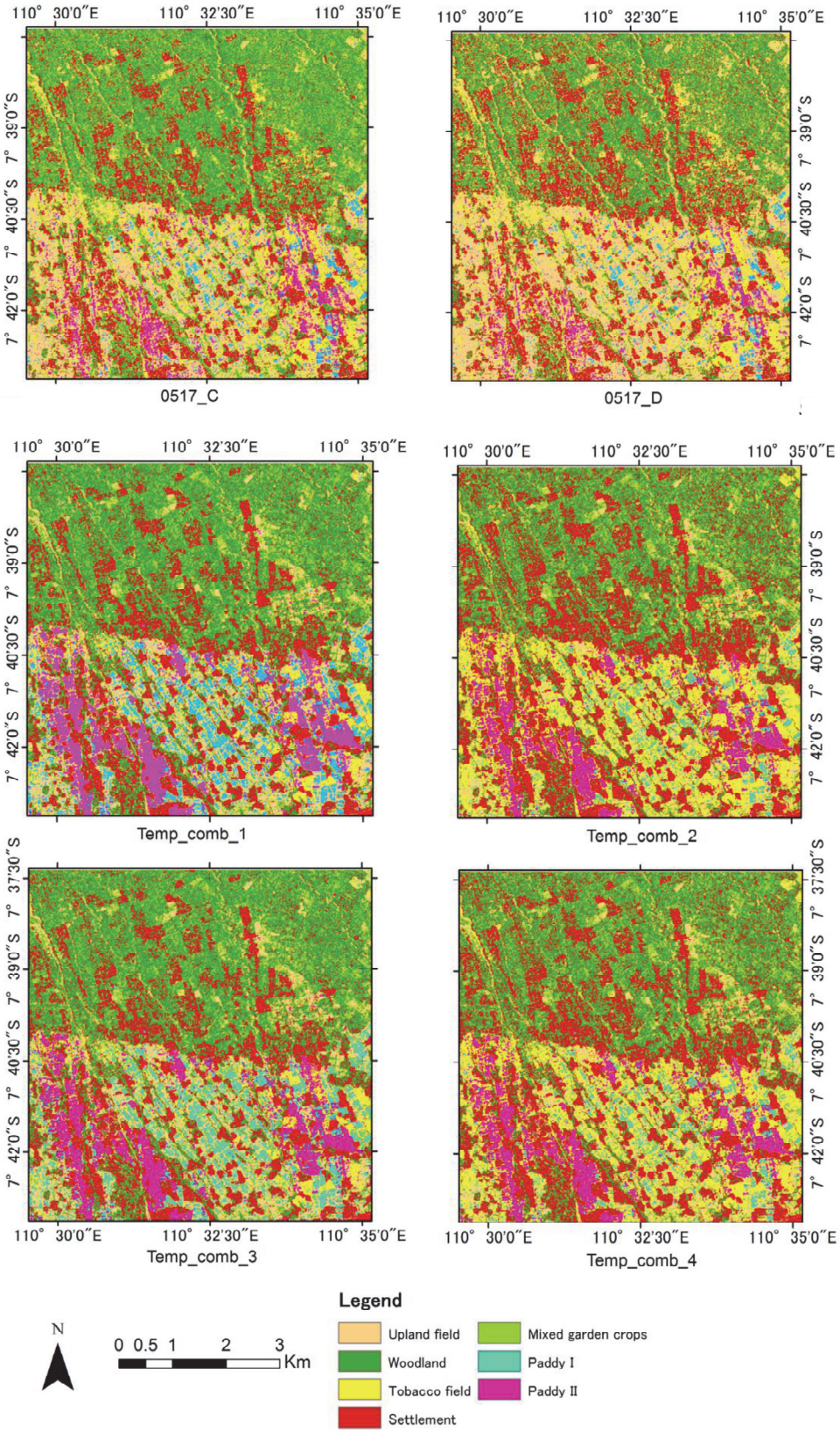

The classification result for 0517_C, 0517_D, Temp_comb_1, Temp_comb_2, Temp_comb_3 and Temp_comb_4

Summary

According to the statistics of Indonesia Statistics Bureau in 2010-2014, the ratio of agriculture, forestry and fisheries sector to gross domestic product shows high value (13.38%). Despite its small area, Java Island in Indonesia plays a central role in agriculture. Rural areas are widely distributed in Central Java province and Eastern Java province. The traditional rural landscapes can be seen at the foot of Merapi volcano in Central Java province. Majority of people living in these traditional rural areas are working as small-scale farmers which cultivate various crops and cultivation types, including paddy. In these small-scale farming systems, the area under management per household is generally as small as 0.3 hectares, and they are irregularly dispersed in more complex terrain shapes. Due to these conditions, it is extremely difficult to map detailed agricultural land use patterns and to grasp the spatial and spatial changes.

Currently, the population of Java is still increasing. The population growth is directly related to the need to increase food production; however, agricultural fields are decreasing due to the expansion of land used for infrastructure purposes. The reduction of agricultural fields could result in less agricultural production. Thus, accurate and updated information on land use and land cover mapping in agricultural areas has become a crucial issue for decision-making on agricultural policy. However, the mapping of agricultural land use and land cover is difficult due to the complexity of farming systems, the diversity of natural conditions, and the rapid development taking place on Java Island. In fact, agricultural statistics are still based on direct surveys of fields, despite the highly time consuming nature of these surveys. In this regard, there are extremely high expectations for geo-spatial technology, such as GIS and remote sensing to obtain information about agricultural croplands. In particular, synthetic aperture radar (SAR) satellite imagery is now being increasingly utilized based on its convenience and utility in overcoming cloud cover in tropical regions.

In this study, the available imagery from L-band SAR systems, such as ALOS/PALSAR, ALOS2/PALSAR2, and C-band SAR named Sentinel-1 was used to classify the land use and land cover of complex agricultural areas in Java Island as well as for discussing methods of classification. There are six objectives that must be met in order to achieve this purpose: (1) to examine the characteristics of complex agricultural cropland that can be identified by using active remote sensing data, (2) to explore the full polarization ability of ALOS/PALSAR, (3) to understand the backscatter value characteristics of paddy field cropping patterns, (4) to test the most effective backscatter value parameters for classifying areas of complex agricultural croplands, (5) to investigate the efficacy of temporal ALOS-2/PALSAR-2 in identifying and classifying croplands, and (6) to analyze the influence of sample point selection based on the backscatter value characteristics for the classification process.

In brief, main component of the SAR image is the transmitted and received waves in horizontal (H) and vertical (V) directions. There are four polarizations that can be generated from these two directions, namely HH,

HV, VH, and VV. The two letters in each abbreviation indicate transmission direction and receive direction. The classification of agricultural land use and land cover type using four polarization mode of L-band SAR, the ALOS/PALSAR, taken in April 2010. The target area covered around 50 km^2 in Central Java province. The four polarizations were processed into two types of decomposition type namely the Freeman and Durden and Yamaguchi 4-component. There are also 33 parameters extracted from these polarization by using the arithmetic calculation, such as add, subtract, multiply and division. The classification of full polarization achieved 67.09% and 0.523 for overall classification and kappa respectively. Meanwhile, the integration between backscatter intensities (HH, HV, VH, VV, and HH+HV) and the three components of the Freeman and Durden decomposition significantly improved the overall accuracy and kappa coefficient (74.11% and 0.6247). This fact implies that the integration of the full polarization and polarimetric decomposition of Freeman and Durden methods was able to compensate for the weakness of each component in discriminating complex agricultural croplands. The dry fields and paddy fields become bare land before the cultivation or after the harvest. These stages lead to the misclassification between both classes. On the other hand, mixed garden crop was surrounding with tree canopy that produced unique backscatter. Consequently, the mixed garden crop could be distinguished from other croplands class. The settlement class is recognized from the building structures that reflect stronger backscatter compared to other classes.

Next, the multi-temporal imageries of C-band SAR, the Sentinel-1, taken on 2017 were applied in the similar study to the second research. The Sentinel-1 data assisted with Sentinel-2 were successfully classified for the complex agricultural area in GEE platform. The threshold of backscatter coefficient less than -17.4852 dB and greater than -31 dB generated a paddy fields area. The detail cropping pattern of paddy fields became possible with the high multi-temporal of Sentinel-1 and the optical of Sentinel-2. A comparison of the backscatter coefficient and NDVI value derived from the Sentinel-2 of these paddy fields classes shows the backscatter coefficient was more sensitive to the surface structure, which led to the shifting time between the backscatter coefficient and NDVI. The combination band of VH, VV, and the subtraction of VH and VV polarization classified with the random forest with 50 number of trees obtained the highest overall accuracy and kappa value as 76.88% and 0.728, respectively.

This research also focuses on classifying agricultural land using the time series imageries from the L-band SAR, ALOS2/PALSAR2. The study area covers around 112 km^2 and consists of several land use and land cover types such as woodlands, paddy fields, upland fields, tobacco fields, settlement and mixed garden crops. There are three of dual polarizations imageries (HH, HV) and one full polarization imagery (HH, HV, VH, and VV). Similar to the previous study, the maximum likelihood classification method was also applied in this study. However, the temporal of ALOS2/PALSAR2 and field survey conducted in this area present there are two types of paddy field cultivation, paddy I for irrigated paddy field and paddy II for rain-fed paddy field. The

significant size of tobacco fields which planted during the dry season increases the difficulty of the classification process. Therefore, the temporal of Landsat-8 imageries were also applied to assist the sample point selection, especially for the tobacco fields. The RGB composite of HH, HV and HV-HH polarizations was used for the separation of these paddy fields' cropping patterns. Sample points were selected based on the characteristic of the RGB composite. The low backscatter coefficient areas, which appeared as dark blue, were categorized as paddy-I. Meanwhile, the paddy fields in a late growing stage showed more roughness and a higher backscatter coefficient and categorized as paddy-II. This method gave higher classification result compared to the first study. The overall accuracy of 85.02% and a kappa coefficient of 0.824 were achieved by using the multi-temporal combination of HH and HV polarization from four temporal data taken between January and September 2015.

In summary, this study presented the capability of SAR imageries for identifying and mapping the complex agricultural croplands in tropical area. This study explored the best parameters generated by using the combination of full polarizations from L-band, the benefit of sample points collection based on the backscatter coefficient of multi-temporal from L-band SAR and the methodology for sample point collection in cloud based system classification for multi-temporal C-band SAR. The results and finding exposed that the characteristic of the cropland derived from the backscatter coefficient is beneficial for classifying the complex agricultural croplands. The multi-temporal polarizations and the optical imageries assistance were also highly affected the accuracy of classification. The cloud based processing is highly favorable to maintain and process big amount of temporal data. Lastly, this study aimed to enhance more knowledge for faster identifying and mapping complex agricultural lands in tropical regions by using C-band and/or the L-band SAR.

Keywords: Agricultural land use, ALOS, PALSAR, PALSAR-2, Sentinel-1, Multi-temporal imageries, Cloud based remote sensing,

Japanese Summary

2010 - 2014 年のインドネシア統計局のデータでは、国内総生産に対する農林水産部門の占める割合は高い値（ 13.38%）を示している。とりわけジャワ島はその面積が小さいにもかかわらず、インドネシア国内にあって農業の中心的な役割を担っている。ジャワ島中・東部の中部ジャワ州、東部ジャワ州には農村地域が広く分布しており、中部ジャワ州のメラピ火山山麓では伝統的な農村景観がみられる。ジャワの伝統的農村とは、水田を基調としながらも経営規模が小さく多種多様な作物・栽培形式を多時期で行う農業が展開している地域を指す。これらの小規模農家では一般的に世帯あたりの経営耕地面積は 0.3 ヘクタールと小さく、さらに複雑な地形形状のなかで不規則に分散している。このために、詳細な農業的土地利用の様相を地図化し、さらにその時空間的変化を把握することは極めて困難な作業であると言える。

現在、ジャワ島の人口は依然として増加している。人口の増加は直接的に食糧増産の必要性に関与するが、一方で人口集積域の拡大によって農地面積減少の問題にも直面する。それ故に、農業地域における正確でアップデートされた土地利用・土地被覆に関する情報は、同国の農業政策に関わる意思決定にとって極めて重要な課題である。しかしながら、ジャワ島における営農体系の複雑さ、自然条件の多様性、急速な開発の進行などにより農業的土地利用・土地被覆の地図化は難しい課題を抱えている。農産物・農業地域の統計は依然として人手による直接調査によっており、精度や更新などは必ずしも頻繁におこなわれているものではない。この点において、衛星リモートセンシングや GIS などの地理空間情報技術への期待は極めて大きい。特に、合成開口レーダ（SAR）衛星画像は熱帯地域の雲量を克服するために、全天候型のセンサーとしてその利便性と効用性について大きく期待されている。

本研究は、ジャワ島の複雑な農業地域の土地利用・土地被覆を分類するために L バンド SAR である ALOS /PALSAR、ALOS 2 / PALSAR 2 および C バンド SAR である Sentinel-1 画像の利用可能性を評価するとともに、その分類手法を議論したものである。この目的のために、以下の 6 つの項目について検討・分析が行われた。すなわち、１）小規模で複雑な農業的土地利用の空間分布を能動型リモートセンシングデータで如何に分類するか、２）ALOS /PALSAR の位相情報（Polarization）の特徴から分類するアルゴリズムの検討、3）水田の作付けパターンの特徴を把握するための最適な後方散乱量の特徴を把握する、4）複雑な農作物畑を分類する際に最も効果的な後方散乱値のパラメータの吟味、5）農作物の分類・抽出のために時系列的な ALOS-2 / PALSAR-2 の利用可能性の検討、6）分類プロセスの後方散乱値特性に基づくサンプルポイントの選定とその評価、である。

SAR 画像の主成分は、水平方向と垂直方向の送受信波で２つの方向から発射される４つの偏波、すなわち HH、HV、VH および VV である。それぞれの略語の 2 文字は、水平方向（H）と垂直方向（V）の送信方向と受信方向を意味している。ここで一番目の研究課題として、本研究では 2010 年 4 月に撮影された L バンド SAR である ALOS / PALSAR の 4 偏波モードのデータを用いて農業的土地利用・土地被覆タイプの分類を中部ジャワ州の約 50 平方キロメートルの範囲を対象に行った。ここで、4 偏波データは２つのタイプの偏波分解（Polarimetric Decomposition）、すなわち Freeman and Durden と Yamaguchi 4-component の 2 通りのアルゴリズムで処理された。加算、減算、乗算、除算の算術計算によりこれらの偏波から、最終的に 33 個のパラメータを抽

出した。４偏波データを用いた画像分類の結果は、総合分類精度および Kappa 係数がそれぞれ 60.84%および 0.52 の値を得た。一方、後方散乱強度（HH、HV、VH、VV および HH＋HV）と Freeman and Durden 分解の３つの成分との間の積分は、総合分類精度および Kappa 係数がそれぞれ 74.11%および 0.62 を得、著しく精度が向上した。このことは、Freeman と Durden の全偏波分解と偏波分解の統合が、複雑な農作物の識別における各成分の弱点を補うことができたことを意味している。畑地と水田は、実際に作付け前と収穫後の土地被覆は裸地になる。こうした農地の季節変動が両クラス間の誤分類に関与している。一方、混交樹園地（Mixed garden crop）はユニークな後方散乱量を示す樹冠で特徴付けられており、結果として他の農地クラスとは容易に区別することができた。集落クラスは、他のクラスと比較して強い後方散乱を反映する建物構造から特徴付けられた。

次に、同様な研究対象地域において、2017 年に撮影された C バンド SAR である Sentinel-1 の多時期画像を用いた解析を行った。データ解析のツールとして Google Earth Engine(GEE)を用いた。分類は、光学衛星である Sentinel-2 のマルチスペクトル情報も補完的に用いて行われた。後方散乱係数の閾値が-17.4852 dB 未満で-31 dB を超えると、抽出・分類された水田面積に差が確認された。水田地域の詳細な作付けパターンは Sentinel-1 の高い時間分解能と Sentinel-2 のスペクトル分解能に補完されてより高い分類精度で抽出・分類が可能になった。 これら水田クラスの Sentinel-2 から導き出された後方散乱係数と NDVI 値の比較は、後方散乱係数が表面構造により敏感であることを示し、それは後方散乱係数と NDVI の間の時間的な差異（ズレ）を反映している。 VH、VV の結合帯域と 50 系統樹のランダムフォレスト法で分類された VH と VV 偏光の減算はそれぞれ 76.88%と 0.728 として、以前と比較して最高の総合分類精度と Kappa 係数値を得ることができた。

本研究では、L バンド SAR の ALOS2 / PALSAR2 の時系列画像データを用いても対象地域の農耕地を如何に分類できるかについて検討を行った。研究対象地域は一番目の研究課題地域に近接した約 112 平方キロメートルの範囲にあり、樹林地、水田、畑地、タバコ畑、集落、混交樹園地の土地利用・土地被覆タイプから構成されている。3 つの二重偏波画像（HH,HV）データおよび 1 つの全偏光画像（HH、HV、VH および VV）データを用いてまず最尤分類法が適用された。この地域では 2 つの異なる作付けパターンを示す水田に加え、乾季に栽培されるタバコ畑の存在によって分類プロセスの難易度は高くなっている。そのため、特にタバコ畑の抽出・分類のトレーニングサンプルを補強するために光学衛星データである Landsat-8 の時系列画像も補完的に用いられた。 HH、HV、HV-HH 偏光の RGB 合成は、これらの水田の作付けパターンの分離するためには有効であった。トレーニングサンプルの抽出点は、これらの RGB カラー合成画像に基づいて決定した。画像上で暗青色示された地域は、低後方散乱係数領域で水田 I として分類された。一方、後期成長段階の水田はより大きな粗度とより高い後方散乱係数を示し水田 II として分類された。この手法では、一番目の研究成果と比較してより高い分類精度を得ることができた。 2015 年 1 月から 9 月までの期間に取得した 4 時期の時系列データから、HH 偏波と HV 偏波の多時時合成画像を使用することで、総合分類精度 85.02%と Kappa 係数 0.824 の値を得、PALSAR-2 画像が複雑な農作物を識別するのに有効であることを実証することができた。　以上要約すると、熱帯地域のジャワ島おける伝統的な農業地域において、小規模で複

雑な耕作農地はSAR画像を用いることで高精度に分類することができた。本研究では、L バンドSARの全偏波の組合せ、同様にL バンド SARの多時期の後方散乱係数に基づく分類およびクラウドベースシステムにおけるサンプル点収集の方法で生成された最良パラメータを探求した。一方、多時期Cバンド SARの分類結果は、後方散乱係数から得られた農地の特性が複雑な農地を分類するために有益であることを示した。多時期偏波および光学画像の併用は分類精度の向上に大きく貢献することが明らかにされた。さらに、GEEのようなクラウドベースシステムを用いたデータ処理は、SAR画像のような大容量データを処理するのに極めて有効なツールであることも分かった。最後に、本研究はCバンドおよびLバンドSARを使用することによって、熱帯地域の小規模で複雑な農耕地の抽出・分類・地図化をより有効・有用であることを実証的に示すことができたことを改めて認識することができた。

キーワード：農業的土地利用、ALOS、PALSAR,PALSAR-2、Sentinel-1、時系列画像、クラウドベースリモートセンシング